Ex Vivo Evaluation of Myocardial β-Adrenergic Receptors in High-Fat Fed STZ and ZDF Models of Diabetes Using [^{3}H]-CGP12177.

James M. Haley

This Thesis is Submitted as Partial Fulfillment of the Master of Science Program in Cellular and Molecular Medicine

Ottawa, Ontario, Canada

Ex Vivo Evaluation of Myocardial β-Adrenergic Receptors in High-Fat Fed STZ and ZDF Models of Diabetes Using [^{3}H]-CGP12177.

MSc Thesis 2014, James M. Haley
Department of Cellular and Molecular Medicine, University of Ottawa
Ottawa, Ontario, Canada

Diabetes mellitus (DM) and hyperglycemia contribute to sympathetic nervous system (SNS) activation and cardiovascular dysfunction. SNS activation and increased norepinephrine levels downregulate cardiac β-adrenergic receptors (β-AR). The ADMIRE-HF trial identified reduced cardiac SNS innervation as an independent prognostic marker in heart failure. The β-AR antagonist [^{3}H]-CGP12177 was used to quantify cardiac β-AR in *ex vivo* biodistribution studies in streptozotocin (STZ)-treated rats after 8 weeks of sustained hyperglycemia, and in the Zucker Diabetic Fatty (ZDF) rat model of type-2 diabetes at the onset of hyperglycemia (10 weeks of age) and after a sustained period of hyperglycemia (16 weeks of age). In some STZ rats, insulin was provided at the onset of hyperglycemia, or after a sustained period of hyperglycemia. Insulin treatment at both time points prevented reduced [^{3}H]-CGP12177 binding (33-38% compared to controls) observed in STZ hyperglycemics. ZDF β-ARs were intact at 10 weeks but became reduced (16-25% relative to the Zucker leans) following 6 weeks of hyperglycemia. This work supports that cardiac β-AR are reduced in models of DM and that restoring insulin signalling to maintain glycemic control can normalize β-AR density whether provided early or after a period of sustained hyperglycemia.

TABLE OF CONTENTS

LIST OF TABLES

LIST OF FIGURES

LIST OF EQUATIONS

LIST OF ABBREVIATIONS

%EF – Percent Ejection Fraction
AMPK – Adenosine Monophosphate Protein Kinase
AC – Adenylate Cyclase
ANS – Autonomic Nervous System
β-AR – β-Adrenergic Receptor
cAMP – cyclic Adenosine Monophosphate
CGP12177 – 4-(3-tert-Butylamino-2-Hydroxypropoxy)-Benzimidazol-2-One
CGP12388 – 4-(3-(Isopropylamino)-2-Hydroxypropoxy)-Benzimidazol-2-One
DAG - Diacylglycerol
DM – Diabetes Mellitus
E/A – Transmitral Early to Atrial Flow
EDTA - Ethylenediamine Tetraacetic Acid
FDG – Flurodeoxyglucose
FFA – Free Fatty Acid
GLUT – Glucose Transporter
Gs – Stimulatory G-Protein
Gi – Inhibitory G-Protein
GPCR – G Protein-Coupled Receptor
GRK – G Protein-Coupled Receptor Kinase
HED – Hydroxyephedrine
HPLC – High-Performance Liquid Chromatography
HR – Heart Rate
IRS – Insulin Receptor Substrate
JAK – Janus Kinase
LCFACoA – Long Chain Fatty Acyl-Coenzyme A
MAPK – Mitogen-Activated Protein Kinase
MVD – Mitral Valve Deceleration
NE – Norepinephrine
NET – Norepinephrine Reuptake Transporter
PDE - Phosphodiesterase
PDK – Phosphoinositide-Dependent Kinase-1
PET – Positron Emission Tomography
PI3-K – Phosphatidylinositol 3-kinase
PKA – Protein Kinase A
RAS – Renin Angiotensin System
PNS – Parasympathetic Nervous System
SNS – Sympathetic Nervous System
SOC – Suppressor of Cytokine Signaling
STAT – Signal Transducer and Activator of Transducer
STZ - Streptozotocin
VMH – Ventral Medial Hypothalamus
ZDF – Zucker Diabetic Fatty
ZL – Zucker Lean
ZO – Zucker Obese

ACKNOWLEDGEMENTS

Following the completion of my thesis, I would like to thank everyone who helped me along the way. I extend my sincerest appreciation to my supervisor Dr. Jean DaSilva for the opportunity to undertake this project as well as the guidance to complete it. I must also thank my co-supervisor Dr. Rob Beanlands for his work with the Molecular Function and Imaging program and for the help he provided me in learning and applying translational research, as well as my committee members Dr. Mario Tiberi and Dr. Ross Milne for their expert advice. I would also like to thank Dr. James Thackeray, whose PhD work laid the foundations for my research project and Dr. Stephanie Thorn who always had time to help with anything. Without their mentorship and support, I would not have been able to complete this work. I extend my appreciation the members of the PET biotesting and radiochemistry labs for their help with the all the problems along the way, specifically Marika, Keegan, and Tayebeh who were adamant in helping me get everything to work from Western blots to flow cells and mobile phases. In addition, I must thank the ACVS staff at OHI, Dan, Caroline, Claire, and Chantal who always made time to help me and provided diligent care. Finally I would like to thank my family and friends, whose company and support provided me the stability and encouragement I needed to get everything done.

Thank you all.

1)INTRODUCTION

1.1)General Introduction

Metabolic syndrome is a term that describes a group of symptoms associated with obesity and an increased risk of cardiovascular disease. While definitions of metabolic syndrome vary, its is generally characterized as including several or all of the following risk factors of obesity, dislipidemia, hypertension, and diabetes mellitus (DM) (Figure 1.1). While each of these symptoms infers cardiovascular risk, the combination of these factors together increases that risk to a greater extent than any of the individual components (Hutchenson and Rocic, 2012). Each of these symptoms is associated with altered sympathetic nervous system (SNS) activity as indicated by increased cardiac and plasma norepinephrine (NE), and a reduction in cardiac SNS receptors contributing to progressive cardiovascular dysfunction. The ADMIRE-HF trial identified that methods assessing SNS integrity *in vivo*, such as by positron emission tomography (PET), may be applied to evaluate the cardiac SNS as an independent prognostic marker of patient outcome in heart failure (Jacobson et al. 2010). Given the close relationship between SNS integrity and cardiovascular risk in heart failure and DM, imaging the cardiac SNS in DM may provide novel insight into disease etiology in small animals and future prognostic insight into treating DM patients. This work will focus on quantifying sympathetic integrity in the heart, at the level of β-adrenergic receptors (β-AR), by characterizing [^{3}H]-CGP12177 retention in *ex vivo* biodistributions, in animal models of hyperglycemia and DM. This project is also a proof of concept model for future work with [^{11}C]-CGP12177 PET in DM and metabolic syndrome.

1.2)Diabetes Mellitus

The prevalence of DM is growing and globally is expected to increase from 366 million in 2011 to 552 million by 2030. The number of people with DM is increasing in every country and almost half of diabetics world wide are undiagnosed (International Diabetes Association, 2011). DM is an important risk factor for heart failure, the main cause of death in diabetics (Falcao-Pires and Leite-Moreira, 2012). In heart failure trials, diabetics represent 20-40% as compared to 5-10% in the general population (Taegtmeyer et al., 2002). Increasing evidence indicates a strong association between obesity, heart failure, and DM (Brodde 1993; Agardh et al. 2011). DM presents in two main forms that vary in their onset and progression. Type-1 DM presents following an autoimmune obliteration of pancreatic β-cells. This results in a drastic reduction of endogenous insulin production and subsequent hyperglycemia and altered lipid metabolism. In type-2 DM, high-fat, high-caloric diets contribute to whole body insulin resistance, so that despite normal or increased insulin production by the pancreas, target cells have reduced insulin-stimulated glucose uptake (Kostis and Sanders, 2005). Type-2 DM presents early on with progressive hyperinsulinemia and hyperglycemia and subsequent hypoinsulinemia as pancreatic β-cells begin to fail. Tissue insulin resistance contributes to a progressive increase in circulating blood glucose. DM, hyperglycemia, dyslipidemia and altered insulin signalling are strongly associated with cardiovascular disease (Taegtmeyer et al. 2002).

1.2.1)Diabetic Heart

The diabetic heart shows significant morphological abnormalities including myocyte hypertrophy, perivascular fibrosis, increased collagen deposition, increased free

fatty acid (FFA) uptake, and oxidative stress (Taegtmeyer et al. 2002). Echocardiography studies have demonstrated reduced heart rate (HR), and increased heart mass, and left ventricular dilation (Young et. al. 2002). The effect of DM on the heart can be identified early on in the left ventricle which loses compliance, developing filling abnormalities despite a preserved percent ejection fraction (%EF) (Choy et al. 2008; Galderisi 2006). Perturbed ventricular filling is characteristic of diastolic dysfunction. Echocardiographic measurements of diastolic function show increased transmitral early to atrial flow (E/A) velocity and increased mitral valve deceleration (MVD) time in humans and animal models of DM. Abnormal diastolic function has been noted in 27-70% of asymptomatic diabetic patients (Pailloe et al. 1989; Zarich et al. 1988) and is thought to precede the development of systolic dysfunction and reduced %EF in diabetics (Thackeray et. al., 2011b; Falcao-Pires and Leite-Moreira, 2012). One of the main factors that appears to underlie many of these changes in the diabetic heart is autonomic dysfunction (Esler et al. 2001, Thackeray et. al. 2011a; Thackeray et. al. 2011b). In DM, sympathetic over activity can be seen by increased NE in the heart and plasma, directly influencing heart rate and contractility (Esler et al. 2001, Thackeray et. al. 2011b).

1.3) Metabolic changes in DM and Sympathetic Activation

One of the predominant physiological changes that occur in obesity and DM is an alteration in metabolism, such as increases in circulating FFA, altered insulin signalling, hyperglycemia, and altered leptin signalling (Thackeray et. al., 2011b; Taegtmeyer et. al., 2002; Young et. al., 2002). These metabolic changes play a role in stimulating SNS activation and contribute to the progression of cardiovascular disease. In DM, different measurements of sympathetic activation have positive correlations with metabolic

perturbations including increases in sympathetic nerve activity reduced plasma NE clearance, increase cardiac and plasma NE (Straznicky et. al., 2012). The specific relationship between these metabolic factors and sympathetic activation in DM will be discussed below.

1.3.1)Free Fatty Acids

Dyslipidemia and steatosis are hallmarks of obesity and DM, and are strongly correlated with the development of insulin resistance and cardiovascular disease. Increases in circulating FFA in these conditions are usually associated with hypercaloric high-fat diets and an inactive lifestyle; the development of insulin resistance is associated with a chronic elevation in circulating fats. Elevated circulating FFA have specific effects in directly augmenting the SNS, but also indirectly by contributing to insulin resistance and subsequent metabolic changes.

Fatty infusions and high fat feeding contribute to increased sympathetic tone. Portal infusions of oleate in rats induced increases in plasma NE (Benthem et. al., 2000). Increased lumbar sympathetic nerve activity was observed in high-fat fed rats after 2 weeks high-fat feeding (Muntzel et. al., 2012), and increased renal sympathetic nerve activity was observed in New Zealand white rabbits fed high-fat diet (Armitage et al. 2012). β-blockers treat heart failure by antagonizing β-AR to reduced hyperstimulation and thereby restore receptor expression. Maison et al. (2000) observed reduced FFA levels in patients treated with β-blockers over the span of four and a half years. Stimulation of cardiac β-AR with isoproterenol was shown to increase heart rates and oxygen consumption post-exercise in humans (Borsheim et. al. 1998). This suggests a reciprocal relationship between β-AR expression and plasma FFA levels, and emphasizes

the close association between cardiac function, metabolism, and β-AR expression. The effects of circulating fats also appear related to insulin signalling. Oral and intravenous fat loads in obese humans were shown to increase HR and decrease HR variability over 8 hours, indicative of increased sympathetic tone. These changes occurred together with increases in plasma insulin, especially with higher concentration infusions, suggesting the relationship between fats and insulin resistance (Gosmanov et. al., 2010). Glucotoxicity and lipotoxicity can act synergistically *in vivo* in rat cardiomyocytes to exacerbate one another's detrimental effects (Dyntar et. al., 2001). This notion is supported by greater SNS activity in obese type-2 DM than in euglycemic obese individuals, and emphasizes the complex and interdependent relationships that exist between these metabolic factors and SNS activation (Lips et. al., 2013).

1.3.2) Insulin Signalling, Free Fatty Acids, and Insulin Resistance

In healthy individuals, insulin binds to insulin receptors and through a series of secondary messengers stimulates glucose transporter (GLUT) 4 translocation to the cell surface to facilitate glucose uptake by target tissues. The insulin receptor at the cell surface consists of two α- and two β-subunits. Insulin binding to the α-subunit activates a tyrosine kinase on the β-subunit, autophosphorylating three tyrosine residues, Tyr 1158, 1162, and 1163 (Kraegan and Cooney, 2008). The phosphorylated β-subunit mediates the activation of insulin receptor substrate (IRS) proteins. IRS proteins mediate the activation of phosphatidylinositol 3-kinase (PI3-K). PI3-K binds to phosphoinositide-dependent kinase (PDK)-1, facilitating the phosphorylation of protein kinase B, also known as Akt, which mediates the translocation of intracellular GLUT4 storage vesicles to the cell surface (Figure 1.2A). GLUT4 translocation may also occur independent of insulin

signaling by activating AS160, through the adenosine monophosphate kinase pathway (AMPK). AMPK is activated by an increased AMP:ATP ratio, such as occurs following a contraction, providing a direct link between the energy status of a cell and its glucose uptake (Cartee and Wojtaszewski, 2007). AMPK-dependent glucose uptake is an important mechanism of the insulin sensitizing drug metformin (Nicholson and Hall, 2011).

A proposed link between insulin resistance and FFA is that increased exposure of organs to circulating FFA raises the intracellular pool of long chain fatty acyl-Coenzyme A (LCFACoA) and their accumulation provides a substrate for non-oxidative processes, such as triglycerides, diacylglycerol (DAG), and ceramide formation (Kraegan and Cooney, 2008; Chess and Stanley, 2008). DAGs are formed from LCFACoA as an intermediate in triglyceride storage which is increased in most organs in obesity and DM. DAGs contribute to the activation of various serine kinases such as protein kinase C, molecular target of rapamycin, and c-Jun N-terminal kinases, which can interact with IRS and reduce its capacity to be phosphorylated by the β-subunit of the insulin receptor. LCFACoA can also form ceramides. Ceramides have been associated with perturbed insulin signalling by affecting the activation further down the insulin signalling cascade at the level of Akt (Chess and Stanley, 2008). Increases in FFA oxidation may also contribute to increases in oxidative stress and the production of reactive oxygen species. Reactive oxygen species have been implicated in reduced GLUT4 translocation through the activation of serine kinases and attenuation of insulin signalling downstream of Akt (Kraegan and Cooney, 2008). These mechanisms are summarized in Figure 1.2B. The

development of insulin resistance can in turn increase lipolysis of adipocytes, further increasing FFA levels and exacerbating insulin resistance.

1.3.3)Altered Insulin Signalling

Altered insulin signalling is central to the metabolic perturbations observed in obesity and DM. In type-2 DM hyperinsulinemia precedes the development of overt insulin resistance and hyperglycemia, and gradually progresses to hypoinsulinemia as pancreatic β-cells fail. Hyperinsulinemia even without hyperglycemia appears to have a direct influence in stimulating the SNS. In type-1 DM, hypoinsulinemia directly contributes to hyperglycemia and subsequent sympathetic activation.

1.3.3.1)Hyperinsulinemia in Type-2 DM

Insulin infusions experiments can demonstrate the acute effects of insulin and hyperinsulinemia on the activation of the SNS. When insulin is administered in physiological doses, it evokes increased muscle sympathetic nerve activity as compared to saline controls in normotensive non-obese humans (Hausber et. al., 1995). In a similar study by Kern *et. al.* (2002), a 360 min high rate insulin infusion [15mU/kg/min] increased HR as well as plasma epinephrine and NE relative to a low rate infusion [1.5mU/kg/min]. Of particular interest is that while insulin levels increased rapidly to a plateau, catecholamine levels did not plateau and had a positive slope over the duration of the infusion in both high- and low-rate groups, suggesting the chronic nature in which hyperinsulinemia may augment the SNS.

The manner in which hyperinsulinemia stimulates the SNS is not entirely clear, but it may act through the ventral medial hypothalamus (VMH). Insulin is transported across the blood-brain barrier and its central concentration is proportional to plasma

insulin levels (Banks et al. 1997). Insulin's transport across the blood-brain barrier can be saturated, and in conditions of hyperinsulinemia, this may contribute to central glucopenia, as not enough insulin can enter the brain to achieve normal glucose uptake (Borg et. al. 1995; Evans et al. 2004). Studies assessing the role of the VMH in SNS activation and DM have shown that 2-deoxyglucose-induced hypoglycemia contributes to elevations in plasma glucose in tandem with increases in plasma epinephrine and NE (Borg et. al. 1995). Sympathetic inputs to the VMH in turn exacerbate some metabolic perturbations associated with obesity, hyperinsulinemia, and DM. Acute NE administration to the VMH rapidly increases plasma glucose, FFA, insulin, and glucagon (De Jong et.al., 1977). Chronic infusions of NE into the VMH induce an obese, hyperinsulinemic, glucose-intolerant state (Cincotta et al.,2000). It appears that in the VMH, systemic hyperinsulinemia contributes to reduced glucose utilization and SNS activation, which may act synergistically to exacerbate one another.

1.3.3.2)Reduced Insulin Signalling in DM

Apart from the direct effects insulin can exert on the SNS, insulin resistance in type-2 DM and reduced insulin signalling due to hypoinsulinemia in type-1 and late stage type-2 DM contributes to metabolic changes characteristic of DM – hyperglycemia, increased circulating FFA, and steatosis. The liver and skeletal muscles are two of the main sites of insulin action and the major storage sites for glucose (Ferrannini, 2012). Impaired insulin signalling in these organs is considered to be one of the main factors contributing to hyperglycemia in DM. In normal conditions, hepatic insulin signalling encourages glucose storage and suppresses glucose output by the liver through inhibition of glycogenolysis and gluconeogenesis (Ferrannini, 2012). When normal insulin

signalling is absent, this suppression is attenuated, and the liver's glucose storage is reduced. Glucose secreting pathways remain constitutively active increasing blood glucose (Kostis and Sanders, 2005; Ferrannini, 2012). In tandem with this increased glucose output by the liver, reduced insulin signalling at the level of the skeletal muscle and most other tissues attenuates glucose uptake increasing blood glucose further (Ferrannini, 2012). Impaired insulin signalling encourages increases in circulating FFA (Weiss et. al., 2013). While it is true that increased FFA catabolism must occur in DM given the reduction in glucose utilization, FFA mobilization is also augmented increasing circulating FFA. Normal insulin signalling in adipocytes encourages fat storage, but as adipocytes become resistant to insulin, lipolysis is augmented and contributes to a net increase in circulating FFA. Additionally, obesity and high-caloric diets characteristic of type-2 DM can also contribute to high circulating FFA levels (Kraegen and Cooney, 2008; Weiss et. al., 2013). Increased FFA mobilization and accumulation in non-adipose tissues can contribute to steatosis and encourage the accumulation of metabolites such as DAG and ceramides, which in turn further exacerbate insulin resistance.

1.3.4)Hyperglycemia

Hyperglycemia is an added risk factor in metabolic disorders and is associated with increased mortality and morbidity therein. While intimately related with insulin signalling and resistance, hyperglycemia carries its own specific effects stimulating the SNS and increasing the risk of cardiovascular disease.

Carbohydrates have a stimulatory effect on the SNS and in their absence stimulation is reduced. In rats an intravenous bolus of glucose [1g/kg] increases plasma NE (Levin, 1991), and hypoglycemia has been associated with reduced SNS outflow

(Young and Landsberg, 1979; Landsberg et al, 1980). Elevated NE levels are characteristic of DM, and appear positively correlated with hyperglycemia. Reducing blood glucose in streptozotocin (STZ) rats with insulin attenuates elevations in plasma and cardiac NE (Thackeray et. al., 2013). As insulin resistance progresses, the worsening of glycemic control contributes to the development of impaired glucose tolerance into type-2 DM, with overt hyperglycemia. A recent study comparing left ventricular function and SNS found that treatment-naïve type-2 DM patients had greater muscle sympathetic nerve activity , atrial NE, and reduced plasma NE clearance compared to unmedicated impaired glucose tolerant patients that were matched for age, gender, body mass index, and blood pressure. Glycemic control and SNS activation appear to be reciprocally related. Increased SNS tone in type-2 DM was correlated with increased left ventricle mass and diastolic dysfunction, highlighting the importance of hyperglycemia in the progression of SNS activation and subsequent cardiovascular dysfunction. (Straznicky et. al., 2013).

The acute effects of glucose on the SNS appear to be mediated by glucose sensing neurons in the hypothalamus. Neurovascular cultures from rat postganglionic sympathetic neurons showed increased NE release in the presence of 25mM glucose as compared to 5mM controls (Damon, 2010). During an intracerebroventricular infusion of glucose (5.6mM) *in vivo* in rats, direct recordings of electrical activity showed an increase in superior sympathetic ganglion activity of 177% and decreased parasympathetic (PNS) superior vagal nerve activity by 39% (Camargo et. al., 2013) . Glucose injections peripherally increase activation of sympathetic preganglionic autonomic neurons as seen by an increase in increase in *c-fos* a marker of neuronal activity. Sympathetic

preganglionic autonomic neurons have distal effects increasing sympathetic nerve activity blood pressure, and HR (Nunn et. al., 2011). An intimate relationship exists between hyperglycemia and sympathetic tone.

1.3.5)Altered Leptin Signalling in DM

1.3.5.1)Hyperleptinemia and Leptin Resistance in Obesity and DM

Hyperleptinemia and leptin resistance occur in obesity and type-2 DM, contributing to the activation of the SNS. Leptin is a hormone secreted by adipocytes and its production is proportional to the amount of white adipose tissue. Leptin is an adipostatic mediator which acts on hypothalamic receptors to limit food intake and to activate sympathetic pathways regulating energy metabolism (Stucchi et. al., 2011). Leptin infusions augment sympathetic outflow from the kidneys (Haynes et. al., 1997). Leptin administration also appears to act synergistically with insulin in increasing HR, a marker of sympathetic activity, greater than insulin alone (Kuo et. al., 2003).

Normally, leptin binding to the leptin receptor, facilitates Janus kinase (JAK)2 phosphorylation on three tyrosine residues (Tyr 985, 1077, 1138 in mice) activating it. JAK2 in turn activates the signal transducer and activator of transcription (STAT)3, which increases forkhead box O-1 gene transcription. Leptin may activate sympathetic projections in the hypothalamus, where forkhead box O-1 promotes expression of pro-opiomelanocortin increasing appetite suppression, and reducing the expression of neuropeptide Y and its appetite promoting signalling (St-Pierre and Tremblay, 2012; Amitani M, et. al., 2013). In the liver, STAT3 regulates glucose homeostasis by suppressing the expression of gluconeogenic genes. Phosphorylated JAK2 also stimulates IRS1/2 phosphorylation, a down-stream target of the insulin receptor. IRS

phoshphorylation activates Akt through PI3-K and phosphatidylinositol (3,4,5)-trisphosphate. Similar to STAT3, Akt increases forkhead box O-1 transcription, promoting appetite suppression. Leptin has been shown to contribute to GLUT4 translocation through stimulation of IRS proteins (Benomar et al., 2006). Leptin signalling promotes fatty acid oxidation through increased peroxisome- proliferators-activated receptor-α (Lee Y, et. al., 2002). In the absence of normal leptin signalling, reduced STAT3, IRS, and peroxisome proliferators-activated receptor α activation promote increased food intake, hyperglycemia a steatosis (Amitani M, et. al., 2013).

Increased adipocity in obesity and type-2 DM is associated with circulating hyperleptinemia and leptin resistance. Leptin resistance appears to have at least two underlying causes, including decreased permeability of the blood-brain barrier to leptin reducing its concentration in the hypothalamus, and through suppressor of cytokine signaling (SOC)3 inhibition of JAK2 activation. Hyperleptinemia is associated with decreased brain leptin concentrations in rodents and humans (Amitani et. al., 2013). The permeability of the blood-brain barrier to leptin is decreased in high-fat diet-induced obese rats despite increased plasma leptin levels, reducing its central effects (Burguera et al., 2000). Leptin induced mRNA expression of JAK-STAT is inhibited by SOC3. Expression of SOC3 mRNA is increased in murine skeletal muscle in the setting of diet-induced and genetic obesity, inflammation, and hyperlipidemia. Leptin and insulin act to regulate one another's production, and leptin is implicated in altered insulin signaling and resistance in obesity and type-2 DM. Leptin signalling inhibits insulin biosynthesis and secretion from pancreatic β-cells and insulin stimulates leptin secretion from adipose tissue. This hormonal regulatory feedback loop is important in the healthy adipo-insular

axis, and dysfunction of this crosstalk plays and important role in the development of hyperinsulinemia and type-2 DM (Amitani M, et. al., 2013).

Leptin signalling does not occur in some model of obesity and DM like the Zucker obese (ZO) and Zucker Diabetic Fatty (ZDF) rats, due to a complete knock-out of the leptin receptor. While this negates the contribution of leptin to sympathetic activation in these models, it is relevant to note that similar to these models, leptin resistance occurs in obesity and type-2 DM. Diet-induced obesity and hyperleptinemia contribute to leptin resistance in the hypothalamus of mice (Munzberg et. al., 2004) and the loss of leptin receptor functionality occurs with age in the livers of C57BL/6J in association with the development of dislipidemia (Stucchi et. al., 2011). Elevated leptin signalling directly decreases insulin secretion, and the absence of leptin signalling may thereby contribute to hyperinsulinemia and insulin resistance in leptin resistant obesity (Park et. al., 2010). While leptin resistance may share some similarities with leptin receptor knock-out models of obesity and type-2 DM, it is also known that leptin repletion in *ob*/*ob* mice, a model in which endogenous leptin production is attenuated but an intact receptor remains, can help to improve dislipidemia and obesity (Sloan et. al., 2011) as well as restore depressed contractility, indicating that leptin resistance and the absence of leptin signalling are not analogous (Minhas et. al., 2005).

1.3.5.2)Leptin Deficiency in DM

Reduced adiposity in type-1 DM contributes to a state of relative leptin deficiency. In uncontrolled insulin-deficient diabetes, decreased body fat stores results in a marked reduction in plasma leptin levels (German et al., 2010; Amitani t. al., 2013). Leptin has antisteatotic actions in peripheral tissues and the absence of leptin signalling

may contribute to steatosis (Oral et. al., 2012). Accumulation of excessive lipids in pancreatic islets was reported to increase ceramide accumulation, fibrosis, and apoptosis. Restoration of leptin signalling recovered pancreatic insulin secretion and ameliorated DM in several rodent models of obesity, leptin resistance, and leptin deficiency (Unger 2005; Oral et. al., 2012). Leptin can improve lipid metabolism in ways that insulin cannot. Restoring leptin signalling can reverse steatosis by promoting β-oxidation of FFA in muscle and liver (Oral et. al., 2012) and by improving insulin sensitivity (Amitani et. al., 2013). Long-term leptin therapy in humans reduced insulin requirements; however, patients did not become insulin free, and c-peptide levels remained undetectable even after 1 year of leptin therapy (Park et. al., 2008; Amitani et. al., 2013; Wasserfall et. al., 2012). Reduced leptin signalling due to resistance in obesity and type-2 DM or due to insufficiency in type-1 DM is implicated in the deregulation of glucose and lipid metabolism, encouraging insulin resistance, hyperglycemia, and steatosis. As discussed above, these factors are directly and indirectly implicated in the metabolic changes associated with DM and contribute to the increased sympathetic tone therein.

1.4)Sympathetic Nervous System

1.4.1) Presynaptic NE Regulation

The autonomic nervous system (ANS) innervates various organs and tissues throughout the body to regulate physiological functions and metabolism. The ANS is divided into two branches, the SNS and the PNS, which contain preganglionic neurons that originate in the central nervous system and synapse with postganglionic neurons in the peripheral ganglia, which innervate target organs such as the heart (Figure 1.3). Stimulation of the PNS releases acetylcholine, which binds parasympathetic cholinergic

receptors, while stimulation of the SNS releases NE and epinephrine, which binds sympathetic adrenergic receptors (Appenzeller and Oribe, 1997). NE dominates SNS signaling in the heart. NE is synthesized from tyrosine in presynaptic cells and stored in vesicles until SNS stimulation facilitates calcium-mediated exocytosis of NE (Currie et. al., 2012). In the synapse, NE availability is tightly regulated. NE can be broken down in the synapse by catechol-*O*-methyl transferase or taken back up by presynaptic cells through norepinephrine-reuptake transporter (NET) where is it metabolized by monoamine oxidase or transported back into vesicles by the vesicular monoamine transporter 2 (Brodde et. al., 2006; Appenzeller and Oribe, 1997; El-Armouche et al. 2003; Thackeray et al., 2012). NE in the synapse may also bind adrenergic receptors on post synaptic cells, activating intracellular pathways (Figure 1.4). Adrenergic receptors exist in two main classes, α and β. These classes further divide into subclasses: α_1, α_2, β_1, β_2, and β_3 (Appenzeller and Orbie, 1997). The two branches of the ANS act in a complimentary but antagonistic manner. The SNS is generally associated with catabolic processes and its activation has a stimulatory *fight or flight* response. The SNS upregulates functions like cardiac output and blood flow to skeletal muscle, increasing the use and mobilization of fuel stores. In contrast, the PNS reduces cardiac output attenuating blood flow to skeletal muscle, while increasing blood flow to organs like the gut. Activation of the PNS contributes to energy sparing process encouraging the body to absorb and store energy for future use (Appenzeller and Orbie, 1997).

1.4.2)β-Adrenergic Signalling

β-AR belong to the super family of G protein-coupled receptors (GPCR) that have seven transmembrane-spanning regions (Broddee, 1993). In the heart, β-AR exist as three

distinct isoforms, β_1-, β_2-, and β_3-AR (Wallukat, 2002). Each β-AR subtype has a distinct molecular structure, pharmacological profile and population density. β_1-AR have the greatest expression in the heart, followed by β_2-AR, and β_3-AR have the lowest expression (Wallukat, 2002; Gauthier et al. 2011). The relative expression of β_1:β_2:β_3-AR in the hearts of healthy rats has been reported to be 62:30:8 (Dincer et al. 2002). With the highest relative expression, β_1-AR have the most important role in regulating cardiac performance in the healthy heart (Altan et al. 2007). β-AR are coupled to stimulatory G-proteins (Gs) and agonist stimulation of cardiac β-AR populations with pharmacological agents like isoproterenol or endogenous agonists like NE increase ionotropy and chronotropy. This effect occurs through Gs-mediated activation of adenylate cyclase (AC) following agonist binding, increasing cyclic adenosine monophosphate (cAMP) levels in cardiomyocytes, stimulating protein kinase A (PKA) production and culminating in increased intracellular calcium cycling, upregulating contractile force and heart rate (Lefkowitz, 1998) (Figure 1.4). Some evidence suggests β_2- and β-$_3$AR may also couple to inhibitory G-proteins (Gi), and their stimulation can mediate negative effects on inotropy and chronotropy, especially in advance heart failure with defective cardiac SNS innervation (Kuschel et. al., 1999). While conclusive data regarding the existence of Gi-coupling to β_2- and β_3-AR remains somewhat controversial, the rational supporting this coupling is that NE binding to Gi-coupled β-AR reduces contractility, potentially though AC inhibiton (Kuschel et. al., 1999; Dincer et al. 2002). The negative ionotropy associated with β_3-AR stimulation has also been attributed to the activation of the endothelial nitrous oxide signaling pathway encouraging vasodilation, attenuating cAMP production through competitive cyclic guanosine monophosphate production, and

by modifying membrane excitability to reduce intracellular calcium by increasing its extracellular transport through the sodium-calcium exchanger (Massion et al. 2003). β_3-AR stimulation has also been implicated in thermogenesis in brown adipose tissue, which increases energy expenditure by reducing the mitochondrial efficiency by modifying it's proton gradient through uncoupling-protein 1.

1.4.3) β-AR Regulation

GPCRs, including cardiac β-AR, are synthesized in the golgi apparatus and shuttled to the plasma membrane where they predominantly reside and where their signal transduction is activated. Agonist binding can desensitize receptors, attenuating intracellular signal transduction. Internalization of receptors from the plasma membrane into the cystol also occurs slowly and increases in the presence of an agonist (Dzimiri, 1999). Upon internalization these receptors may translocate back to the plasma membrane or to lysosomes where they are degraded. The relationship between ligand availability, receptor desensitization, internalization and degradation provides a mechanism to regulate ligand receptor interactions and subsequent intracellular responses. This provides a point of control at the level of the target cell, reducing receptor expression at the plasma membrane when agonists are abundant, which can be reversed when they are not, protecting cells from excessive receptor stimulation. In pathological conditions where agonists are chronically elevated, excessive binding can favour desensitization and degradation of receptors, leading to reduced surface expression of GPCRs and a chronic attenuation of intracellular signalling cascades (Figure 1.5) (Zhang and Mende, 2011).

1.4.3.1) Desensitization

Desensitization of GCPRs, such as the cardiac β-AR, is a regulatory mechanism that helps mediate intracellular responses resulting from receptor stimulation. Desensitization is defined as decreased AC activation and reduced intracellular response from a GPCR following ligand binding (Hadcock and Malbon, 1991). Desensitization is a short-term mechanism that is both rapid, occurring within seconds to minutes of ligand binding, and reversible, with AC responsiveness capable of returning within 15-30 min after agonist removal (Hadcock and Malbon, 1991; Lefkowitz, 1998). There are three main proteins involved in β-AR regulation – PKA, G protein receptor-coupled kinases (GRK), and β-arrestin. PKA and GRKs contribute to desensitization by phosphorylating intracellular aspects of β-AR reducing their GPCR coupling and stimulation of AC. β-arrestin can bind to phosphorylated receptors and facilitate their internalization. Desensitization can be heterologous (non-agonist specific) or homologous (agonist specific).

1.4.3.1.1)Heterologous Desensitization

Heterologous desensitization does not require agonist-specific stimulation of a GPCR, but results from stimuli that increase secondary intracellular messenger kinases. When intracellular cAMP levels become elevated, PKA is activated. PKA can phosphorylate β-AR on the third intracellular loop (Bouvier et al., 1988; Hausdorff et al., 1989; Brodde, 1993), causing a conformational change that prevents interaction with G-proteins, attenuating signal transduction (Lefkowitz, 1993). When PKA is inhibited or its target putative phosphorylation sites are mutated, this desensitization is attenuated (Lohse et. al., 1990; Hausdorff et. al., 1989). Secondary messenger kinases other than PKA may also influence β-AR phosphorylation and heterologous desensitization. Protein kinase C

has been implicated in the desensitization of several receptors including the m1 muscarinic receptor, the vasopressin receptor, and the angiotensin II receptor (Haga et. al., 1996; Zhang et. al., 1996; Oppermann et. al., 1996).

1.4.3.1.2) Homologous Desensitization

Homologous desensitization occurs following the stimulation of GPCRs by an agonist. Agonist binding of β-AR recruits β-AR receptor kinases, also know as GRK to the agonist-bound receptor. GRKs can be present in the membrane or in the cystol. GRKs 2, 3, 5, and 6 have been identified in the heart, with GRK2 and GRK3 residing in the cystol and GRK5 and GRK6 in the membrane (Drake et. al., 2006). Following agonist stimulation, GRKs are recruited to β-AR and phosphorylate the intracellular C-terminus of agonist-occupied receptors. Receptor phosphorylation by GRKs facilitates β-arrestin binding, preventing G-protein interactions and suppressing signal transduction. β-arrestin bound receptors attract clathrin and internalize the receptors into clathrin-coated pits (Tseng et. al., 2001; Dzimiri et. al., 1999). Internalized receptors are dephosphorylated (Sibley et al., 1986) and can be recycled back to cell surface as active receptors or directed to lysozomes for degredation (Hausdorff et al 1990; Pierce and Lefkowitz 2001; Luttrell and Lefkowitz, 2002). In a normal state, a balance exists between receptor production, desensitization, internalization and degradation (Tseng et al., 2001). Persistent stimulation of receptors can shift this balance in favour of degradation, reducing GPCR expression. Reduced β-AR expression in conditions of elevated SNS tone in heart failure and diabetes is one such example.

1.4.3.2)Downregulation

Downregulation is defined as a decreased in total receptor numbers caused by exposure to agonists for days or more. Downregulation results from long-term persistent

agonist receptor stimulation through a reduction in steady state mRNA and enhanced receptor degradation (Bohm et. al., 1997). Chronic incubation of hamster vas deferens cells with isoproteronol reduces β_2-AR mRNA by reducing the stability and half life of transcripts (Hadcock et. al., 1989). This reduces the translation of functional β_2-AR, downregulating the rate of production of new receptors. Persistent stimulation of β_2-AR increased lysosomal targeting reducing receptor expression. This increased lysosomal targeting appears related to an increased phosphorylation and upregulation of the recycling rate constant of receptor internalization, where each successive recycling internalization increases the probability a receptor may be targeted to lysosomal degredation (Moore et al 1999). Agonist-induced downregulation of GPCRs like the β-AR can take two weeks or more to recover receptor populations (Hadcock and Malbom 1991) and may only recover 50-90% of initial receptor density (Wang et al 1990). Internalization and downregulation is complex and overlapping point between desensitization and downregulation (Moore et al 1999).

1.4.4) Reduced β-AR Expression in DM

DM and hyperglycemia are associated with elevated plasma and cardiac NE (Thackeray et al. 2011b). NE levels positively correlate with disease progression and poor outcome in HF and DM (Young et. al., 2002; Jacobson et al. 2010; Thackeray et. al., 2011b). Elevated NE in the heart leads to a chronic hyperstimulation of β-AR and subsequent receptor desensitization, internalization and downregulation (Ganguly et. al., 1987; Roof et. al., 2011, Thackeray et. al., 2011a). Reduced β-AR density has been described in the diabetic heart (Dincer et al. 2002, Altan et. al., 2007, Thackeray et. al., 2011a). The expression of the three β-AR subtypes in the heart is affected differently by

DM (Brodde, 1993). Subtype-specific assessment of cardiac β-AR in DM indicates that β_1-AR expression is reduced (Dincer et. al., 2002; Thackeray et. al. 2011a), β_2-AR expression may be reduced or increased (Dincer et. al., 2002; Thackeray et. al. 2011a), and that β_3-AR expression is increased (Dincer et. al., 2002; Gauthier et. al. 2011). In 14 weeks of untreated DM, the relative expression of β_1:β_2:β_3-AR has been reported to be 40:36:23, as compared to 60:30:8 in the healthy heart (Dincer et. al., 2002). The shift in expression patterns brings greater emphasis on β_2- and β_3-AR, potentially counteracting the heightened release of NE by enhancing negative ionotropy and vasodilation (Liu et al. 1998). β_2- and β_3-AR are shown to have a lower affinity for NE, further suggesting an important role when catecholamine levels are elevated in DM (Gauthier et. al., 2011). The role of these changes in β-AR density and function in DM are still not fully understood. The relationship between β_3-AR, negative ionotropy and vasodilation in the heart, as well as the thermogenic dissipation of excess calories in brown adipose tissue make it an emerging therapeutic target in heart failure, DM, and obesity (Massion et al. 2003). The improved success of the third generation β-blocker Nebivolol is thought to be due in part to its β_3-AR agonism promoting cardioprotective vasodialtion (Rozec et. al. 2009). Examining how β-AR expression changes in the heart during DM and how glycemic control impacts this change may provide insight into understanding the effect of DM and hyperglycemia on cardiac function and β-AR expression.

1.5)Animal Models of Diabetes

1.5.1)High-Fat Fed Low-Dose STZ Rats

STZ is a diabetogenic agent consisting of a cytotoxic methylnitrosourea moiety attached to a 2-deoxyglucose molecule (Figure 1.6) (Lenzen, 2008). STZ is the most

widely used chemical to induce a diabetic state in experimental DM (Lenzan, 2008; Salem et. al. 2009; Choi et al. 2002; Khong et al. 2011). STZ is hydrophilic preventing its uptake in many tissues; however it is preferentially taken up by pancreatic β-cells through the GLUT2 transporter, where it alkylates DNA, leading to β-cell necrosis, ultimately impairing or eliminating native insulin production (Lenzen, 2008). A rat model of DM combines high-fat diet feeding to induce insulin resistance with an moderate intraperitoneal injection (45mg/kg) of STZ to partially impair insulin secretion in affected pancreatic β-cells and promoting the overproduction of insulin by surviving β-cells, leading to β-cell wasting and hypoinsulinemia (Reed et. al., 2000; Srinivasan et. al., 2005; Zhang et. al., 2003). The intraperitoneal route of administration theoretically reduces the effective dose of STZ delivered in each animal as compared with intravenous injection, resulting in a milder form of DM (Reed et al. 2000). These animals have been shown to exhibit characteristics of DM, including impaired glucose tolerance, sustained hyperglycemia, hypoinsulinemia, and dyslipidemia (Ganguly et al. 1987, Thackeray et. al 2011a, Thackeray et. al. 2011b). Insulin has been shown to be effective in inducing euglycemia in this model, providing a means of assessing the effects hyperglycemia on β-AR density, but also the role of insulin-induced euglycemia on preserving or restoring receptor expression. This model has been used previously in our group to study sympathetic dysfunction in DM (Thackeray et. al 2011a, Thackeray et. al. 2011b).

1.5.2) Zucker Rats

1.5.2.1) Zucker Obese and Zucker Lean Rats

ZO rats are a well characterized model of obesity and pre-DM, owing to a missence mutation (*fa*/*fa*), resulting in a truncated leptin receptor and hyperleptinemia

(Zucker and Zucker, 1961). Impaired leptin signalling in ZO rats contributes to the development of obesity starting between three and five weeks of age (Chua et. al., 1996a; Chua et. al., 1996b; Phillips et. al. 1996) with increased levels of circulating leptin, insulin, and FFA relative to Zucker lean (ZL) (+/+) rats (Pico et. al., 2002; Hardie et. al., 1996), their non-obese counterparts with intact leptin receptors and signalling. ZO rats display insulin resistance, high levels of circulating insulin (apparent at three weeks of age) (Beck, 2000), and FFA (Bugger and Abel, 2009), while blood glucose levels remain normal. ZO rats provide a better pre-DM euglycemic obese control for studying the effects of hyperglycemia on cardiovascular disease in type-2 DM than ZL rats alone.

1.5.2.2)Zucker Diabetic Fatty Rats

The ZDF rat is the most widely studied model of type-2 DM. ZDF was developed by selective breeding for hyperglycemia in the ZO (*fa/fa*) strain. Studies in ZDF rats have shown altered myocardial metabolism, with a shift toward increased FA oxidation (Bugger and Abel, 2009). Cardiac dysfunction has also been identified in ZDF rats using echocardiography (Fredersdorf et. al., 2004; Marsh et. al., 2007; Zhou et. al., 2000) and pressure-volume analysis (Radovits et. al., 2009), including reduced %EF, increased MVD, and reduced HR. Greater increases in NE levels have been observed in ZDF than in their euglycemic obese ZO counterparts and compared to ZL rats by 14 weeks of age (Marsh et al. 2007). The effect of elevated NE on cardiac β-AR and function is still not well studied in ZDF; specifically, the time course of altered β-AR expression in ZDF needs to be explored. This will help establish time points for future experiments assessing cardiac SNS in ZDF rats and potentially the effect of glycemic control with insulin sensitizers on the progression of DM and its relationship with altered β-AR expression.

1.6)Hypoglycemic Therapies and Reduced SNS

1.6.1)Insulin Replacement

Treatment of type-2 DM focuses on reducing blood glucose and/or increasing insulin sensitivity. Insulin replacement is used to treat type-1 DM or as a last stage of treatment of type-2 DM as β-cell exhaustion and apoptosis evokes hypoinsulinemia (Nicholson and Hall, 2007). Good glycemic control has been associated with improved sympathetic innervation in the heart (Stevens et. al., 1999) and normalization of blood glucose by insulin has been associated with restoration of SNS innervation, decreased NE levels and normalization of β-AR expression patterns in the heart (Ramanadham et. al., 1983; Dincer et. al., 2002; Thackeray et. al., 2013; Sherma et. al., 2008). Studies assessing the role of insulin therapy in restoring β-AR expression provide strong evidence as to the role of hyperglycemia and altered insulin signalling in cardiovascular disease at the level of the β-AR (Dincer et. al., 2002). Less is known about the temporal nature of insulin replacement therapy on cardiac SNS innervation. It remains unclear if insulin therapy provided after a period of sustained hyperglycemia is as effective at inducing euglycemia and restoring cardiac β-AR expression in the heart as when it is provided at the onset of hyperglycemia.

1.6.2)Insulin Sensitizers

Unlike reducing blood glucose with exogenous insulin, insulin sensitizers act to improve the body's responsiveness to endogenous insulin to reduce blood glucose. Metformin, is a biguanide that is one of the main pharmacological approaches to the management of insulin resistance in type-2 DM (Stumvoll et. al., 2007). Metformin acts to improve insulin sensitivity and reduce blood glucose. While the exact mechanisms of

metformin's actions are not fully understood, it appears to exert its function by stimulating AMPK (Zhou et. al., 2001; Viollet et. al., 2009). AMPK can mediate GLUT4 translocation independent of insulin signaling through the Rab GTP-ase activating protein AS160 (Kramer et al. 2006). Metformin-mediated improvements in glucose uptake have effects in several tissues such as decreased hepatic glucose output (Nicholson and Hall, 2011) as well as increased glucose deposition and utilization in peripheral tissues like the skeletal muscle, ultimately reducing blood glucose. Metformin has been used extensively in managing hyperglycemia in both type-1 and type-2 DM since it can act independently of circulating insulin levels and tissue insulin resistance. Blood glucose levels, glucose tolerance, and insulin sensitivity are improved in ZDF rats treated with metformin (Shoghi et. al., 2009).

Rosiglitazone is a second generation thiazolidinedione used in the treatment of type-2 DM (Nicholson and Hall, 2011). Rosiglitazone acts predominantly on adipocytes and skeletal muscle, activating peroxisome proliferators-activated receptor-γ to alter gene expression of proteins involved in FFA metabolism in adipocytes. This mechanism leads to decreasing circulating FFA by 20-40% and improves insulin sensitivity (Fonseca et. al., 2000; Phillips et. al., 2001; Fonesca 2008). Rosiglitazone also helps redistribute fat from visceral to subcutaneous deposits, and increases the ratio of high-density to low-density lipoproteins, both of which are cardioprotective (Adams et. al., 1997; McGuire and Inzucchi et. al., 2008). In contrast to this cardioprotection, rosiglitazone may be associated with an increased instance of myocardial infarction and heart failure (Nissen and Wolski et. al., 2007), but subsequent investigations have not found a clear link between rosiglitazone and adverse cardiovascular outcomes (Woo, 2009). More recently,

rosiglitazone has been associated with impairment of beneficial exercise-induced reverse remodeling in the left ventricle, which may be due to fluid retention (Roes et. al., 2011). It has been suggested that rosiglitazone may have vascular complications but remains neuroprotective (Palomares et. al., 2012). Myocardial imaging studies in ZDF rats have shown improvements in myocardial substrate utilization when treated with rosiglitazone (van der Brom et. al., 2009). Attempts to induce euglycemia in STZ rats with metformin and rosiglitazone by our group have been unsuccessful, presumably due to the lack of native insulin production. This may suggest a model of type-2 DM that exhibits hyperinsulinemia may be more successful. In future experiments, normalizing blood glucose levels and improving insulin sensitivity with these drugs in ZDF rats should reduce NE levels in the heart and plasma, restoring β-AR expression and left ventricular function.

1.7)PET and the SNS

PET is an imaging modality that uses radiolabelled compounds in tracer doses to visualize and quantify pathways and receptor targets in the body in three dimensions. Compounds or drugs that interact with specific pathways or receptors are coupled with cyclotron-produced radionuclides to form PET tracers. PET tracers undergo positive beta decay, emitting a positron (antiparticle of an electron), which will collide with an electron in an annihilation reaction near the origin of the decay, producing a pair of collinear gamma photons at 511 keV traveling in opposite directions. The two photons are then detected by scintillation crystals in the PET cameras surrounding the body in 360^{o}. The opposite but collinear nature of the decay allows the two gamma photons to be detected simultaneously, defining a line of response by electrical collimation, which is then

reconstructed to produce an image (Figure 1.7). In PET, the image produced has a colour scale, where brightness is proportional to tracer retention, giving an indication of receptor density or metabolic activity within an organ *in vivo* (Figure 1.8). PET imaging has high spatial resolution (6-10 mm), high molecular sensitivity (10^{-11}-10^{-12} mol/L), high temporal resolution (2-10 seconds), and high radiotracer sensitivity relative to other imaging techniques, making it a useful tool for characterizing biological processes *in vivo* in different tissues of the body (Matthews et. al., 2011). The high spatial resolution of PETrelative to other imaging modalities like SPECT, is due to PETs lower positron range and electrical collimation, making it a powerful too for assessing the SNS *in vivo*, especially in small animals or patients with elevated body mass where sensitivity may be inherently reduced (Rahmim and Zaidi, 2008).

1.7.1)PET as Guide to Heart Disease and Therapy

Little progress has been made in altering the clinical course of heart failure, and cardiovascular disease remains a leading cause of death world wide. Cardiovascular disease is not a single entity, but a common pathway for a number of cardiac and non-cardiac processes. Patient populations are diverse and individual responses to pharmacological intervention can vary widely. PET and its ability to study metabolic pathways and receptors *in vivo* may provide some insight into treating cardiovascular disease by allowing more stringent stratification of patient populations and by providing evidence for pathological patterns of metabolism and receptor expression (Matthews et. al., 2011; Bengel, 2011). Pathological changes in metabolism, such as changes in glucose and lipid metabolism in the heart (Welch et. al., 2006), and receptor expression, such as changes in β-AR expression (Bengel, 2011; Naya et al. 2009), can be identified by PET.

Monitoring these changes *in vivo* using PET may provide insight into the etiology of an individual patient's cardiovascular disease to determine and optimize a specific personalized therapeutic approach. Furthermore, baseline readings of such processes can be compared with readings after therapeutic interventions to determine if a particular treatment is having the desired effect and if not allow for alternate approaches (Matthews et. al., 2011). [^{18}F]- fluorodeoxyglucose (FDG) PET/CT is being applied in such a manner to help identify lymphoma based on increased glucose uptake and then stratifying patients to optimize therapy (Hutchings and Barrington, 2009). Given the prognostic utility identified in the ADMIRE-HF trial, assessing the SNS is an attractive target for PET in characterizing and optimizing treatments for cardiovascular disease in individuals to improve patient outcomes (Bengel, 2011). Assessing SNS integrity in animal models can similarly provide insight into the role of the SNS in the development of several cardiovascular pathologies like DM and how pharmacological treatments can impact this integrity within individual animals at multiple timepoints.

1.7.2)PET Tracers for SNS

The two main targets for PET in assessing SNS in the cardiovascular system are the presynaptic and postsynaptic neurons. Presynaptic neurons regulate NE production, release, and metabolism to control NE concentration within the synapse and its availability to bind postsynaptic receptors on cardiomyocytes. In the heart, postsynapatic β-AR bind NE and mediate its cellular responses related to cardiomyocyte function. A brief review of PET tracers that have or may be applied by our group to assess cardiac SNS innervation are below (Figure 1.4).

1.7.2.1)Presynaptic

1.7.2.1.1)[^{11}C]-Hydroxyephedrine

[^{11}C]-hydroxyephedrine (HED) is the most common PET tracers of presynaptic sympathetic innervation. Like NE, HED is taken up with high affinity by NET in presynaptic neurons, but unlike NE, HED is not metabolized by catechol-*O*-methyl transferase and is resistant to oxidative deamination by monoamine oxidase (Cheng, 2006). Characterization studies established high affinity for [^{11}C]HED for NET (k_i=20.9nM) (Raffel and Chen, 2004), with 85-90% specific uptake determined by desipramine pretreatment in rats (Thackeray et, al. 2007). A direct correlation exists between [^{11}C]HED retention and NET expression. Previous work by our group has identified that [^{11}C]HED retention is reduced after 8 weeks of STZ-induced hyperglycemia in high-fat fed rats (Thackeray et. al., 2011b), and that retention is restored when blood glucose is normalized with insulin (Thackeray et al., 2013). Metformin was less successful in reducing blood glucose and failed to restore [^{11}C]HED retention in this model, potentially because despite any improvement in insulin sensitivity, native insulin production is very low. This suggests that a truer model of type-2 DM, with intact endogenous insulin production, may be a better for assessing the role of insulin sensitizers in reducing blood glucose and restoring SNS integrity.

1.7.2.2)Postsynaptic

1.7.2.2.1)[^{11}C]-CGP12177

The β-AR antagonist 4-(3-tert-Butylamino-2-Hydroxypropoxy)-Benzimidazol-2-One (CPG12177) (Figure 1.9), has been used to study β-AR populations in various tissues, including the heart (Van Waarde et. al., 1992; Naya et. al., 2009; Thackeray et. al., 2011a). CGP12177 is hydrophilic, binding to cell surface receptors, giving a better

representation of active cell surface receptor populations compared to other lipophilic radiotracers such as such as [^{3}H]-dihydroalprenolol, which can cross the cell membrane and bind inactive receptors in the cytoplasm. Moreover, CGP12177 exhibits increased specificity and appears to bind only β-AR, compared to tracers like [^{125}I]-iodocyanopindolol that may also bind non-specifically to serotonin receptors in the brain (Morin et. al. 1992; de Jong et. al., 2002). [^{11}C]-CGP12177 has been used to study β-AR populations in cardiac disease states such as idiopathic dilated cardiomyopathy *in vivo* using PET (Delforge et. al., 2002; Naya et. al., 2009). While [^{11}C]-CGP12177 has not yet been synthesized by our group, [^{3}H]-CGP12177 provides an opportunity to explore this tracer in a proof-of-concept model, for the utility of longitudinal imaging studies with [^{11}C]-CGP12177, to serially evaluation β-AR density in diabetic animal models and patients. [^{3}H]-CGP12177 has been used to study β-AR populations in *ex vivo* biodistributions (Van Waarde et. al., 1992; Thackeray et. al., 2011a), binding with high affinity to β_1-AR (K_d=0.3nM) and β_2-AR (K_d = 0.9nM) and with lower affinity to β_3-AR (K_d = 90nM) (Mohell and Dicker, 1989; Van Waarde et. al., 1992). While *ex vivo* biodistributions are limited by the terminal nature of the experiment only allowing for a single time point to observe receptor binding, biodistributions also provide a direct quantitative assessment of receptor binding in a tissue without any reconstruction. Previous work in our lab has demonstrated the specificity of [^{3}H]-CGP12177 binding by blocking uptake with unlabeled CGP12177 and the non-selective β-AR antagonist propanolol and that [^{3}H]-CGP12177 retention in the heart is reduced after 8 weeks of sustained hyperglycemia in high-fat fed STZ rats (Thackeray et. al., 2011a).

1.7.2.2.2) [^{11}C]-CGP12388

Similar in structure to CGP12177, 4-(3-(Isopropylamino)-2-Hydroxypropoxy)-Benzimidazol-2-One (CGP12388), is an interesting alternative to CGP12177 in quantifying β-AR. CGP12388 has a simpler radiochemical synthesis that CGP12177 by circumventing [^{11}C]-phosgene and using the labeling synthon [^{11}C]-acetone to improve the efficiency and specific activity of synthesis (Elsinga et. al., 2001). Characterization has show similar kinetics to CGP12177 (Momos et. al., 2004 ; Elsinga et. al., 2001; Doze et. al., 2002). While CGP12388 has not been used previously in our group, it may provide an attractive alternative to [^{11}C]-CGP12177 with a more robust and reproducible synthesis for future work using PET.

1.7.2.2.3) (R)- [^{11}C]-Rolipram

(R) - [^{11}C]-Rolipram does not assess β-AR, but acts within cardiomyocytes to quantify post-receptor secondary messaging at the level of phosphodiesterase (PDE)4. In the heart, β-AR stimulation by NE increases cAMP levels. PDE4 enzymes terminate cAMP signalling by catalyzing second messengers to their inactive 5'-adenosine monophosphate derivatives (Zhao et. al., 2003). PDE4 isozymes are inhibited by rolipram and (*R*)-[^{11}C]-Rolipram has been applied as a PET tracer used for the evaluation of PDE4 levels and alterations in cAMP signalling pathways in the brain and heart. (Lorenco et al. 1999; Kenk et. al., 2011). High contrast in cardiac tissue uptake compared to surrounding tissues, combined with the involvement of PDE4 in cardiac contractility and pathological remodeling make this tracer a promising tool for *in vivo* imaging of myocardial diseases (Kenk et. al., 2011). Rolipram may provide unique information regarding post-adrenergic receptor signalling within cardiomyocytes and may be useful in quantifying β-AR signalling in individuals receiving β-blocker therapy. Our group has

demonstrated a dose dependent increase in PDE4 binding in response to NE in biodistributions with *(R)* - [^{11}C]-Rolipram (Lourenco et. al. 2006) and that in the myocardium this binding is specific to PDE4 and not other PDE isoforms (Kenk et. al., 2007). Changes in PDE4 activity have been observed using (*R*)-[^{11}C]-Rolipram PET following cardiomyocyte stimulation with the β-AR antagonist desipramine (Thomas et. al. 2011). These tracers provide tools to assess cardiac sympathetic integrity at pre- and post-synaptic sites as well as at an intracellular level. This work will contribute to the development of CGP12177 in assessing cardiac β-AR expression in models of DM. In the long term, this will help develop PET tracers capable of assessing the cardiac SNS at multiple levels.

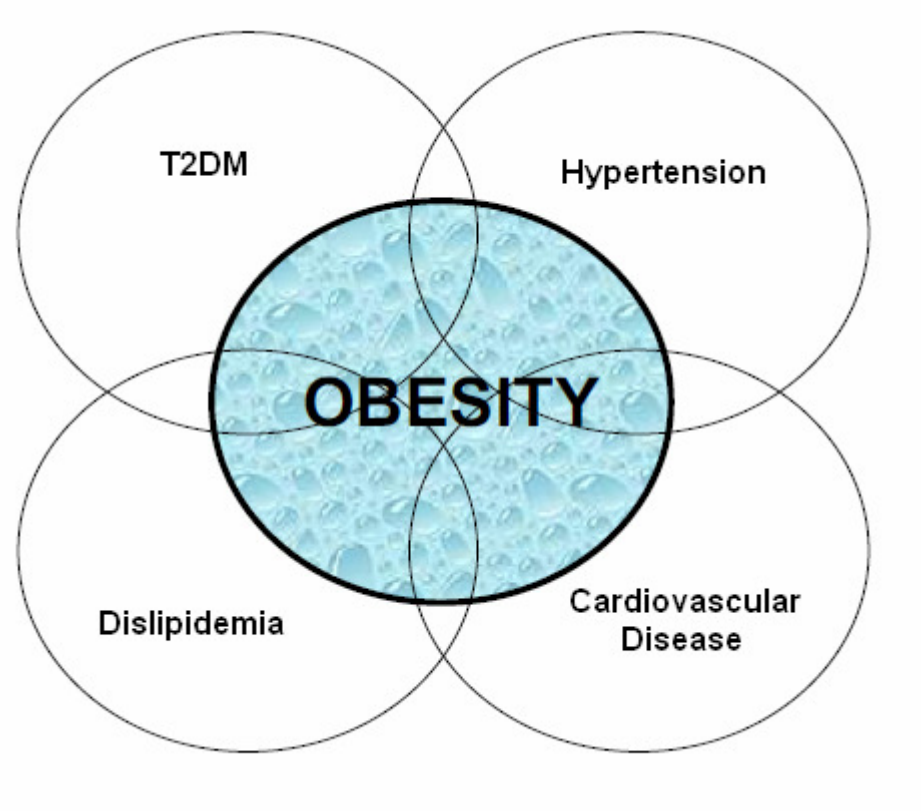

Figure 1.1: Common symptoms associated with metabolic disease. (Adapted from Maric-Bilkan, 2013.)

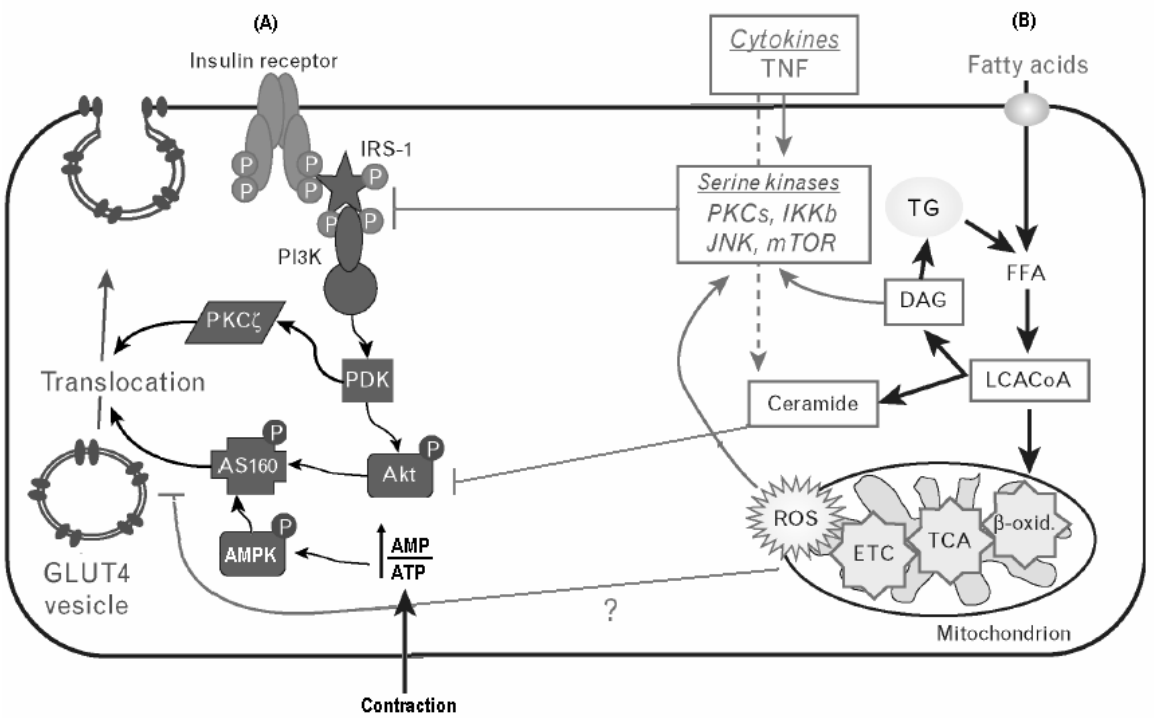

Figure 1.2: Overview of normal insulin signalling, AMPK mediated GLUT4 translocation **(A)**, and how FFA contribute to the impairment of insulin-stimulated GLUT4 translocation **(B)**. In normal insulin signalling, insulin binding autophosphorylates the insulin receptor activating insulin receptor substrate (IRS). IRS mediates the activation of PI3-K. PI3-K binds to PDK-1, facilitating GLUT 4 translocation through protein kinase C (PKC)ζ activation as well as through the phosphorylation of protein kinase B, also known as Akt, which mediates the translocation of intracellular GLUT4 storage vesicles to the cell surface via AS160 for glucose uptake. AS160 can also be activated by AMPK in the absence of insulin when there is an increase in the AMP to ATP ratio, such as may occur following a contraction. In insulin resistance, increased FFA uptake raises intracellular LCFACoA and provides a substrate for non-oxidative processes, such as triglyceride, DAG, and ceramide formation. DAGs contribute to the activation of various serine kinases such as PKC isoforms other than PKCζ, molecular target of rapamycin (mTOR), and c-Jun N-terminal kinases (JNK), which may reduce the capacity of IRS to be activated by insulin binding to the insulin receptor. Ceramides perturb insulin signalling by attenuating Akt phosphorylation. Increases in FFA oxidation may also contribute to increases in oxidative stress and the production of reactive oxygen species (ROS). ROS have also been implicated in reduced GLUT4 translocation through the activation of serine kinases and attenuation of insulin signalling downstream of Akt. (Adapted Kraegan and Cooney, 2008)

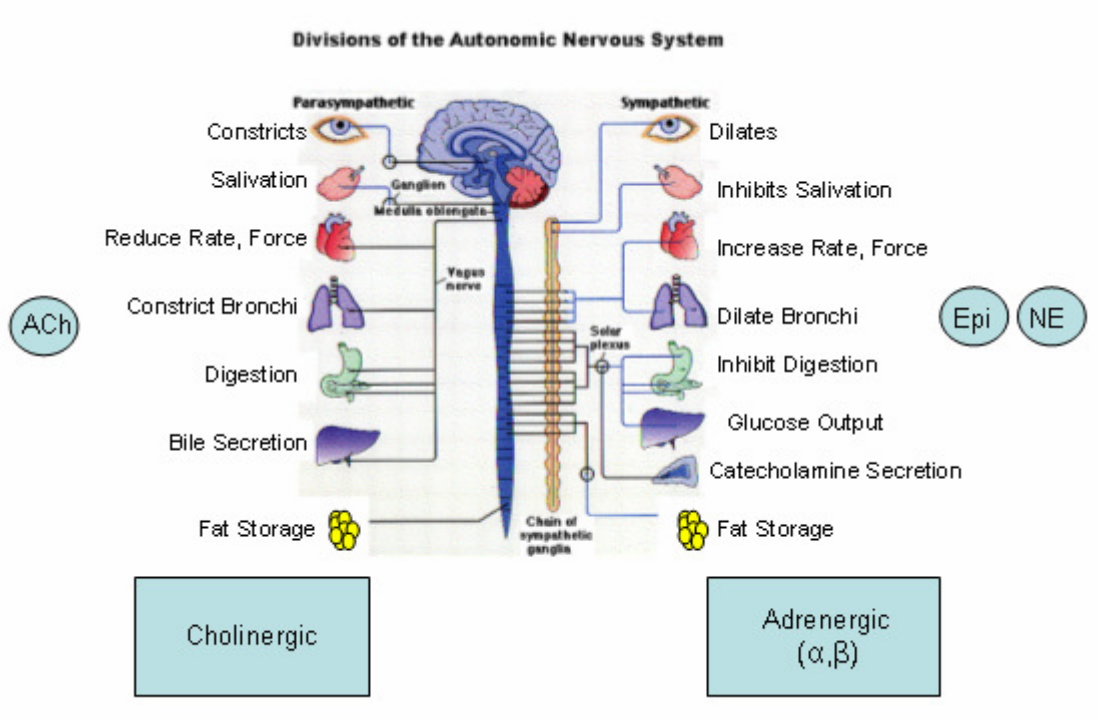

Figure 1.3: Illustration of the autonomic nervous system with its parasympathetic and sympathetic branches as well as specific target organs and physiological responses to stimulation. Parasympathetic signaling molecule acetylcholine (Ach) and cholinergic receptor family are indicated on the left. Sympathetic signalling molecules epinephrine (epi) and norepinephrine and the α- and β-adrenergic receptor family are indicated on the right. Generally, the stimulatory effects of the sympathetic branch are antagonized by the parasympathetic branch. (Adapted from www.users.rcn.com. (Accessed September 24, 2013).

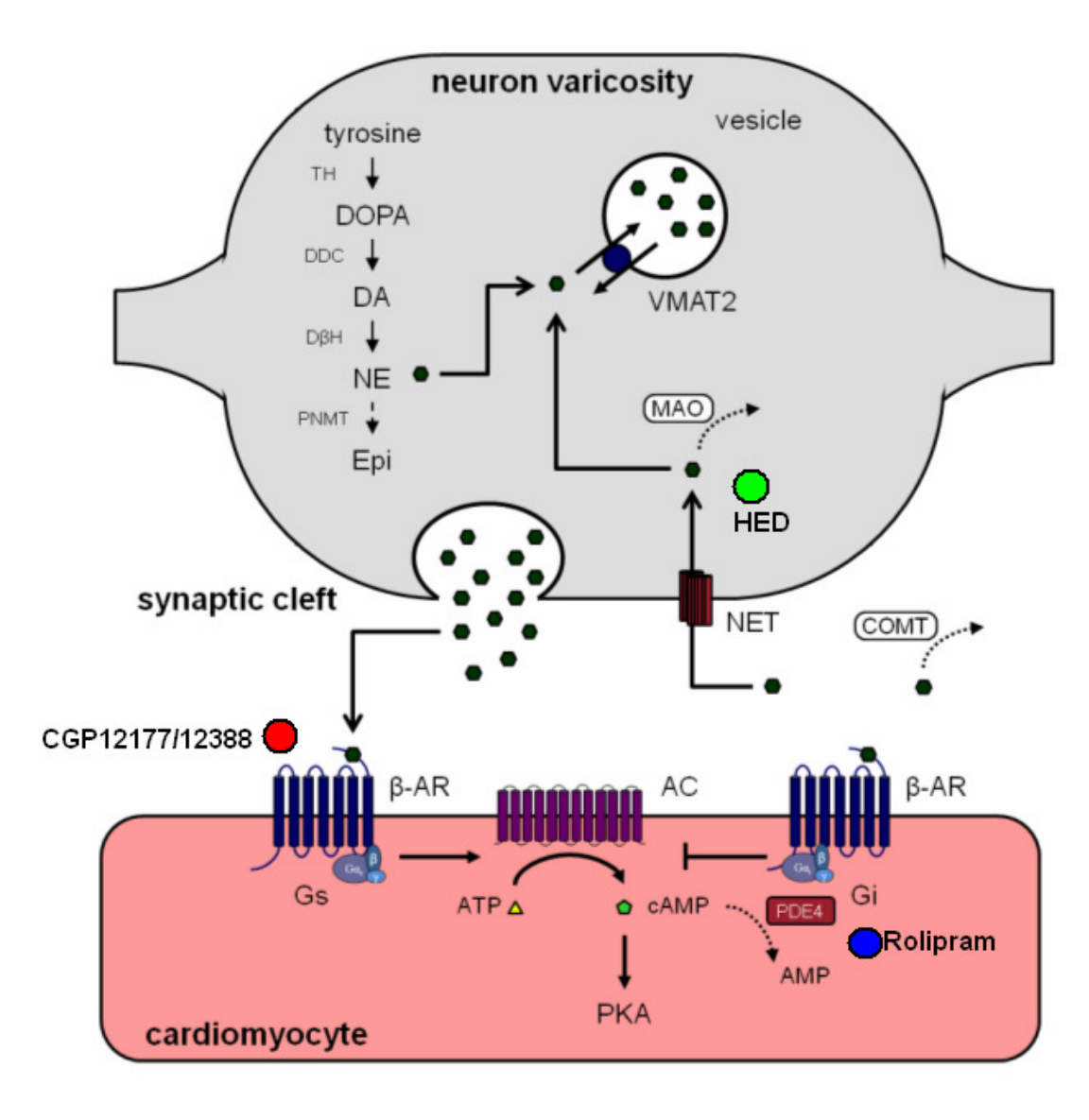

Figure 1.4: Pre-synaptic synthesis and release of NE ( ) into the synaptic cleft. Post-synaptic stimulation of β-AR and subsequent Gs-facilitated activation of AC, converting ATP to cAMP, stimulating PKA to increase intracellular calcium is indicated on the left. The potential mechanism of inhibitory Gi signalling inactivating AC, reducing cAMP and preventing PKA-mediated increases intracellular calcium is indicated on the right. Site of action of SNS PET tracers are within the cleft are indicated. Presynaptic [^{11}C]HED ( ) acting at NET, postsynaptic [^{11}C]-CGP12177 and 12388 ( ) acting at the β-AR, and intracellular *(R)*- [^{11}C] Rolipram ( ) acting at PDE4. (Adapted from Thackeray et. al. 2012.)

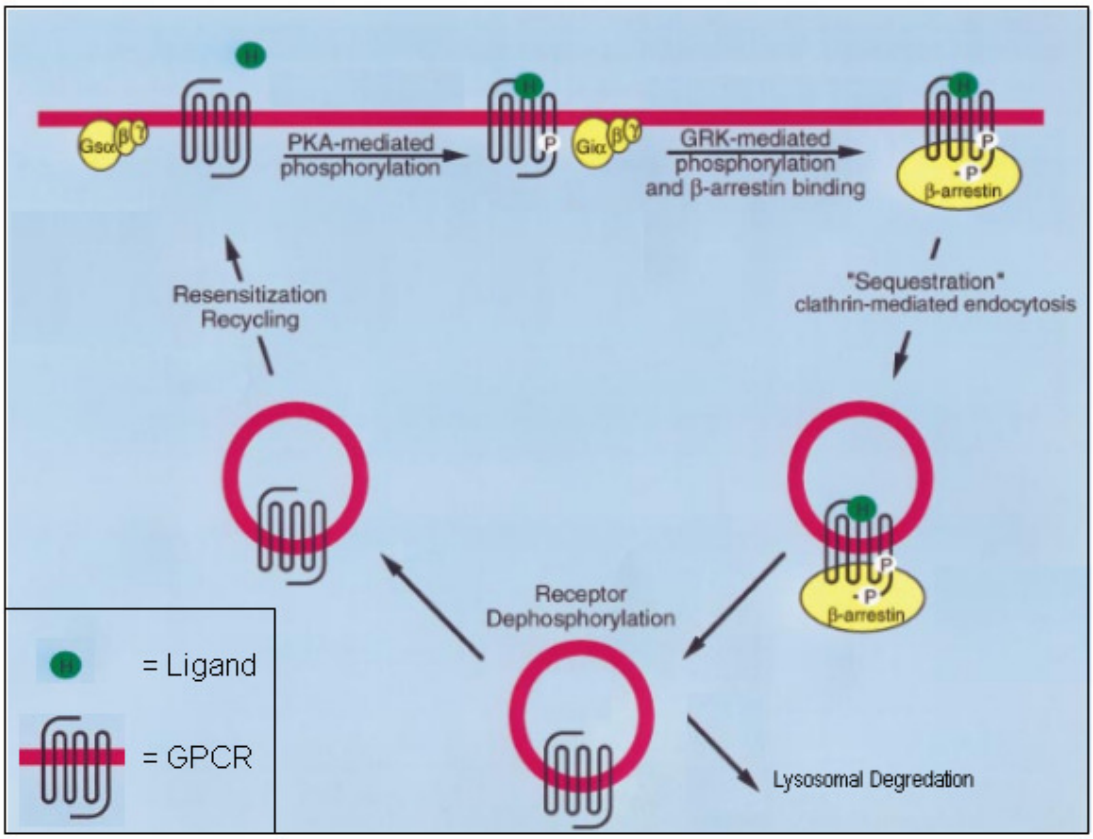

Figure 1.5: General illustration of receptor desensitization, internalization and recycling. Following non-specific or specific stimulation of a GPCR, activated PKA can mediate heterologous desensitization through receptor phosphorylation on the third intracellular loop. Agonist-specific stimulation can also induce receptor phosphorylation on the C-terminus by GRK. β-arrestin can bind GRK phosphorylated receptors to facilitate clathrin-mediated endocytosis. Internalized receptors are dephosphorylated and recycled back to the plasma membrane, or shuttled to lysosomes for degradation. (Adapted from Lefkowitz, 1998.)

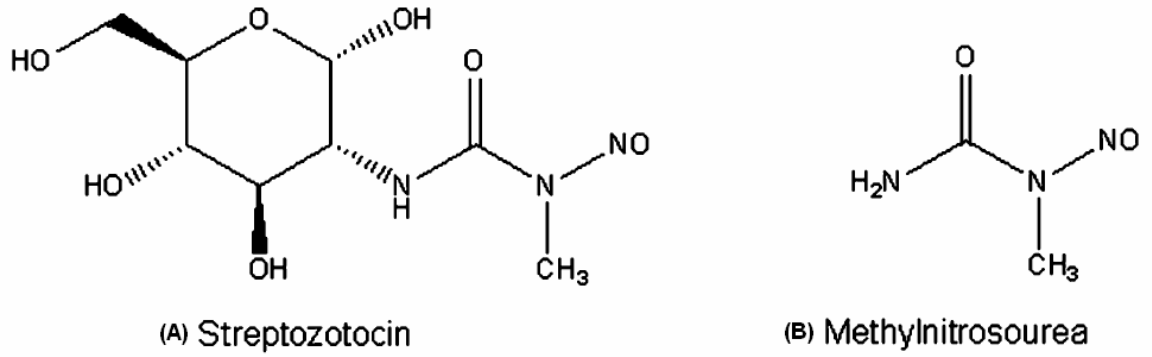

Figure 1.6: (A) The chemical structure of streptozotocin **(B)** and its methylnitrosourea moiety responsible for its apoptotic effects through DNA alkylation. (Adapted from Lenzen. 2008.)

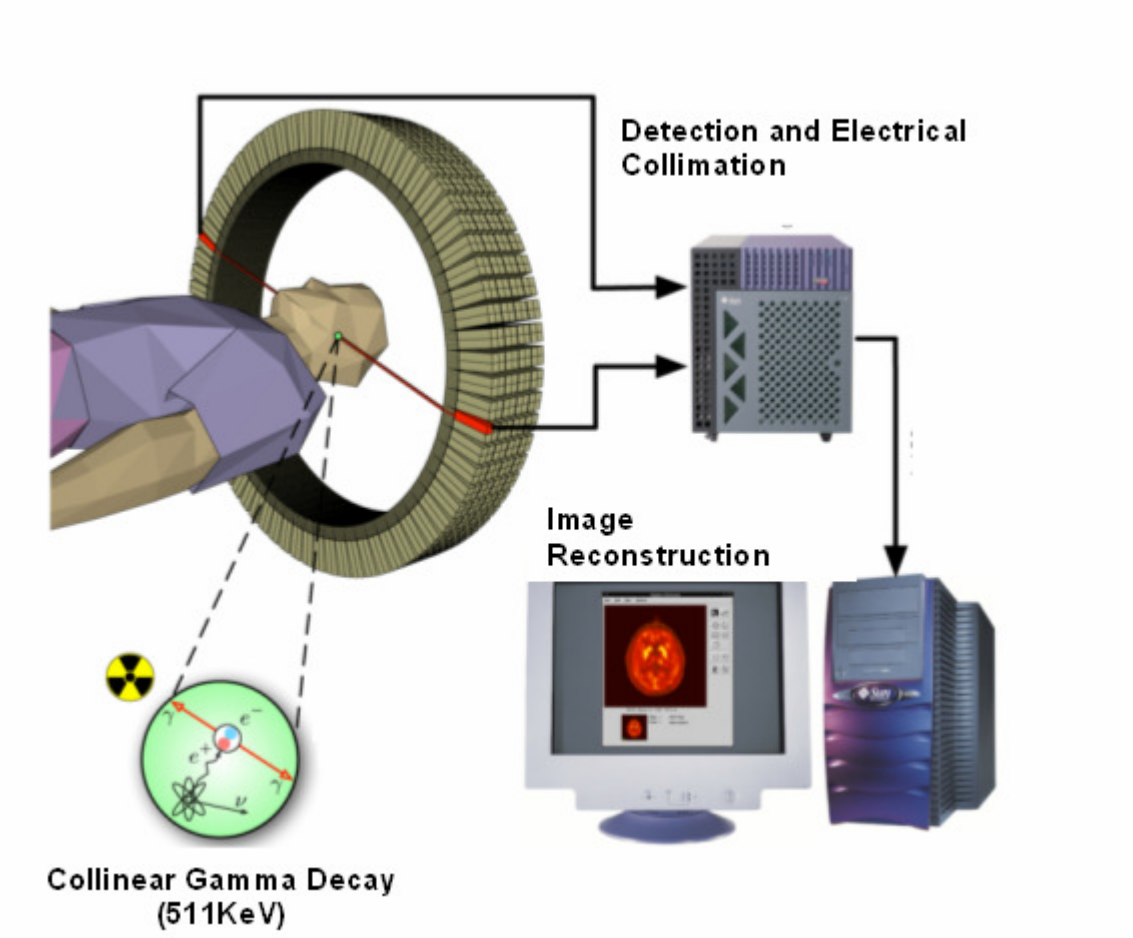

Figure 1.7: Overview of PET scan. PET tracers acting at a specific site undergo a positron decay that travels a short distance until colliding with an electron in an annihilation reaction, releasing two gamma rays (γ) traveling 180^{o} to one another. These gamma rays are detected by cameras surrounding the subject in 360^{o}. This information is reconstructed using the line of response of the gamma rays to determine where the radioisotope decay took place. This provides an *in vivo* image, and based on the PET tracer used, will indicate receptors density or metabolic processes like glucose uptake, relative to a colour scale of intensity, with brighter areas indicating increased tracer binding and darker areas a reduction in tracer binding. (Adapted from: www.jens-langner.de_ftp_MScThesis.)

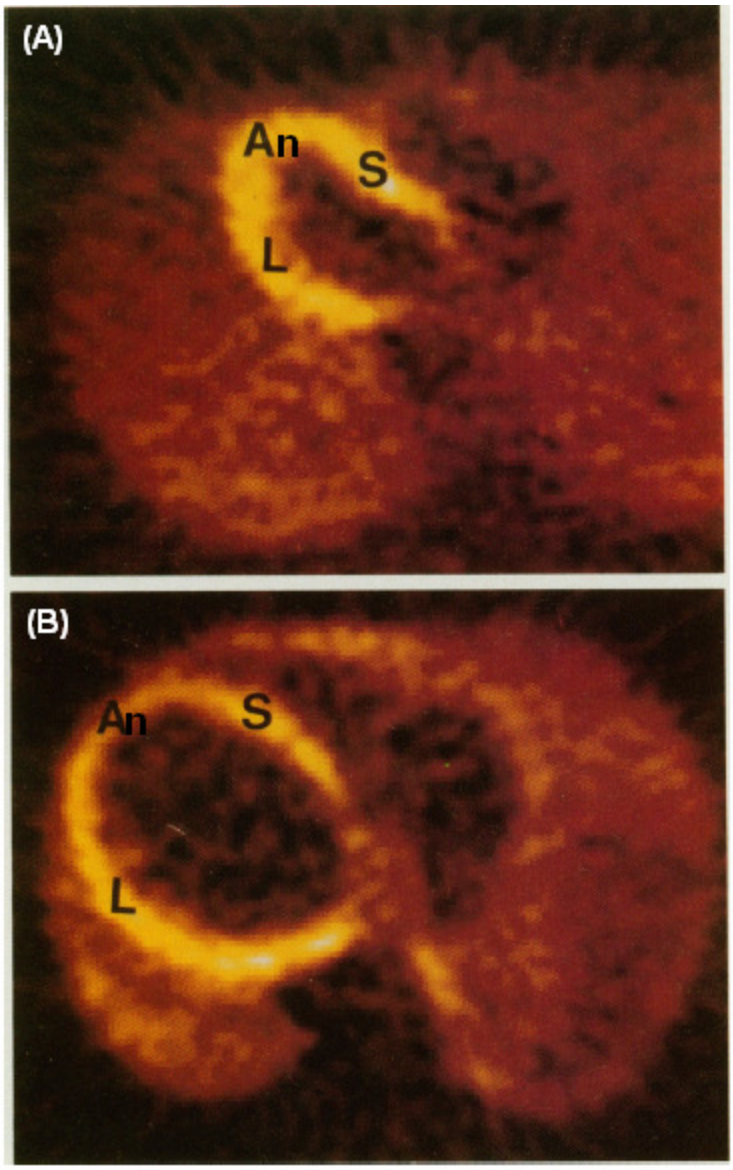

Figure 1.8: PET Colour Scale. Greater myocardial distribution of [^{11}C]-CGP12177 uptake obtained by PET in a normal subject (A) compared to a patient with left ventricular dysfunction related to idiopathic dilated cardiomyopathy (B). The left ventricular anterior (An), intraventricular septal (S), and left ventricular lateral (L) walls are indicated. (Adapted from Merlet et. al., 1993.)

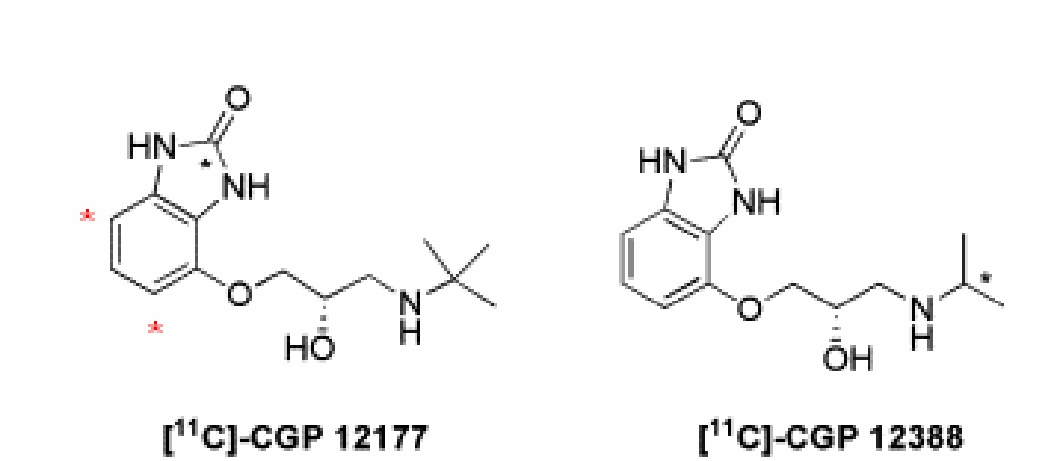

Figure 1.9: Structure of CGP12177 and CGP12388. Site for [^{11}C] and [^{3}H] radioisotope labels indicated by (*) and (*) respectively.

2) HYPOTHESIS AND OBJECTIVES

2.1)Hypothesis

The primary hypothesis is that elevated blood glucose levels and increased plasma and cardiac NE levels will lead to the downregulation of β-AR expression in the heart that will be identified with [^{3}H]-CGP12177, and will contribute to the deterioration of left ventricular function.

The secondary hypotheses are:

1. Elevated NE and reduced β-AR expression correlate with progressive diastolic dysfunction as estimated by echocardiography
2. *In vitro* measurements of NE and β-AR subtype expression correlate to *ex vivo* [^{3}H]-CGP12177 binding results.

2.2)Objectives

The primary objective of this study is to explore the development of cardiac SNS dysregulation at the level of the β-AR in two rat models of DM – high-fat fed moderate-dose STZ and ZDF – as compared to strain- and age-matched controls in two separate experiments. Measurements obtained serially by non-invasive techniques will be corroborated by terminal invasive procedures and correlated with *in vitro* data collected post-mortem.

Specific aims are:

2.2.1) High-Fat Fed STZ Hyperglycemic Rats

1. Assess [^{3}H]-CGP12177 retention in control and diabetic groups after treatment with insulin to normalize blood glucose.

2. To compare the effect of insulin treatment and decreased blood glucose on NE and β-AR density when provided early (1 week) or late (6 week) post-STZ.
3. Serial and non-invasive evaluation of left ventricular systolic and diastolic function using echocardiography.
4. Serially measure of blood glucose to identify hyperglycemia in diabetic groups and to evaluate the ability of insulin to reduce it.
5. Western blotting and high-performance liquid chromatography (HPLC) will be performed to corroborate [^{3}H]-CGP12177 findings by determining cardiac $\beta_{1\text{-}3}$-AR protein expression and by evaluating plasma and cardiac NE levels *in vitro*, respectively.
6. Commercially available kits will be used to measure specific metabolic markers, including insulin (ELISA), FFA (coulometric), leptin (RIA).

2.2.2) Zucker Rats

1. Assess [^{3}H]-CGP12177 retention in ZL, ZO and ZDF at 10 weeks of age, at the onset of overt hyperglycemia.
2. Assess [^{3}H]-CGP12177 retention in ZL, ZO and ZDF at 16 weeks of age, after the ZDF have undergone a sustained period of hyperglycemia.
3. Serial and non-invasive evaluation of left ventricular systolic and diastolic function using echocardiography.
4. Serially measure blood glucose and insulin to identify hyperglycemia in diabetic groups.

5. Western blotting and HPLC will be performed to corroborate [^{3}H]-CGP12177 findings by determining cardiac $\beta_{1\text{-}3}$-AR protein expression and by evaluating plasma and cardiac NE levels *in vitro*, respectively.
6. Commercially available kits will be used to measure specific metabolic markers in plasma including insulin (ELISA), FFA (ELISA), leptin (RIA).

3) MATERIALS AND METHODS

3.1) Animals, Drugs, and Materials

3.1.1) Animals

Animal experiments were conducted in accordance with the recommendations of the Canadian Council on Animal Care and with the approval of the Animal Care Committee of the University of Ottawa. Animals were housed in single or in pairs and maintained on a 12h light/dark cycle with *ad libitum* access to food and water.

3.1.1.1) High-Fat Fed STZ Hyperglycemic Rats

Male Sprague-Dawley rats (150-175g) were purchased from Charles River Canada (Montreal, QC). Upon arrival, animals were maintained on regular chow diet (Harlan Teklad 2019), consisting of 22% fat, 55% carbohydrate, and 23% protein per kcal for one week. Following this period of environmental adjustment, animals were switched to a high-fat diet (Research diets D12266B) consisting of 32% fat, 51% carbohydrate, 17% protein by kcal for 10 weeks (Thackeray et. al,. 2011a, Thackeray et al., 2011b)

3.1.1.2) Zucker Rats

Male ZL (+/+), ZO (*fa/fa*), and ZDF (*fa/fa*) were purchased from Charles River Canada (Montreal, QC), at 7 weeks of age. Upon arrival animals were maintained on Purina5008 (Purina Lab diets, St. Louis, MA, USA), consisting of 17% fat, 56% carbohydrate, 27% protein as recommended by the manufacturer and widely used in literature (Fu et. al., 2005; Jain et. al., 2010). Animals were given one week for environmental adjustment, and then maintained on the same diet from 8 to 10 weeks of

age or 8 to 16 weeks of age dependent on the predetermined experimental endpoint.

3.1.2) Drugs

[^{3}H]-CGP12177 (41.6 Ci/mmol) was purchased from Perkin Elmer Health Sciences (Toronto, ON, Canada). Sustain release insulin implants were purchased from Linshin Canada (Toronto, ON). STZ was purchased from Sigma Aldrich (Toronto, ON, Canada).

3.1.3) Materials

3.1.3.1) ex vivo Biodistribution

Scintillation fluid and tissue solubilizer were purchased from GE Healthcare (Montreal, QC, Canada). H_2O_2 (30%) was purchased from Columbus Chemical Industries (Colombus, WI, USA). Isopropanol (70%) was purchased from Ricca Chemical Company (Arlington, TX, USA). Glacial acetic Acid (99^+%) was purchased from Alfa Aesar (Ward Hill, MA, USA).

3.1.3.2) Western Blotting

Antibodies against rat β_1-AR (Ab3546-100, lot #720174) were purchased from AbCam (Cambridge, MA, USA) (Thackeray et. al., 2011a). Antibodies against β_2-AR (SC-570, lot #G2611) (Dincer et. al., 2001), β_3-AR (SC-1473, lot # B2411) (Dincer et. al., 2001), and GAPDH (SC-32233) (Thackeray et. al., 2011a) were purchased from Santa Cruz Biotechnologies (Santa Cruz, CA, USA). Secondary horseradish peroxidase conjugated IgG antibodies goat anti-rabbit (SC-2004), donkey anti-goat (SC-2020), and donkey anti-mouse (SC-2314) were also purchased from Santa Cruz Biotechnology.

3.1.3.3) in vitro Assays

Rat insulin and high range insulin ELISA kits were purchased from ALPCO

Biotechnologies (Salem, NH, USA). FFA coulometric quantification kit was purchased from Biovision Research Products (Mountain View, CA, USA). Rat Leptin RIA was purchased from EMD Millipore (Billerica, MA, USA).

3.1.3.4) HPLC

Alumina oxide (activity grade: super1, type WA-4: acid), ammonium formate, and L-(-)-norepinephrine bitartrate salt monohydrate (≥99%) were purchased from Sigma-Aldrich (Oakville, ON, Canada). Methanol, formic acid (98%), and 1-octanesulfonic acid sodium salt monohydrate were purchased from EMD (Mississauga, ON, Canada). Ethylenediamine tetraacetic acid (EDTA) was purchased from VWR (Radnor, PA, USA). UV detection was performed with Waters 486 Tunable Absorbance detector (Milford, MA, USA). NE was isolated using a Phenomenex Partisil SCX analytical column (250 x 4.60mm) (Torrance, CA, USA). Electrochemical detection was performed with ESA Coulochem III electrochemical detector (Sunnyvale, CA, USA).

3.2) Animal Models

3.2.1) High-Fat Fed STZ Hyperglycemic Rats

Male Sprague-Dawley rats were fed high fat diet for 2 weeks prior to STZ administration. Following this period of high fat feeding, animals were administered a single moderate intraperitoneal dose of STZ (45mg/kg) dissolved in 0.1M sodium citrate buffer, producing STZ hyperglycemic, or they received vehicle alone producing euglycemic STZ controls (Thackeray et al., 2011a, Thackeray et. al. 2013). STZ-hyperglycemic animals were stratified 1 week post-STZ, keeping those with a blood glucose >11mM as STZ-hyperglycemics, and removing those that were <11mM as euglycemics. To determine the temporal effects of glycemic control, some STZ-

hyperglycemic rats were administered subcutaneous sustain release insulin implants (4U/day) at either 1 week post-STZ (early insulin) or 6 weeks post-STZ (late insulin) to induce euglycemia until the terminal endpoint at 8 weeks post-STZ (Thackeray et. al., 2013).

Fed state blood glucose was measured weekly between 8-10am; body mass, and diet consumption were monitored twice per week for 10 weeks, from 2 weeks pre-STZ to 8 weeks post STZ. Fed state saphenous blood samples were collected prior to terminal biodistribution at 8 weeks post-STZ. Fed state trunk blood was collected at 8 weeks post STZ following decapitation for *in vitro* assays. Serial echocardiography was performed at 0, 6, and 8 weeks post-STZ to measure systolic and diastolic function. Separate groups excluded from the biodistribution were terminated by decapitation at the 8 week post-STZ terminal endpoint to provide non-tritiated cardiac samples for Western blotting and NE HPLC. Fasted samples were not collected for STZ groups as insulin treatment and the associated risk of hypoglycemia precluded fasting in this model. Animal model timeline is illustrated in Figure 3.1A.

3.2.2) Zucker Rats

Male ZL *(+/+)*, ZO *(fa/fa)*, and ZDF *(fa/fa)* were fed Purina 5008 from 8 weeks of age until the experimental endpoint at either10 or 16 weeks of age. Fed state blood glucose was measured weekly between 8-10am; body mass, and diet consumption was monitored twice per week from 8 weeks of age until 10 or 16 weeks of age. Fed state saphenous blood samples were collected at terminal endpoints at 10 or 16 weeks and prior to terminal endpoints. Prior to terminal biodistributions animals were fasted overnight to provide fasted state trunk blood for *in vitro* measurements at 10 and 16

weeks of age. Serial echocardiography was performed at 10 and 16 weeks of age to measure systolic and diastolic function. Separate groups excluded from the biodistribution were terminated by decapitation at 10 and 16 week terminal endpoints to provide non-tritiated cardiac samples for Western blotting and NE HPLC and fed state trunk blood samples for *in vitro* assays. Animal model timeline is illustrated in Figure 3.1B.

3.2.3) Characterization of Animal Models

3.2.3.1) Blood Glucose Measurements

Fed state blood glucose was measured weekly between 8 and 10am using the Accu-Chek Advantage blood glucose meter from Roche Diagnostics (Laval, QC, Canada) (Thackeray et. al., 2011a). Animals were restrained; the right leg was shaven then cleaned with isopropanol swabs to expose the saphenous vein, which was punctured using a 23G needle to draw blood.

3.2.3.2) Diet Consumption

Diet consumption per cage in kcal was calculated at the indicated time points by subtracting the mass of food remaining in the cage, from the mass of food that was provided, then dividing by the number of days elapsed, to determine g consumed per cage per day. If animals were housed in pairs, this number was divided by 2. Paired animals were always matched for treatment or genotype. To determine kcal per animal, the average daily mass of food in grams consumed by a rat was multiplied by the energy content of the diet. The energy content of the respective diets was 4.41 kcal/g for the high-fat diet (Research Diets D12266B) fed to the STZ rats and 4.15 kcal/g for the Purina 5008 diet fed to the Zucker rats (Equation 1).

$$DietConsum\ \ ption\ (kcal\ /\ day\ /\ Rat\ ) = \left[\frac{\left(\frac{Food\ \ \mathrm{Pr}\ ovided\ \ (g) - Food\ \ \mathrm{Re}\ maining\ \ (g)}{DaysElapse\ \ d} \right)}{RatsPerCag\ \ e} \right] xEnergyCon\ \ tent\ (kcal\ /\ g\ )$$

Equation 1: Diet consumption in kcal per day per rat.

3.2.3.3) NE Measurements by HPLC

NE measurements were performed on venous plasma samples and whole cardiac homogenates (Thackeray et al., 2011b). At indicated time points, blood samples were collected from restrained animals via the saphenous vein using EDTA-coated microvette vacuum tubes. Blood samples were spun at 2100xg for 5min to isolate plasma, which was aliquoted and stored at -80^{0}C until use. Hearts were extracted following decapitation and flash frozen in liquid nitrogen then hand-powdered and stored at -80^{o}C until use. Myocardial aliquots of ~100mg were homogenized in 80:20 ethanol:formic acid, centrifuged at 16 000 xg for 30min. Supernatant evaporated in a rotary evaporator and samples were reconstituted under 1ml 0.1 M formic acid and 1ml 1.5M TRIS 0.05M EDTA (pH=8.5), and filtered with PharmAssure 0.2µm filters (Pall Corporation, East Hills, NY, USA).

In a two pump column-switching approach (Figure 3.2), plasma or cardiac samples ~100µl were injected in solution with 250µl 0.1M formic Acid and 250µl 1.5M TRIS 0.05M EDTA (pH=8.5) and delivered by pump1 (Water 515 HPLC pump) (1ml/min) to an inline activated alumina oxide capture (Alltech Inline Refillable Guard Column, 2x2mm, Mandel, Guelph, ON, Canada) which binds NE. After a 10min wash with milliQ H_20 to elute macromolecules and clear TRIS buffer monitored by UV

detection (254nm), a valve switch reverses flow of pump 1 to waste and pump 2 (Waters 510 HPLC pump) (1ml/min) elutes the contents of the capture cartridge onto a cation exchange analytical HPLC column (Phenomenex Partisil SCX, 250 x 4.6mm, 10µm). Eluent is monitored by electrochemical detection (Coulochem III, ESA) with an applied voltage of +100mV across the guard cell, +250mV across the E1 analytical cell and +700mV across the active E2 analytical cell. Area under the curve is proportional to mass of NE (Wang et. al., 1998; Thackeray et. al., 2011b; Thackeray et al., 2013).

3.2.3.4) Insulin, Leptin, and FFA Quantification

Trunk blood was collected from animals following decapitation in EDTA-coated tubes and kept on ice. Blood samples were centrifuged at 2100 x g for 5min to isolate plasma, which was aliquoted and stored at -80^{o}C until use. Only fed state measurements were determined for STZ groups as insulin therapy and the subsequent risk of hypoglycemic hyperinsulinemic shock precluded fasting. In ZDF groups both fasted and fed state measurements were taken.

3.2.3.4.1) Insulin Measurements

Insulin was measured using commercially available Rat Insulin and High Range Insulin ELISA kits (ALPCO Biotechnologies, Salem, NH, USA). Rat Insulin ELISA kits were used for the quantification in STZ animals, while the High Range Insulin ELISA was used to quantify ZL, ZO, and ZDF animals due to hyperinsulinemia in ZO and ZDF groups.

3.2.3.4.1.1) Rat Insulin ELISA

STZ animals were quantified using Rat Insulin ELISA kits. Briefly standards, controls, and samples were added to 96-well microplate strips coated with a monoclonal antibody specific for insulin. Working Strength Conjugate buffer is then added and

incubated for 2h RT at 800rpm. Contents are decanted and wells are washed 6 times with 350ul of Working Strength Wash Buffer per well. TMB Substrate is added to each well and the plate is incubated for 15min at RT at 800rpm. After the addition of Stop solution, the plate is read at 450nm. A sigmoidal standard curve is constructed by comparing the standards of known concentration to their experimentally determined absorbance. Sample insulin is determined by extrapolation from this standard curve using the respective absorbencies (Thackeray et. al., 2011b; Thackeray et. al., 2013).

3.2.3.4.1.2) Rat High Range Insulin ELISA

Due to hyperinsulinemia in ZO and young ZDF animals that exceeded the quantifiable range of the rat insulin ELISA, rat high range insulin ELISA kits were employed to quantify insulin levels in the Zucker groups. Methods are similar to those of the Rat Insulin ELISA with the exception that the standards used to construct the standard curve having a larger range (Johnson et. al., 2007)

3.2.3.4.2) Leptin Measurements

Leptin was measured using a commercially available RIA (EMD Millipore, Billerica, MA, USA). Briefly, a fixed concentration of [^{125}I]-labeled leptin is mixed with the assay buffer, rat leptin antibody and standard or sample plasma over a three day procedure. After the addition of a precipitating reagent, tubes are centrifuged for 20min, 2500xg at 4^{o}C to obtain a pellet. All tubes are counted in a Cobra II series auto-gamma counting system (Packard Biosciences Company, Mississauga ON, Canada) for one minute. An inverse relationship exists between the labeled reference leptin binding and binding of unlabeled leptin in sample plasma, such that low radioactivity indicates high leptin concentration and vice versa. A standard curve is constructed using the provided

known standards and ng/ml of rat leptin in samples is calculated by extrapolation from this standard curve (Evans et. al., 2010)

3.2.3.4.3) FFA Measurements

FFA were measured using a commercially available coulometric quantification kit (Biovision Research Products, Mountain View, CA, USA). Briefly palmitic acid standards or sample plasma were mixed with assay buffer then ACS Reagent in a 96-well plate and incubated again at 37^{o}C for 30 min. Following incubation, Reaction Mix was added to each well and incubated at 37^{o}C for 30 min. Absorbance was measured at 570nm. Sample concentration was calculated by extrapolation from the standard curve (Thackeray et. al., 2011b; Thackeray et. al., 2013)

3.3) *Ex vivo* Biodistribution

Ex vivo biodistributions were performed as described elsewhere (Figure 3.3) (Thackeray et. al., 2011a). Briefly, restrained rats were injected via tail vein with 8μCi of [^{3}H]-CGP12177 in a 200μL bolus of saline then killed by decapitation 30min post-tracer injection. Hearts were rapidly excised and dissected into left and right atria, left and right ventricle free walls, and intraventricular septum. Trunk blood was also collected and after aliquoting 100 μl for liquid scintillation counting was spun at 2100 x g for 5min to acquire plasma.

Samples were processed for liquid scintillation counting. Briefly, ~100mg samples were incubated at 60^{o}C in 1ml quaternary ammonium hydroxide tissue solubilizer, except blood and plasma, shaking at 50^{o}C for 2h at 100rpm. The solubilized tissues were decolorized to prevent interference with scintillation detection by the addition of 400 μl isopropanol and 400 μl hydrogen peroxide then incubated at 50^{o}C for 30min shaking at 100rpm. For blood samples 600μl of both isopropanol and hydrogen

peroxide were added as it we previously determined larger volumes were required to decolorize blood samples (Parsa-Nezhad Master's Thesis, 2008). Finally, 10ml of scintillation fluid was added with 60µl of glacial acetic acid to neutralize chemiluminescence. Samples were counted using a Packard Tri-Carb liquid scintillation analyzer model 2100TR (Meriden, CT, USA), with 0.1% dilutions (0.008µCi) of the [^{3}H]-CGP12177 injected dose. Total tissue uptake was calculated using Equation 2 below (Lourenco et. al., 2006; Thackeray et. al, 2007; Thackeray et. al., 2011a).

$$TotalUptake = \frac{CPM\_\text{Recovered}/g\_Tissue}{CPM\_Injected/g\_BodyMass}$$

Equation 2: Calculation of total [^{3}H]-CGP12177 uptake in tissues in *ex-vivo* biodistributions.

3.4) Echocardiography

Echocardiography was performed at the indicated time points under light anesthesia (1-2% isoflurane) using the Vevo 770 high-resolution *in vivo* micro-imaging system (VisualSonis, Toronto, ON, Canada) with the RMV 716 probe at 23.5 MHz. Parasternal long axis views were recorded as sequencial ECG-gated M-mode sweeps (EKV-mode), generating two dimensional cines of the left ventricle. The endocardial and epicardial areas were traced on the two-dimentional parasternal long axis cine and used to calculate left ventricular volumes at end systole and end diastole. Calculations for %EF and HR were complete using VisualSonics software. Diastolic function was assessed using pulse-wave Doppler across the mitral valve from the apical four chamber view. Tracing E/A flow velocity and MVD time provided and indication of diastolic function (Thackeray et. al., 2011b; Thackeray et. al., 2013).

3.5) Western Blotting

To validate [^{3}H]-CGP12177 binding studies and to determine changes in β-AR subtypes, groups separate from biodistribution studies were maintained for Western blotting of β_1-AR, β_2-AR and β_3-AR. Rats were sacrificed by decapitation and hearts were rapidly removed and frozen in liquid nitrogen. Hearts were hand-powdered and stored at -80^{o}C until use. Total protein lysate was extracted by adding 5ml lysis buffer per gram of tissue and homogenizing. Triton X100 was added to a final concentration of 2% and tissue was left to lyse on ice for 1h then spun at 13 000 x g for 15min at 4^{o}C. The supernatant was aliquoted and stored at -80^{o}C, with 10µl being used for protein determination by bicinchoninic acid assay. Sodium dodecyl sulfate-polyacrylamide gels were performed with 8% reducing gels loading 15-20µg of protein per lane, run for approximately 1.5h at 150V. Transfer to an Immobilin-P PVDF transfer membrane (Millipore, Belirica, MA, USA) was performed at 40V, 0.12A at 4^{o}C overnight. Membranes were incubated for 1 to 3h, shaking at 100rpm at RT in primary antibody: rabbit anti-β_1-AR (1:1000 with 2% bovine serum albumin in TBST), rabbit anti-β_2-AR (1:200 with 2.5% skim milk in TBST), goat anti-β_3-AR (1:200 with 2% skim milk in TBST), and mouse anti-GAPDH (1:4000 in 2.5% skim milk TBST). Membranes were washed in TBST and incubated shaking at 100rpm for 1h in the respective horseradish peroxidase conjugated IgG secondary antibody: goat anti-rabbit (1:5000 in 2.5% skim milk TBST), donkey anti-goat (1:5000 in 2.5% skim milk TBST), or donkey anti-mouse (1:2000 in 2.5% skim milk TBST). Proteins were visualized using enhanced chemiluminescence substrate for Western blotting (Perkin Elmer Health Sciences, Toronto, ON, Canada) and the FluorChem 9900 Imaging System (AlphaInnotech/Cell

Biosciences, Santa Clara, CA), with exposure over 0.5 to 4min. Blots were analyzed using AlphaEase FC software with protein band densities normalized to GAPDH and expressed as a percentage of the controls (Thackeray et. al., 2011a).

3.6) Statistical Analysis

Statistical analyses were carried out using one-way analysis of variance (ANOVA) with Bonferroni's post hoc analysis. Significance was set as $p<0.05$. The n-values are indicated in corresponding figures and tables.

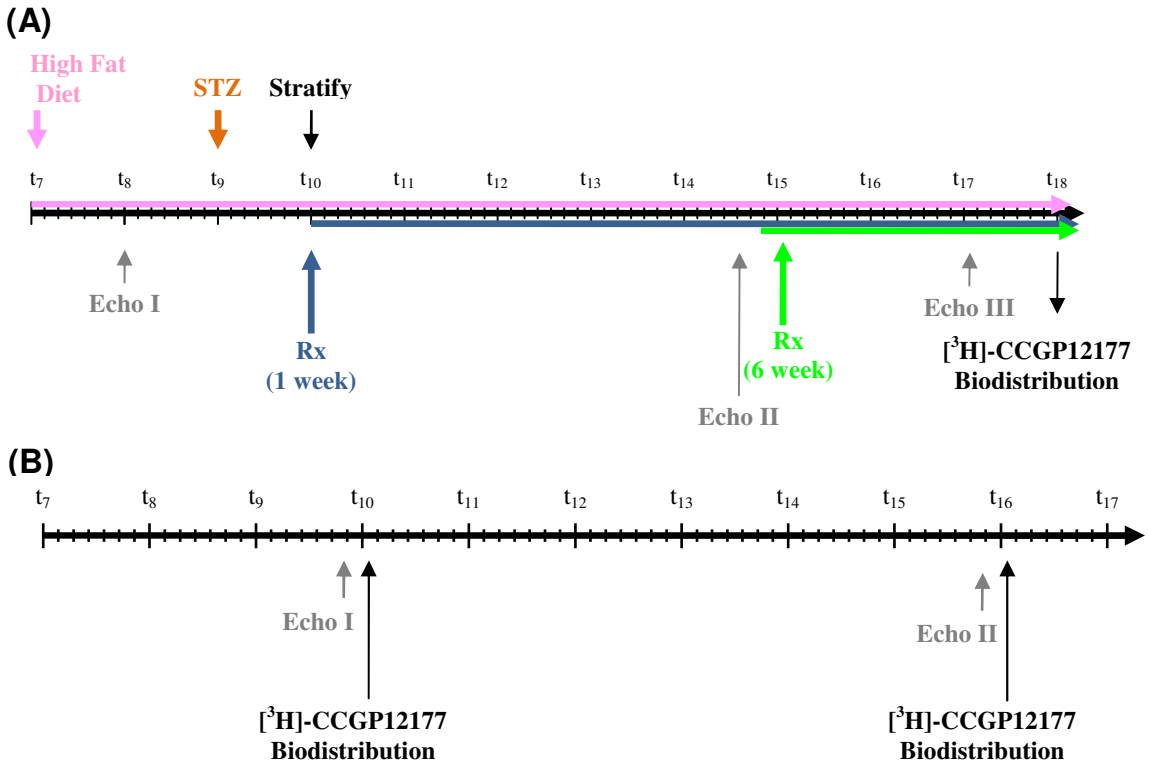

Figure 3.1: Experimental timelines. **(A)** STZ model over 10 weeks with 8 weeks of hyperglycemia, started at 7 weeks old and complete at 18 weeks of age. Echocardiography conducted at 0, 6, and 8 weeks post-STZ. [^{3}H]-CGP12177 biodistribution study performed at the terminal endpoint. **(B)** ZDF model of type-2 DM, started at 8 weeks old and completed at 16 weeks of age. Echocardiography conducted at 10 and 16 weeks of age prior to terminal biodistributions. [^{3}H]-CGP12177 biodistribution study was performed at 10 weeks and at 16 weeks of age.

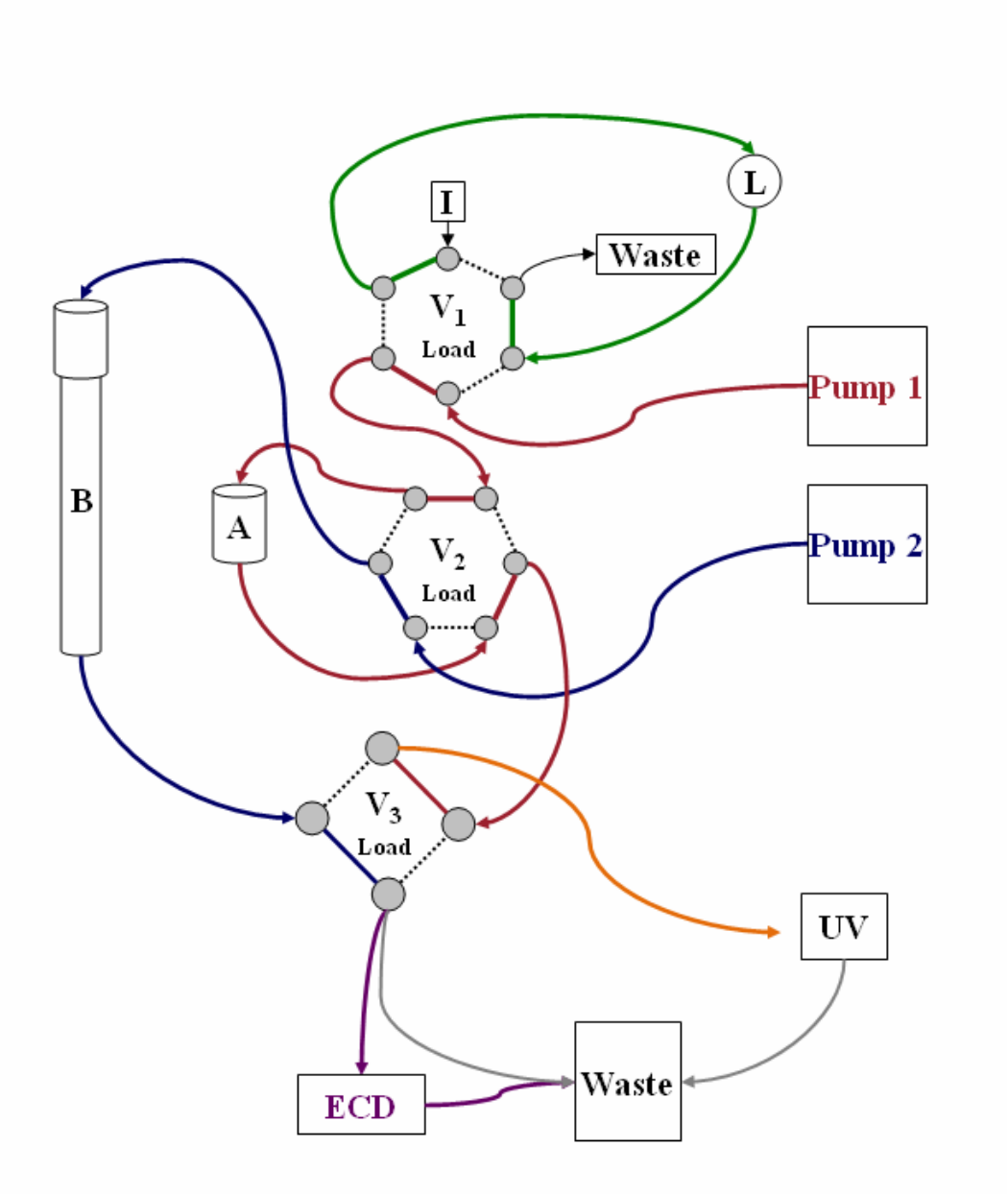

Figure 3.2: Setup of two pump column-switching approach for the quantification of plasma and cardiac NE. Sample is injected through the injection port (I) into the loop (L) prefilled with 1.5M TRIS 0.05M EDTA. Sample is delivered to the capture cartridge (A) containing activated alumina oxide, binding NE, and then the capture cartridge is washed with H_2O to remove any residual TRIS, as monitored by UV detection at 254nm. A valve switch at V_2 reverses the flow of pump 1 across the capture cartridge, eluting NE onto the Phenomenex Partisil SCX analytical column (B). Eluent from the analytical column is monitored by the Coulochem III electrochemical detector at +700mV for the detection of NE.

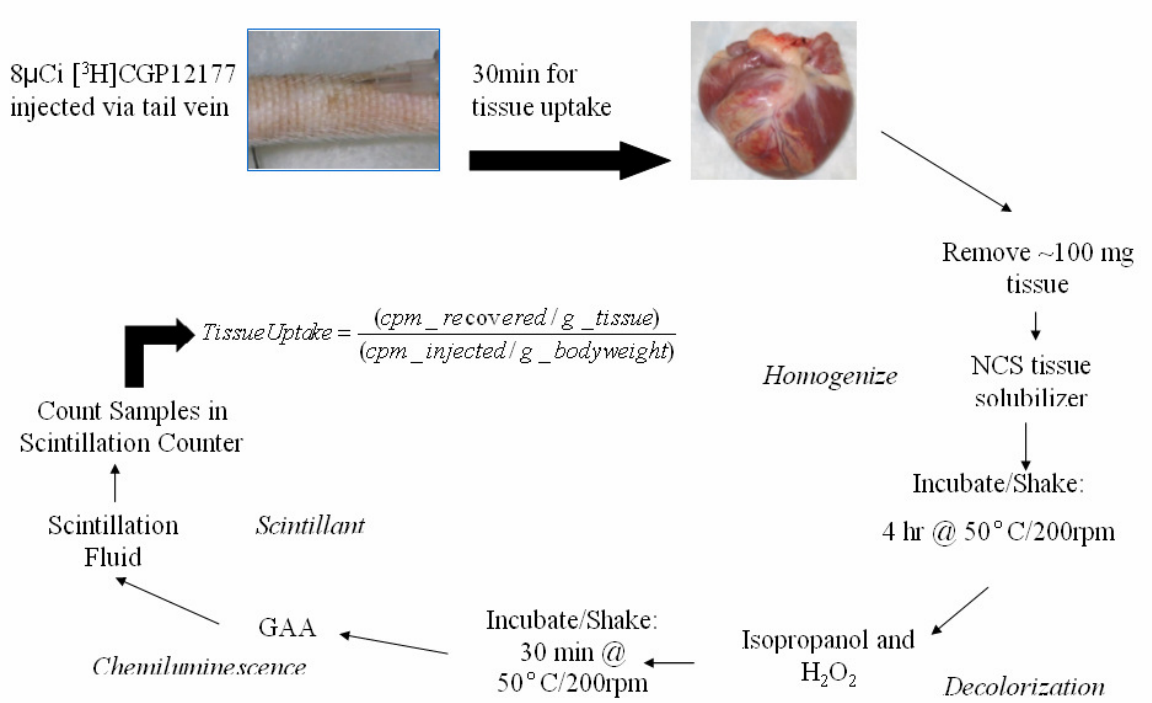

Figure 3.3: Overview of *ex vivo* biodistribution protocol. Animals are injected with 8µCi of [^{3}H]-CGP12177 and following termination by decapitation at 30min post-injection tissue is rapidly excised and dissected into ~100mg samples. Tissue solubilizer is added to all samples except plasma and blood, and samples are incubated for 4 hours at 50^{o}C shaking. Samples are decolorized by the addition of isopropanol and H_2O_2 and incubated again at 50^{o}C shaking for 30min. Glacial acetic acid is added to reduce pH and prevent chemiluminescence. Finally scintillation fluid is added and samples are counted in a Packard Tri-Carb liquid scintillation analyzer model 2100TR with 0.1% dilutions (0.008µCi) of the [^{3}H]-CGP12177 injected dose. Total uptake is normalized to tissue and body mass.

4) RESULTS

4.1) Animal Model Characteristics

4.1.1) High-Fat Fed STZ Hyperglycemic Rats

Blood glucose (Figure 4.1A) levels were similar between all groups for the initial 2 weeks of high fat feeding. One week after treatment with STZ, hyperglycemic, early insulin, and late insulin groups had significantly higher blood glucose than vehicle-treated controls. STZ-treated hyperglycemics maintained significantly elevated glucose relative to controls until termination at 8 weeks post STZ. In the early insulin group, insulin therapy 1 week post-STZ normalized blood glucose to control levels and remained significantly lower than hyperglycemics until 8 weeks. Late insulin treatment blood glucose was also normalized by insulin therapy at 6 weeks post-STZ and remained similar to controls and significantly lower than hyperglycemics until the experimental endpoint was reached at 8 weeks post-STZ.

Body mass (Figure 4.1B) was similar between the four groups for 2 weeks of high-fat feeding prior to STZ administration. At 1 week post-STZ, hyperglycemic, early insulin, and late insulin groups has significantly lower body mass than controls. STZ hyperglycemics body mass remained significantly lower than controls 8 weeks post-STZ. Following insulin therapy at 1 week post-STZ, the early insulin treatment increased in body mass, approaching controls levels and becoming significantly higher than hyperglycemic and late treatment groups by 2 weeks post-STZ until termination at 8 weeks post-STZ. Upon receiving insulin therapy at 6 weeks post-STZ, rats in the late treatment group began to gain mass; however late treatment rats still had a significantly lower mass than controls and early treatment until termination at 8 weeks.

Diet consumption (Figure 4.1C) was calculated at -2, 0, 6, and 8 weeks post-STZ. Diet consumption was similar between each group at -2 and 0 weeks. STZ hyperglycemics consumed significantly more than controls and early treatment at 6 and 8 weeks post-STZ. Early insulin treatment had a similar caloric intake to controls at 6 and 8 weeks post-STZ, significantly less than hyperglycemics. Late insulin treatment consumed significantly more calories that controls and early treatment at 6 weeks, but this significant increase in diet consumptions was lost by 8 weeks, after insulin therapy.

4.1.2)Zucker Rats

Starting at 8 weeks of age, ZDF rats had significantly higher blood glucose (Figure 4.2A) than ZL and ZO controls. ZDF blood glucose gradually increased, becoming overtly hyperglycemic by 10 weeks of age and beginning to plateau at 12 weeks around 20mM, increasing modestly to 21.84mM by 16 weeks of age. ZO animals remain euglycemic throughout with blood glucose similar to ZL animals at 16 weeks of age. It should also be noted that 4 of 16 ZDF rats kept to 16 weeks remained euglycemic and did not exhibit fed state hyperglycemia. These animals were excluded from the study.

ZDF and ZO animals had a significantly greater body mass (Figure 4.2B) than ZL controls starting at 8 weeks of age. ZO animals continued to increase in body mass until 16 weeks, remaining significantly greater in mass than ZL. ZDF animals initially increased in mass, but not at the same rate as ZO, becoming significantly lower in mass by 10 weeks of age. As ZDF body mass began to plateau it was no longer significantly greater than ZL by 12 weeks. ZDF began to show a trend toward a lower body mass than ZL by 14 weeks until 16 weeks but not significantly.

Diet consumption (Figure 4.2C) was assessed at 10 and 16 weeks in line with

terminal biodistributions. At 10 weeks, ZO and ZDF animals were consuming significantly more kcal each day than ZL controls. At 16 weeks, diet consumption by ZO remained significantly higher than ZL. ZDF diet consumption was significantly greater than both ZL and ZO controls at 16 weeks.

4.2) Plasma Metabolic Characteristics

4.2.1) High-Fat Fed STZ Hyperglycemic Rats

4.2.1.1)Fed State Insulin, FFA, and Leptin 8w post-STZ

Plasma insulin, FFA, and leptin levels were assessed at 8 weeks post-STZ (Table 4.1). Insulin levels were similar between vehicle treated controls, early insulin, and late insulin treatments. Insulin treatment groups showed an elevation relative to controls but this was not significant. STZ-treated hyperglycemics showed significantly lower insulin levels than controls and both early and late treatments.

Plasma FFA levels were significantly elevated in hyperglycemic animals compared to controls. Early and late insulin treatments had significantly lower FFA levels than hyperglycemics, but were not statistically different from vehicle-treated controls at 8 weeks post-STZ.

Plasma leptin was significantly reduced in hyperglycemic animals relative to controls at 8 weeks post-STZ. Early insulin treatments showed no difference compared to controls and were significantly greater than hyperglycemics. Late insulin treatments showed significantly reduced leptin levels relative to controls and significantly greater leptin levels than hyperglycemics. Late insulin treatments did not show a significant reduction in leptin compared to early, but leptin levels in the late group tended to be lower than the early.

4.2.1.2)NE levels

4.2.1.2.1)Plasma NE

At 8 weeks post-STZ, no significant differences were observed in plasma NE. Hyperglycemic and late treatment groups appear to exhibited elevated plasma NE relative to controls, but this is not significant. Early treatments had plasma NE similar to controls (Figure 4.3A).

4.2.1.4.2)Cardiac NE

Hyperglycemic animals exhibited elevated cardiac NE relative to controls at 8 weeks post-STZ. Early and late treatment cardiac NE was not significantly different than controls. (Figure 4.3B).

4.2.2)Zucker Rats

4.2.2.1) Fed State Insulin, FFA

Fed plasma Insulin and FFA (Table 4.2) were measured at 10 and 16 weeks. At 10 weeks, ZO animals exhibited an elevation in fed state insulin compared to ZL. ZDF animals also had a significant elevation in fed-state insulin levels compared to ZL at 10 weeks, but ZDF insulin levels were significantly lower than ZO. ZDF fed state insulin was similar to ZL at 16 weeks and remained much lower than ZO. Plasma FFA were also elevated in ZO animals at 10 and 16 weeks. Fed state plasma FFA in ZDF were not significantly different than ZL controls, but were significantly lower than ZO animals.

4.2.2.2) Fasted Insulin, FFA, and Leptin

Plasma insulin, FFA, and leptin (Table 4.3) were also measured at 10 and 16 weeks in fasted animals, showing some differences compared to fed state measurements. At 10 weeks, fasted plasma insulin was significantly higher in both ZO and ZDF animals. Unlike the fed state, ZO insulin only displayed a modest elevation and was not

significantly different than ZDF. By 16 weeks, fasted plasma insulin was increased in ZO animals staying significantly elevated compared to ZL. In ZDF animals, fasted plasma insulin decreased, and was no longer significantly different than ZL but significantly lower than ZO. Fasted plasma FFA were significantly elevated in ZO and ZDF animals at 10 and 16 weeks of age compared to ZL controls, and while similar at 10 weeks, 16 weeks FFA levels were significantly lower in ZDF animals compared to ZO. Fasted plasma leptin was significantly greater in ZO animals at 10 and 16 weeks. ZDF animals also showed increases in plasma leptin compared to ZL but ZDF levels remained significantly lower than ZO at both 10 and 16 weeks.

4.2.2.3)NE Levels

4.2.2.3.1)Plasma NE

At 10 and 16 weeks of age plasma NE was similar between all treatments. ZDF plasma NE appears to be increasing at16 weeks, but this did not reach significance. (Figure 4.4A)

4.2.2.3.2)Cardiac NE

No significant differences were observed in cardiac NE between groups at 10 or 16 weeks of age. (Figure 4.4B).

4.3)Myocardial [^{3}H]-CGP12177 Binding

4.3.1) High-Fat Fed STZ Hyperglycemic Rats 8 weeks post-STZ

[^{3}H]-CGP12177 binding was significantly reduced in STZ hyperglycemic animals in all myocardial regions (33-38% compared to controls) (Figure 4.5). In early insulin and late insulin groups, [^{3}H]-CGP12177 binding was similar to controls and significantly greater than hyperglycemic animals, with the exception of the intraventricular septum in the early insulin group which did not show significance compared to hyperglycemics

(p=0.081). No differences in blood or plasma [^{3}H]-CGP12177 uptake were observed.

4.3.2)Zucker Rats at 10 and 16 weeks of age

[^{3}H]-CGP12177 uptake was assessed in ZL, ZO, and ZDF animals at 10 and 16 weeks of age (Figure 4.6). At 10 weeks, myocardial regions had similar [^{3}H]-CGP12177 uptake in ZL, ZO, and ZDF animals. ZO animals showed some elevations in [^{3}H]-CGP12177 uptake but these were not significant, except in the intraventricular septum, where ZO [^{3}H]-CGP12177 uptake was significantly greater than ZL animals, but not than ZDF (p=0.063). Small but significant increases were observed in ZO and ZDF blood and plasma relative to ZL.

At 16 weeks, ZO uptake was significantly increased in all myocardial regions relative to ZL and ZDF. Conversely, ZDF animals had a significant reduction in [^{3}H]-CGP12177 uptake in all myocardial regions of ~16-25% relative to ZL and ~36-42% relative to ZO. Small but significant increases were observed in ZO and ZDF blood compared to ZL. ZDF plasma also had a small but significant decrease in uptake relative to both ZL and ZO controls.

4.4)Western Blotting β-AR Subtypes

4.4.1)STZ β-AR Subtypes

Western blotting for β-AR subtypes provide insight into how these subtypes may be affected by DM and hyperglycemia, and giving some context in which to interpret [^{3}H]-CGP12177 binding to myocardial β-AR (Figure 4.7). At 8 weeks post-STZ, hyperglycemic animals showed a significant reduction in β_1-AR of 22.5±16.3% relative to controls. Early insulin and late insulin groups had significantly higher β_1-AR expression than hyperglycemic animals with percent control expression of 98.4±14.1%

and 99.3±9.9% respectively. β_2-AR expression was also reduced in hyperglycemic animals, showing 65.1±15.9% expression relative to controls. Early insulin animals had a slight elevation in β_2-AR expression, which was not significant, of 112.8±16.6%. Early insulin β_2-AR expression was significantly higher than hyperglycemics. Late insulin β_2-AR expression was similar to STZ hyperglycemics, 66.7±22.0% relative to controls, significantly lower than control and early insulin groups. β_3-AR expression was not significantly different between any groups.

4.4.2)Zucker Rats β-AR Subtypes

4.4.2.1)10 week Measurements

Western blotting at 10 weeks of age (Figure 4.8) showed no difference in β_1-AR expression between ZL, ZO, and ZDF animals. No significant difference was observed between ZL and ZO β_2-AR, but ZDF had an expression of 79.2±9.7 relative to controls, significantly lower than controls, but not compared to ZO. β_3-AR was similar between groups.

4.4.2.2)16 week Measurements

Western blots performed at 16 weeks of age (Figure 4.9) revealed a significant reduction in β_1-AR in ZDF animals, with an expression of 72.4±13.7% relative to ZL. ZDF were not significantly reduced compared to ZO animals (p=0.072), who had an expression relative to ZL controls of 89.1±7.89. β_2-AR expression was not reduced in ZO with expressions of 88.3±9.27%, but was reduced in ZDF, with an expression of 63.0±14.7% relative to ZL. No differences were observed in β_3-AR expression.

4.5)Echocardiography

4.5.1) High-Fat Fed STZ Hyperglycemic Rats

At 0 weeks, prior to STZ treatment, measurements of systolic and diastolic function by echocardiography were similar between control, hyperglycemic, early insulin and late insulin treatments (Figure 4.10). At 6 weeks post-STZ, significant reductions in HR were evident in hyperglycemic and late insulin groups, compared to vehicle-treated controls and early insulin therapy. No changes were evident in %EF, mitral E/A, or MVD. MVD appears prolonged in both hyperglycemic and late insulin at 6 weeks, but it is not significant. At 8 weeks, HR remained significantly slower in hyperglycemic and late insulin groups compared to controls; %EF and mitral E/A were similar between all groups. MVD was more prolonged in hyperglycemics and significantly slower than controls. Late insulin MVD was not significantly different from other groups.

4.5.2)Zucker Rats

At 10 weeks of age, no differences in HR, %EF, mitral E/A, or MVD were evident between ZL and ZO animals (Figure 4.11). ZDF animals had a significantly slower HR than ZL animals but not than ZO. At 16 weeks, ZL and ZO animals showed no differences in echocardiographic measurements. A small but insignificant increase was observed in ZO %EF compared to ZL. ZDF animals showed a reduction in HR compared to 10 week values, however this reduction was no longer significant at 16 weeks relative to ZL and ZO due to high standard deviation. ZDF %EF was reduced at 16 weeks compared to ZO, but not ZL animals

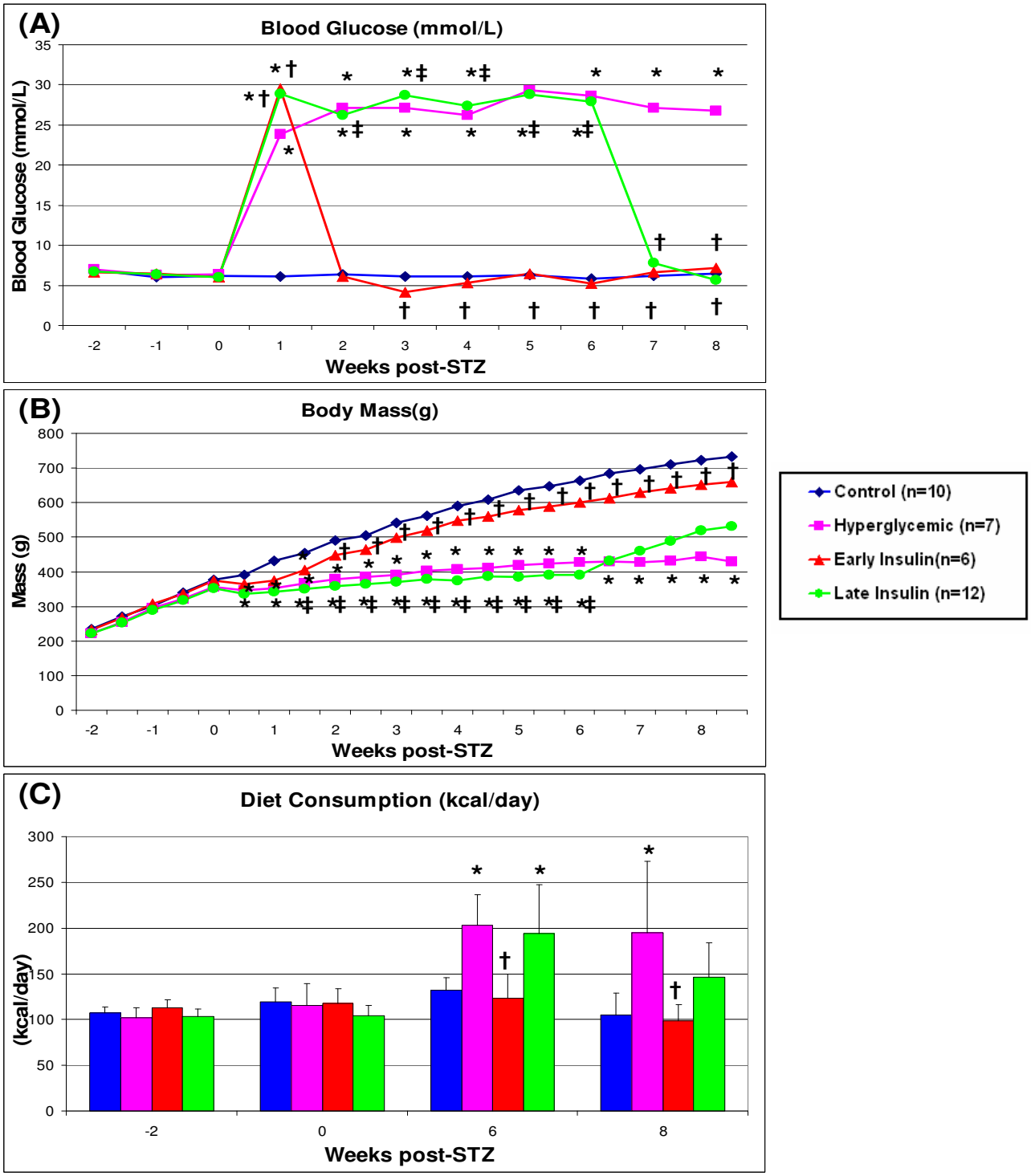

Figure 4.1: Animal Model Characteristics of STZ rats: Blood glucose **(A)**, body mass **(B)**, and diet consumption **(C)** in vehicle-treated controls and STZ-treated hyperglycemic, early insulin, and late insulin groups over 10 weeks from 2 weeks prior to STZ treatment until 8 weeks post-STZ. *p<0.05 to controls, †p<0.05 to hyperglycemic, and ‡p<0.05 to early insulin. One-way ANOVA, Bonferroni post-hoc.

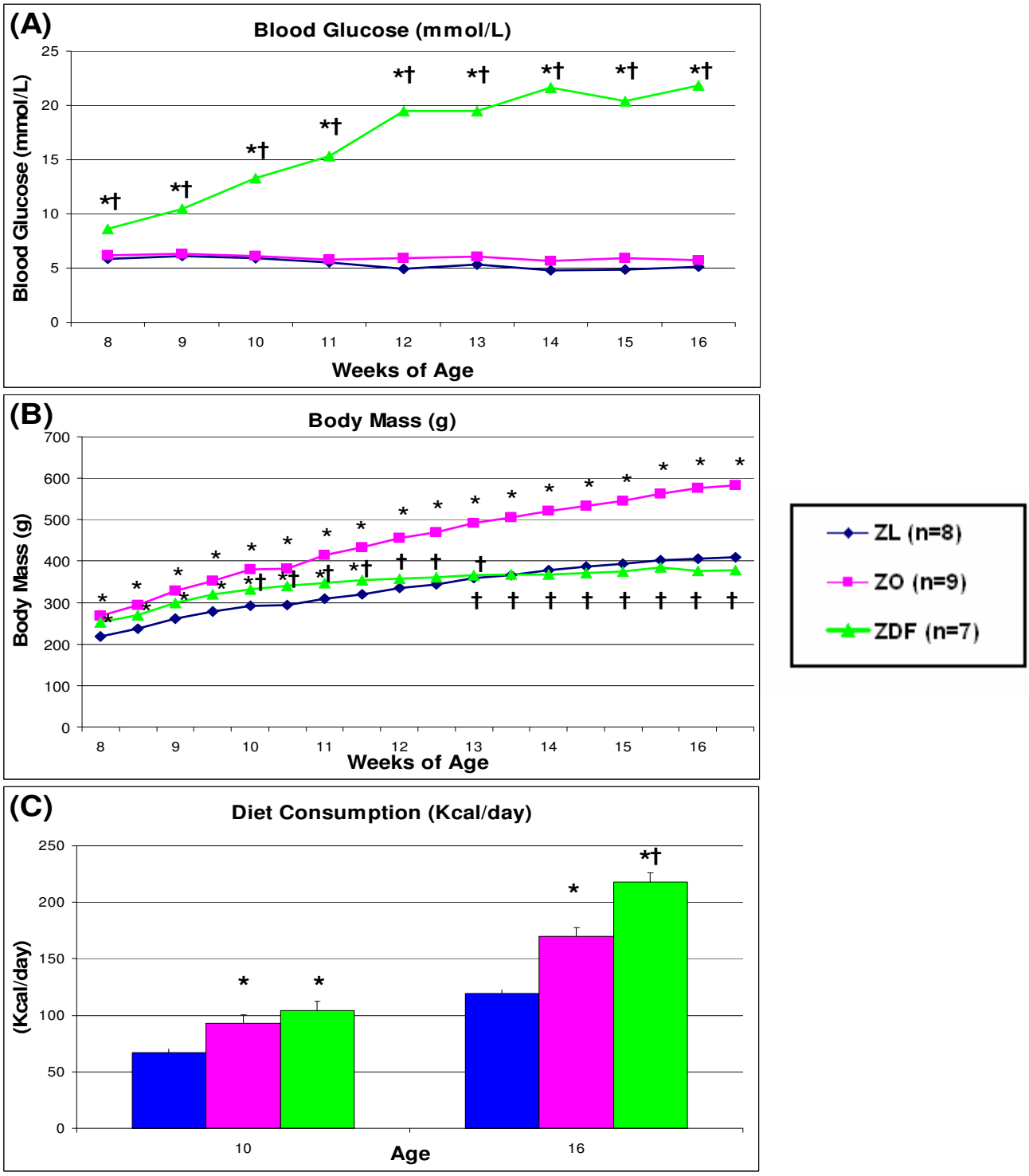

Figure 4.2: Animal Model Characteristics of ZDF rats: Blood glucose (**A**), body mass (**B**), and diet consumption (**C**) in ZL, ZO, and ZDF animals between 8 and 16 weeks of age. *p<0.05 to ZL, †p<0.05 to ZO. One-way ANOVA, Bonferroni post-hoc.

Table 4.1: Fed-state insulin, FFA, and leptin 8 weeks post-STZ			
Group	**Insulin (ng/ml)**	**FFA (mmol /L)**	**Leptin (ng/ml)**
Control	2.72 ± 0.82 (n=9)	0.103 ± 0.06 (n=6)	24.52 ± 9.5 (n=6)
Hyperglycemic	0.11 ± 0.10 * (n=6)	0.351 ± 0.25* (n=6)	1.89 ± 0.46* (n=6)
Early Insulin	3.8 ± 1.16 † (n=9)	0.03 ± 0.02† (n=7)	24.52 ± 8.71† (n=6)
Late Insulin	3.21 ± 1.21 † (n=12)	0.067 ± 0.02† (n=6)	12.83 ± 4.53 *† (n=6)

*p<0.05 to controls, †p<0.05 to hyperglycemic, and ‡p<0.05 to early insulin. One-way ANOVA, Bonferroni post-hoc.

Table 4.2: Zucker Fed-state insulin and FFA levels at 10 and 16 weeks of Age				
Group	**Insulin (ng/ml)**		**FFA (mmol/L)**	
Age	10 weeks	16 weeks	10 weeks	16 weeks
ZL (n=3)	1.94 ± 0.29	3.15 ± 0.94	0.12±0.05	0.16±0.06
ZO (n=3)	41.37 ± 4.02*	40.45 ± 8.56*	0.90±0.25*	1.90±0.60*
ZDF (n=3)	6.89 ± 1.06*†	2.57 ± 0.42†	0.050±0.04†	0.08±0.05†

*p<0.05 to ZL and †p<0.05 to ZO. One-way ANOVA, Bonferroni post-hoc.

Table 4.3: Zucker Fasted-state insulin and FFA levels at 10 and 16 weeks of Age						
Group	**Insulin (ng/ml)**		**FFA (mmol/L)**		**Leptin (ng/ml)**	
Age	10 weeks	16 weeks	10 weeks	16 weeks	10 weeks	16 weeks
ZL (n=5)	1.48 ± 0.29	1.57 ± 0.32	0.08 ± 0.02	0.06 ± 0.01	2.55 ± 1.09	5.28 ± 0.55
ZO (n=5)	4.09 ± 0.84*	11.29 ± 4.93*	0.43 ± 0.07*	0.39 ± 0.07*	46 ± 4.47*	48.69 ± 6.09*
ZDF (n=5)	4.06 ± 1.39*	2.29 ± 0.43†	0.34 ± 0.12*	0.27 ±0.04*†	29.8 ± 4.22*†	30.4 ± 13.89*†

*p<0.05 to ZL and †p<0.05 to ZO. One-way ANOVA, Bonferroni post-hoc.

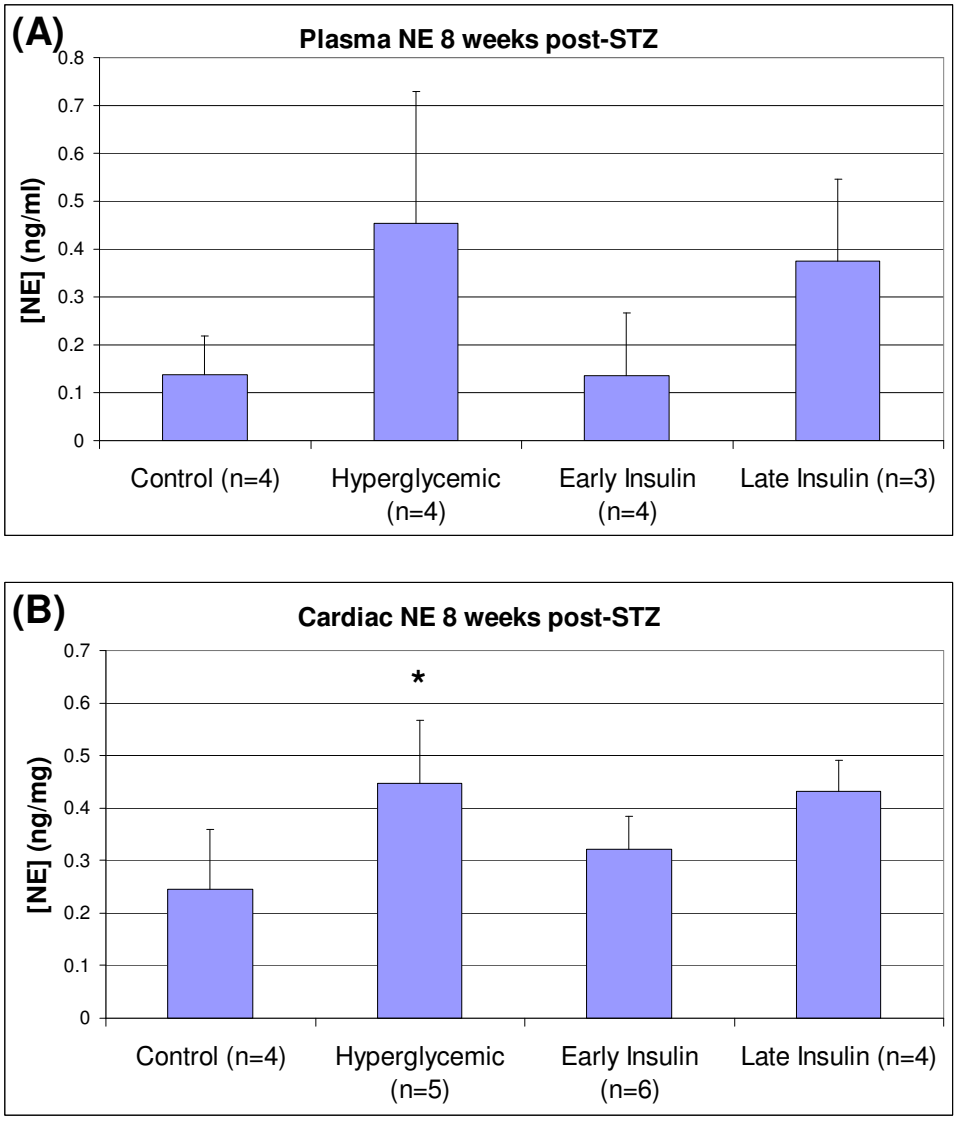

Figure 4.3: Plasma (A) and cardiac (B) NE measurements, 8 weeks post-STZ in vehicle-treated controls and STZ hyperglycemic, early insulin and late insulin. *$p<0.05$ to controls, †$p<0.05$ to hyperglycemic, and ‡$p<0.05$ to early insulin. One-way ANOVA, Bonferroni post-hoc.

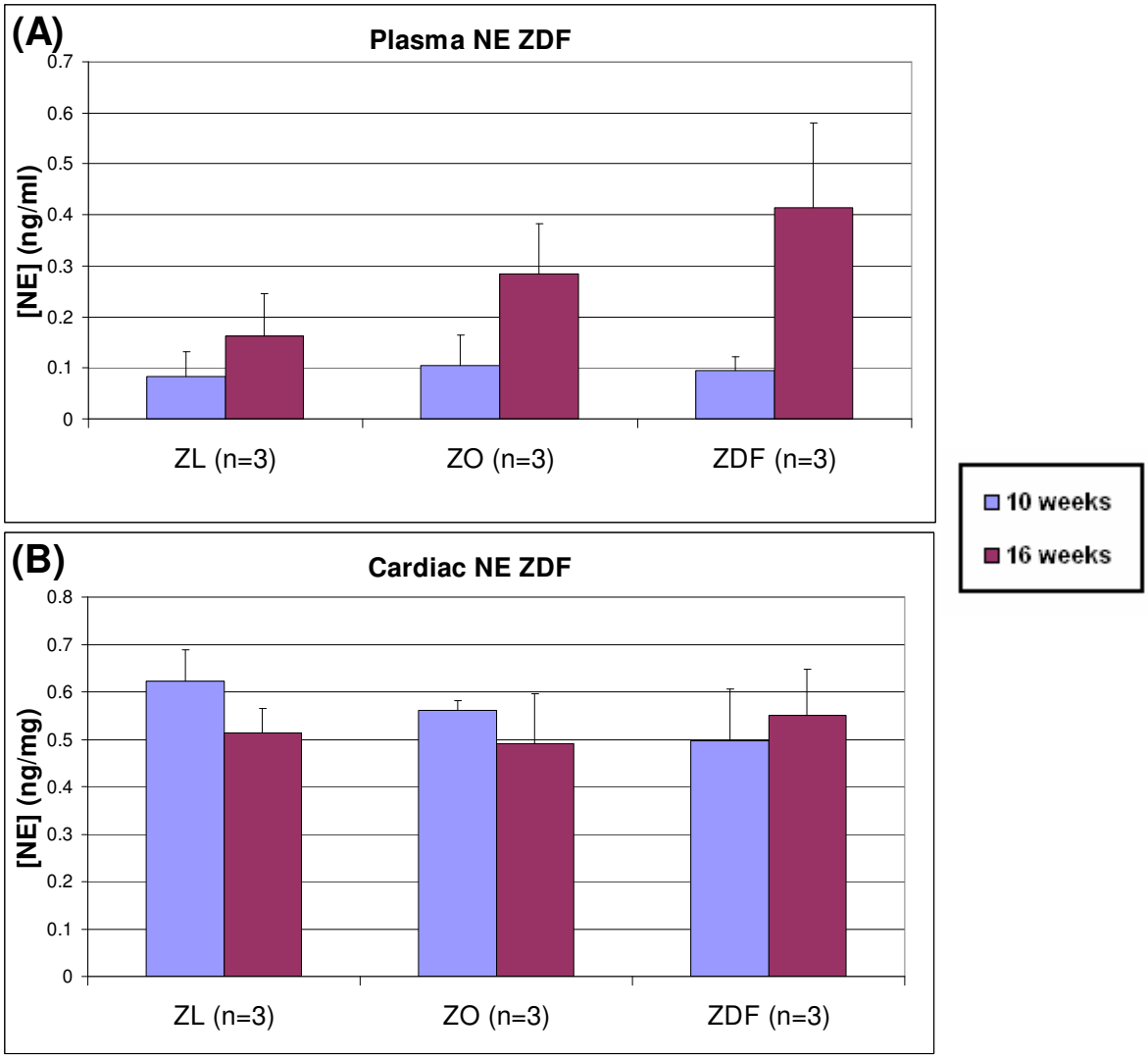

Figure 4.4: Plasma (A) and cardiac (B) NE measurements at 10 and 16 weeks of age in ZL, ZO, and ZDF. One-way ANOVA, Bonferroni post-hoc.*$p<0.05$ to ZL and †$p<0.05$ to ZO, age matched.

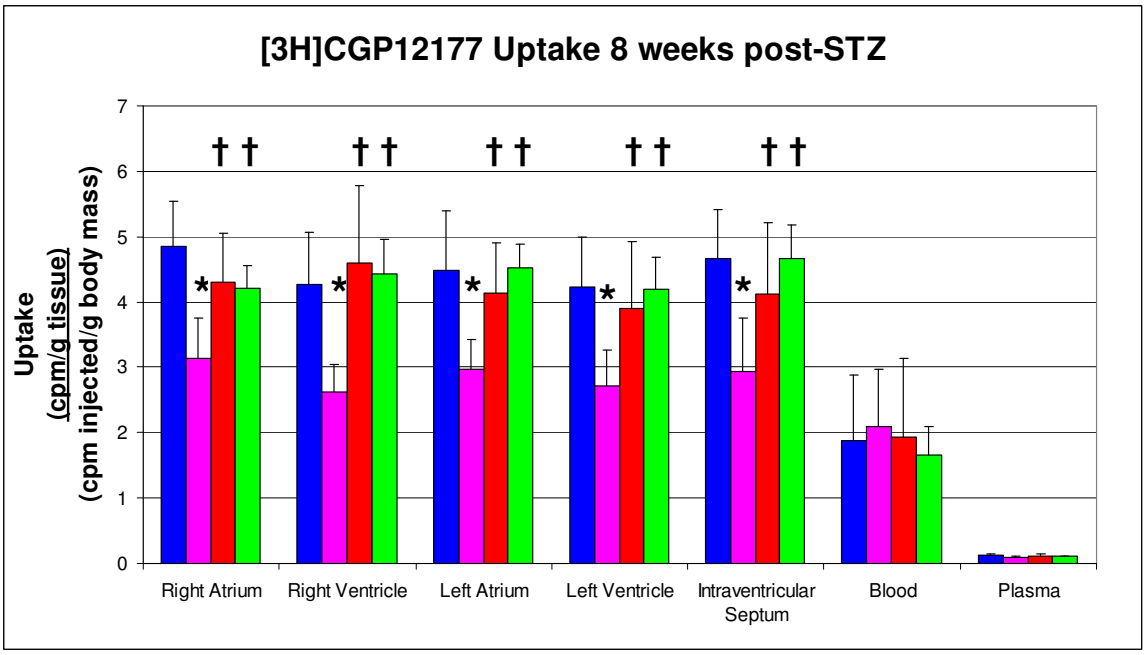

Figure 4.5 : Uptake of [^{3}H]-GGP12177 in different myocardial regions, blood, and plasma, 8 weeks post-STZ in vehicle-treated controls and STZ hyperglycemic, early insulin and late insulin. Uptake expressed as [(cpm / g tissue) / (cpm injected / g body mass)]. *p<0.05 to controls, †p<0.05 to hyperglycemic, and ‡p<0.05 to early insulin. One-way ANOVA, Bonferroni post-hoc.

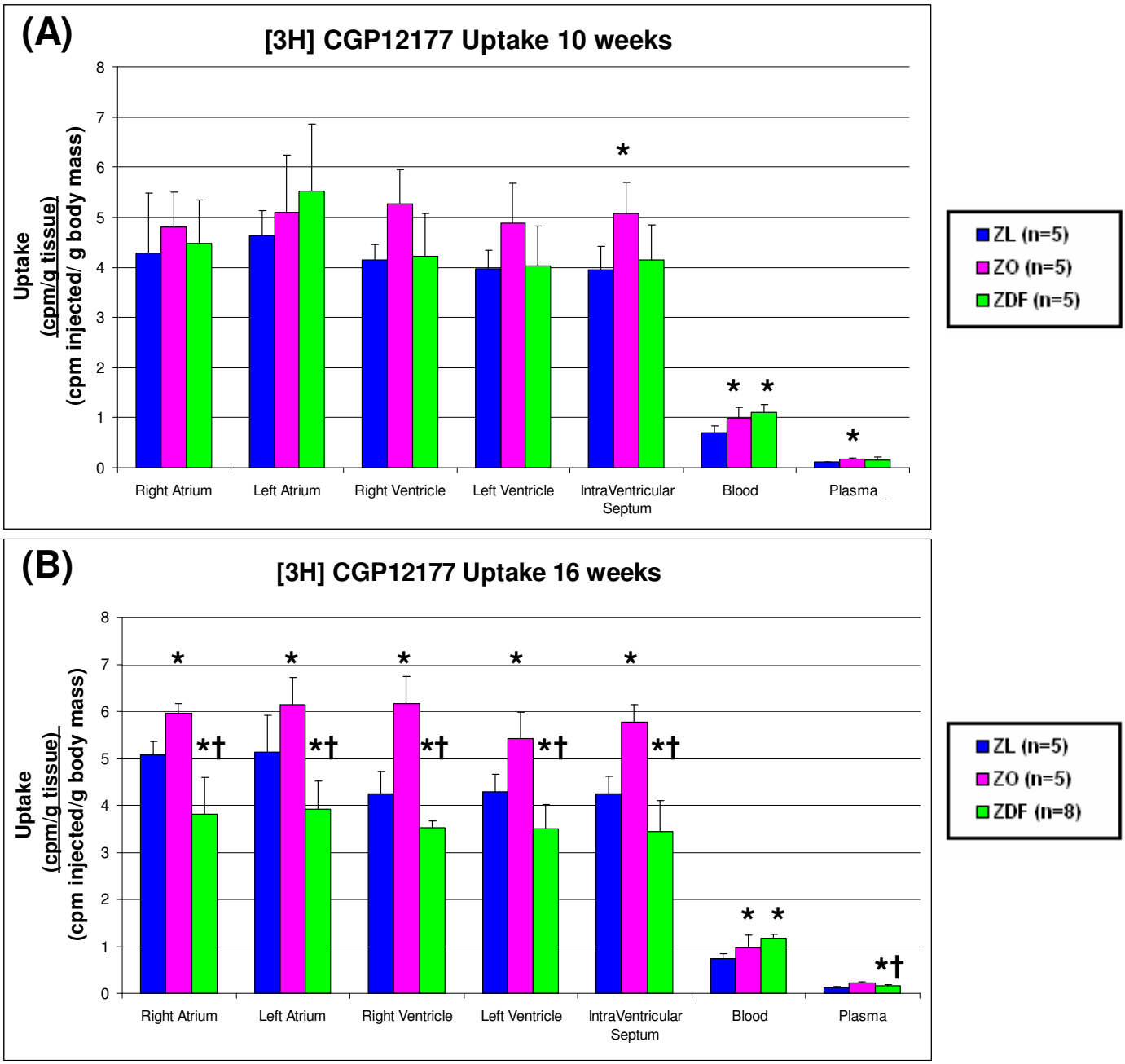

Figure 4.6: Uptake of [^{3}H]-GGP12177 in different myocardial regions, blood, and plasma, at 10 and 16 weeks of age in ZL, ZO, and ZDF. Uptake expressed as [(cpm / g tissue) /(cpm injected / g body mass)]. *p<0.05 to ZL and †p<0.05 to ZO. One-way ANOVA, Bonferroni post-hoc.

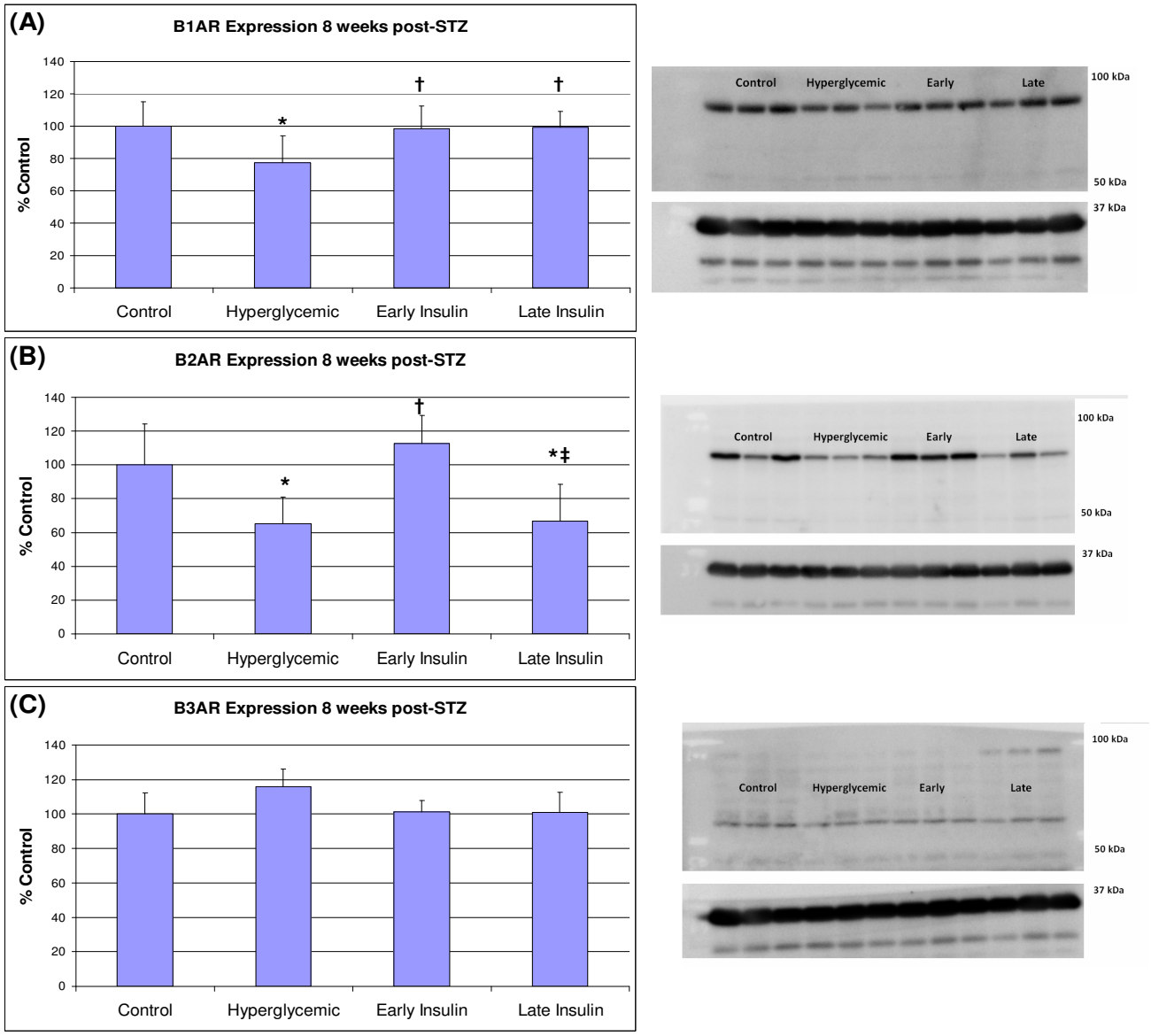

Figure 4.7: Western blot analysis of β_1-AR(**A**), β_2-AR(**B**), β_3-AR(**C**) subtypes (left) and representative blots (right) 8 weeks post-STZ in control, hyperglycemic, early insulin, and late insulin. Relative expression as compared with controls is combined from multiple Western blot analyses with (n=3) per group. *$p<0.05$ to controls, †$p<0.05$ to hyperglycemic, and ‡$p<0.05$ to early insulin. One-way ANOVA, Bonferroni post-hoc.

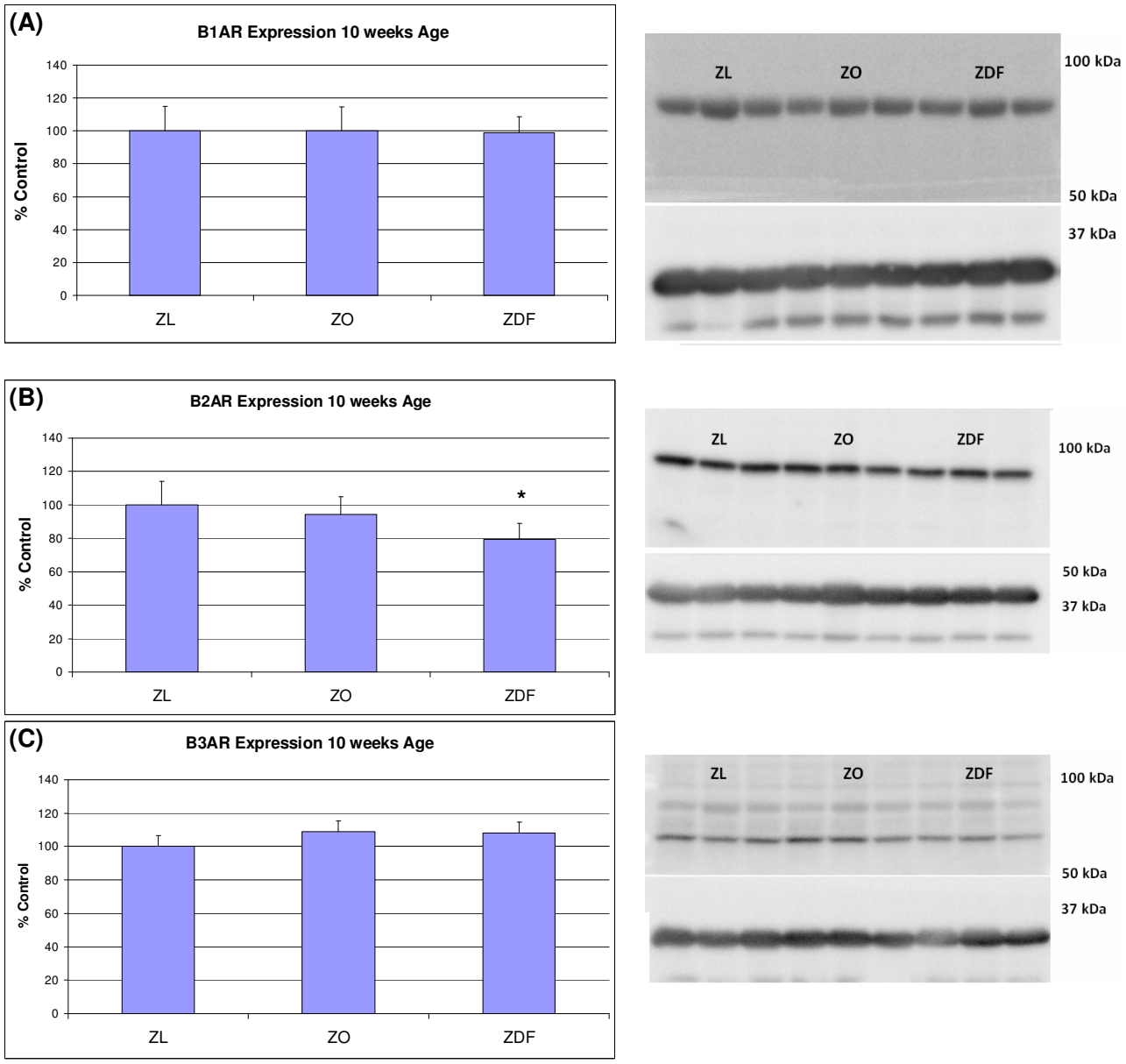

Figure 4.8: Western blot analysis of β_1-AR(**A**), β_2-AR(**B**), β_3-AR(**C**) subtypes (left) and representative blots (right) in 10 week old ZL, ZO and ZDF animals. Relative expression as compared with ZL controls is combined from multiple Western blot analyses with (n=3) per group. *p<0.05 to ZL, †p<0.05 to ZO. One-way ANOVA, Bonferroni post-hoc.

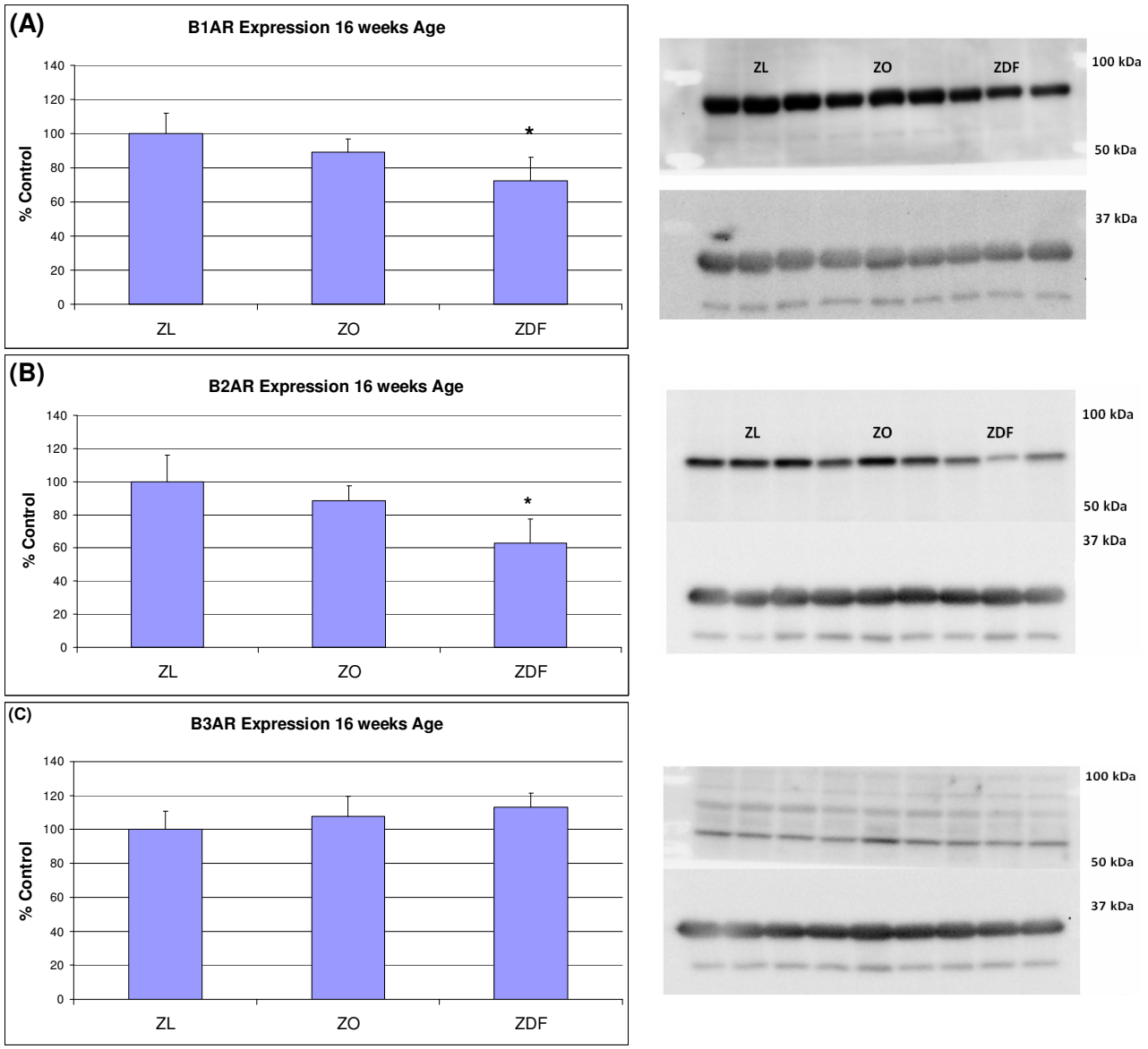

Figure 4.9: Western blot analysis of β_1-AR(**A**), β_2-AR(**B**), β_3-AR(**C**) subtypes (left) and representative blots (right) in 16 week old ZL, ZO and ZDF animals. Relative expression as compared with ZL controls is combined from multiple Western blot analyses with (n=3) per group. *p<0.05 to ZL, †p<0.05 to ZO. One-way ANOVA, Bonferroni post-hoc.

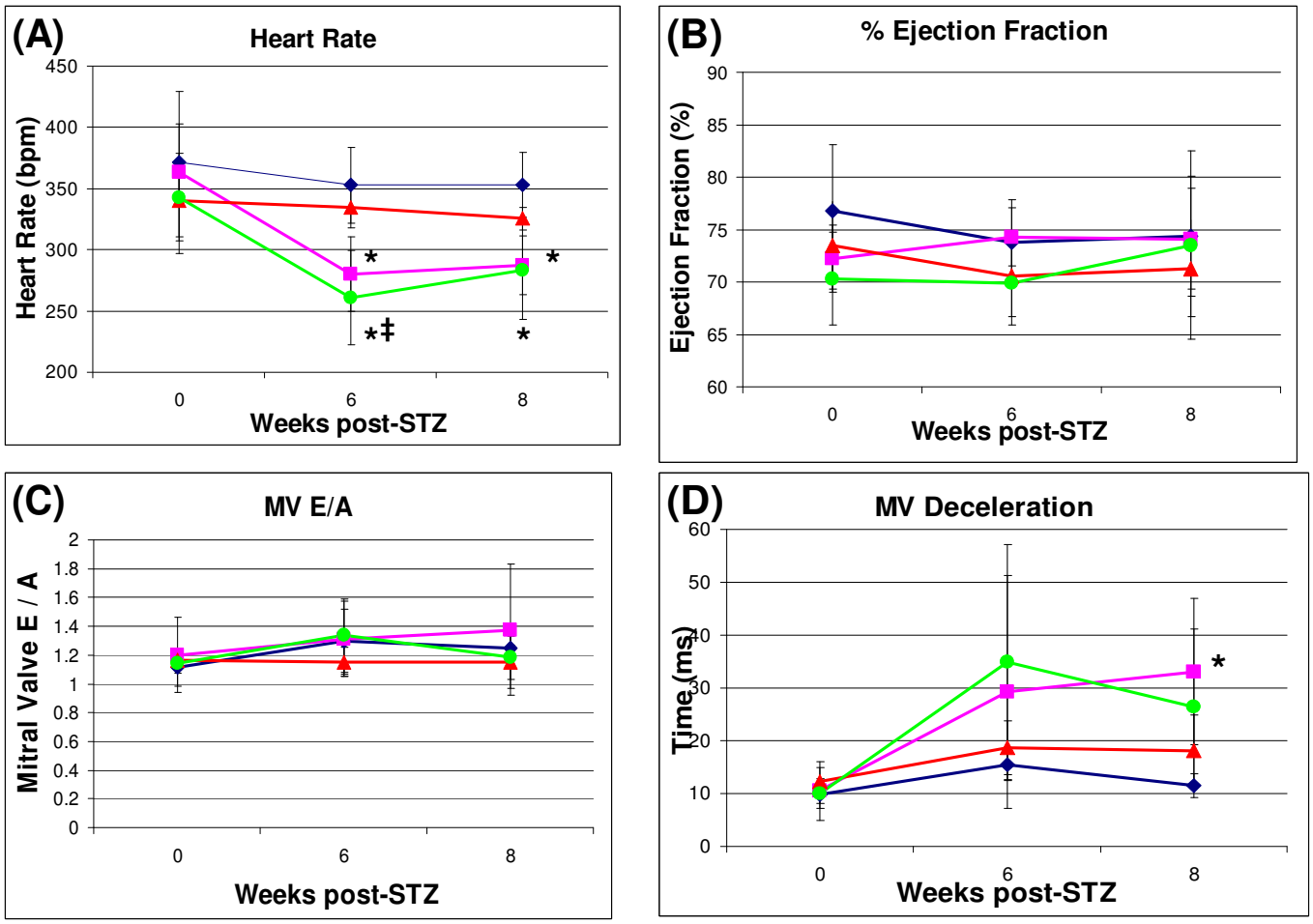

Figure 4.10: Heart rate **(A)**, %EF **(B)**, MV E/A **(C)**, and MVD **(D)** measured by echocardiography in vehicle-treated controls and STZ-treated hyperglycemics, early insulin, and late insulin at 0, 6, and 8 weeks post-STZ. *p<0.05 to controls, †p<0.05 to hyperglycemic, and ‡p<0.05 to early insulin. One-way ANOVA, Bonferroni post-hoc.

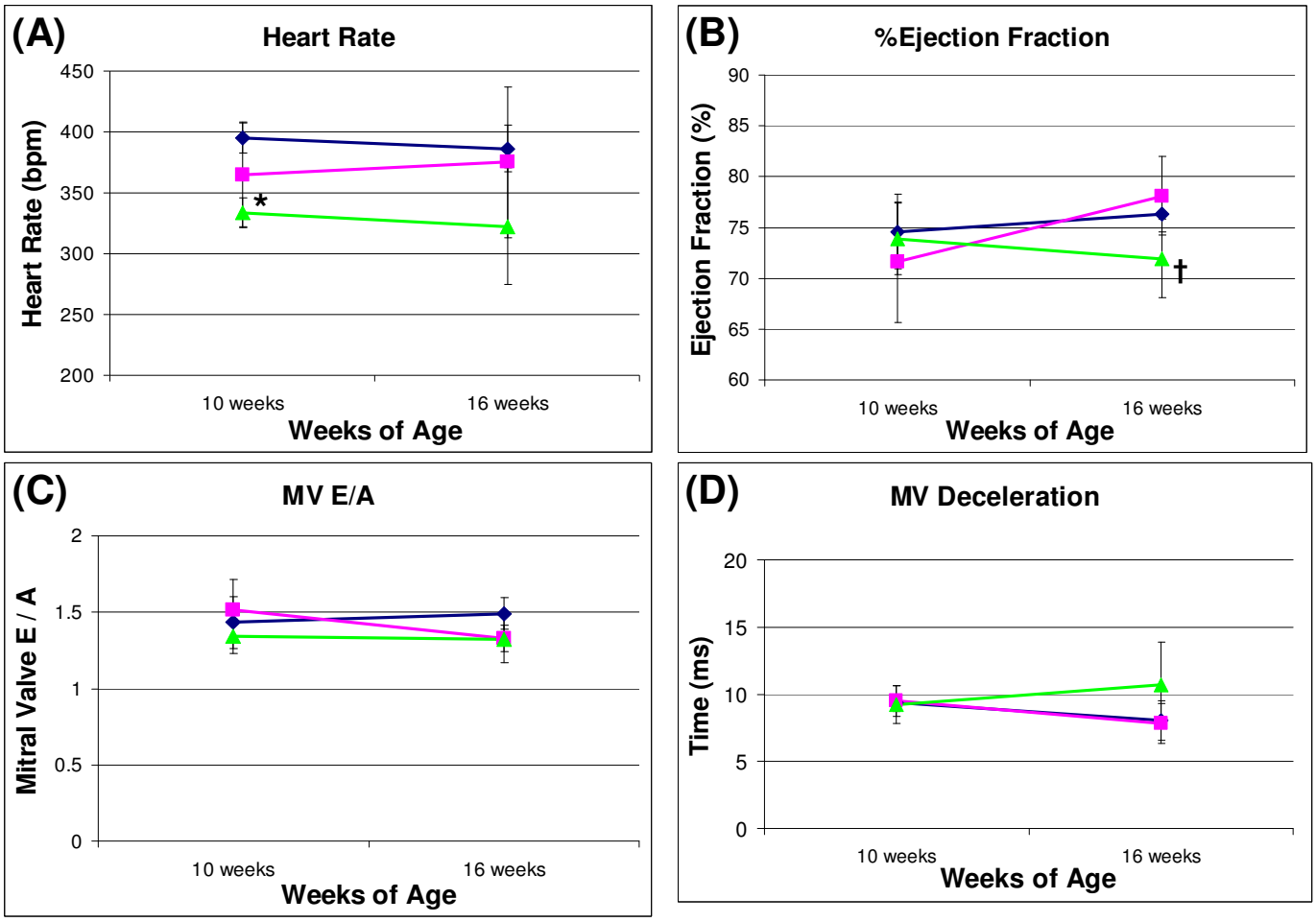

Figure 4.11 : Heart rate **(A)**, %EF **(B)**, MV E/A **(C)**, and MVD**(D)** measured by echocardiography in ZL, ZO, and ZDF at 10 and 16 weeks of age. *p<0.05 to ZL and †p<0.05 to ZO. One-way ANOVA, Bonferroni post-hoc.

5) DISCUSSION

5.1)Myocardial β-AR Expression in High Fat Fed, Hyperglycemic STZ Rats and its Modulation with Insulin Therapy

5.1.1) High-Fat Fed STZ Hyperglycemic Rats Animal Model Characteristics

The rapid and marked elevation blood glucoses at 1 week post-STZ observed in all STZ-treated groups is similar to other reports in this model (Thackeray et. al., 2011a; Thackeray et. al., 2011n; Reed et. al., 2000; Dincer et. al., 2002). STZ is rapidly taken up by pancreatic GLUT2 transporters where it alkylates DNA leading to β-cell death and hypoinsulinemia. The consistently elevated blood glucose levels of ~30mM maintained in STZ hyperglycemics until the end of the experiment at 8 weeks provides a powerful model for assessing the effects of glycemia on the cardiac SNS.

Despite a similar body mass during high-fat feeding, STZ-treatment and subsequent hyperglycemia appear to contribute to reduced weight gain in this model. Coupled with the role of insulin in carbohydrate metabolism and its effects as a growth factor, hypoinsulinemia is likely implicated in this attenuated weight gain. Although hyperglycemic animals showed a modest increase in body mass over the 8 weeks following STZ treatment, this increase is relatively static when compared to the controls. A reduced capacity to gain body mass is typical of DM, especially in insulin-insufficient type-1 DM and during the later insulin-insufficient stages of type-2 DM. This attenuation of weight gain had been observed previously in this model (Thackeray et. al., 2011a; Thackeray et. al., 2011n; Reed et. al., 2000).

The apparent positive relationship between hyperglycemia and hyperphagia in this model has been observed previously (Thackeray et al. 2011a; Thackeray et al. 2011b)

as well as in other models of DM. Since energy from carbohydrate food sources is not being catabolised effectively in these animals, it is expected they will consume more total calories in compensation. Interestingly, diet consumption has a positive association with sympathetic activation, with fasting contributing to a suppression of sympathetic outflow (Young and Landsberg, 1977b), and overfeeding contributing to its activation (Young and Landsberg, 1977a).

5.1.2) Metabolic Markers of STZ Hyperglycemic Animals

To better characterize the hyperglycemic state in these animals, specific metabolic markers associated with obesity and DM were assessed in the plasma at 8 weeks post-STZ – insulin, FFA, and leptin. Measurements were only performed in the fed state, as exogenous insulin supplementation precluded fasting due to the risk of hypoglycemic complications in early and late insulin treatment groups. As expected with STZ treatment, circulating insulin was reduced in hyperglycemic animals, underlying the cause of hyperglycemia in this model as being closer to a type-1 DM. In the absence of insulin-stimulated glucose uptake, and reduced suppression of hepatic glucose output, blood glucose levels are augmented (Reed et. al., 2000; Ferrannini, 2012). The absence of insulin-stimulated glucose uptake means more fats must be mobilized as a fuel source in hyperglycemic animals. Reduced insulin signalling also augments FFA output directly by encouraging adipocyte lipolysis (McTernan et. al., 2002; Ferrannini, 2012). Indirect calorimetry has identified a lower respiratory exchange ratio in this model, indicative of increased utilization of fats as a fuel source (Thackeray et. al., 2011b). This may explain why STZ-treated animals exhibited a much lower body mass than controls, as insulin insufficiency leads to increased catabolism of fatty stores. Leptin levels were reduced in

hyperglycemic animals. In healthy animals, leptin is proportional to adipocity and helps to regulate it. When fat mass is increased, so is leptin production, which acts centrally to suppress appetite and prevent weight gain (Friedman, 2000). Given the preferential use of fats as a fuel source and the reduced body mass in hyperglycemic animals, reduced adiposity likely contributes to reduced leptin levels.

Cardiac NE was elevated in hyperglycemic animals. Elevated NE levels in the heart are characteristic of DM and cardiovascular disease (Ganguly et. al., 1987; Taegmeyer et. al., 2002; Thackeray et. al., 2011a;). In healthy humans, sympathetic nerves of the kidneys and skeletal muscle are the major sources of NE release, accounting for about 25% of the total, while the heart, skin, gastrointestinal tract and liver each are responsible for <10% of plasma NE (Esler et. al., 1988; Goldstein et. al., 1988; McCance et. al., 1989); however, the heart appears to have a disproportionately large NE spillover in conditions of cardiac failure. Regional spillover of NE to plasma in patients with cardiac failure shows a 10-fold increase in cardiac NE spillover, compared to less than 3-fold increase in renal NE spillover, and with no increased spillover from the gut and liver (Esler et. al., 1988). Chronic SNS activation in the heart adversely affects excitation-contraction coupling (Piacentino V 3rd et. al., 2003) and enhances apoptotic pathways (Olivetti et al. 1997). A strong association exists between sympathetic activation, hyperglycemia, DM, and cardiovascular disease.

5.1.3) Effects of Insulin Therapy on Animal and Metabolic Characteristics

Insulin appears to help restore metabolic parameters associated with DM and sympathetic activation assessed. Exogenous insulin supplementation was effective in restoring plasma insulin to control levels as well as return blood glucose to control levels.

Increased utilization of plasma glucose as a fuel source contributed to a reduction in plasma FFA. Leptin levels were restored to control levels in early insulin groups. In late groups, leptin was significantly higher than hyperglycemics, but still significantly lower than controls, this is likely due to lower body mass and may have recovered to control levels with additional time.

The ability of insulin therapy to normalize animal model and metabolic characteristics to values similar to vehicle-treated controls appears to contribute to a reduction in cardiac NE and restoration of cardiac β_1-AR in this model when provided early or late in the progression of hyperglycemia. Early and late insulin-treated groups displayed plasma and cardiac NE levels not significantly different from controls. Late insulin-treated rats display a trend toward higher cardiac and plasma NE levels than early insulin-treated groups, but this was not significant. The efficacy of insulin in inducing euglycemia suggests this model may be limited in studying type-2 DM, which is characterized by insulin resistance. The rapid reversal of the diabetic phenotype with insulin therapy is more similar to type-1 DM; however, oral glucose tolerance tests have identified mild insulin resistance in this model (Thackeray et. al., 2011b; Reed et al,. 2000).

5.1.4) Myocardial β-AR Expression

5.1.4.1)[^{3}H]-CGP12177 Uptake

After 8 weeks of hyperglycemia, [^{3}H]-CGP12177 binding to cardiac β-AR was reduced in hyperglycemic animals. Hyperglycemic retention of [^{3}H]-CGP12177 was between 33-38% lower across myocardial regions, with a 35.7% reduction in the left ventricle. These results confirm previous reports that β-AR expression is reduced in

hyperglycemic high-fat fed STZ rats, and that [^{3}H]-CGP12177 can detect this reduction in *ex-vivo* biodistributions (Thackeray et al., 2011a). This reduction in [^{3}H]-CGP12177 retention was not observed in early or late insulin treated groups. This finding is consistent with previous reports of insulin therapy restoring β-AR expression (Dincer et. al., 2001). Interestingly, unpublished data from our group found that cardiac NET, is not restored after 7 weeks of insulin therapy similar to our early treatment group. This may suggest presynapatic receptors regulating NE in the synaptic cleft may respond more slowly to insulin-induced euglycemia than postsynaptic β-AR. Previous histological observations in high-fat fed STZ rats by our group did not identify any overt structural defects after 8 weeks of untreated hyperglycemia (Thackeray, et. al. 2011b). This coupled with the restoration of [^{3}H]CGP12177 binding in both early and late insulin treatment groups suggests that in the absence of structural remodeling glycemic control with insulin therapy can restore myocardial SNS integrity with similar efficacy when provided at the onset of or after a sustained period of untreated hyperglycemia. The absence of a significant increase in septal uptake of [^{3}H]CGP12177 in the early insulin treated group relative to STZ hyperglycemics is not ideal. This may be explained in part by increased β-AR density in the septum relative to other myocardial regions other than left ventricle (Baker et. al. 1980). Moreover, β-AR density increases toward the apex of the heart, which is largely comprised of septal myocardium (Lyon et. al. 2008). Increased receptor density in the septum may have made it more resistant to downregulation in the STZ hyperglycemics, as suggested by the greater standard deviation in this tissue, which appears to have reduced significance in the early treatment group.

5.1.4.2)Western Blotting for β-AR Subtypes

To provide insight into the specific changes in β-AR subtypes occurring, Western blotting with antibodies specific to β_1-, β_2-, and β_3-AR was performed on whole heart homogenates. β_1-AR expression was reduced in hyperglycemic animals, but in early and late insulin treatment groups, this reduction was not observed. This finding is consistent with other reports of β_1-AR expression in this model of DM (Thackeray et. al., 2011a) and the effect of insulin therapy on this expression (Dincer et. al., 2001). In hyperglycemic animals, β_2-AR expression was reduced. While early insulin β_2-AR expression was not affected, late insulin-treated groups showed a reduction in expression similar to hyperglycemics. The nature of β_2-AR expression is unclear in models of DM and hyperglycemia, with reports suggesting increases (Thackeray et. al., 2011a) and other suggesting a decrease (Dincer et. al., 2001). This data supports the latter observation. This appears to support [^{3}H]-CGP12177 binding results as they predominantly reflect β_1-AR expression which is restored, and suggests that β_2-AR may recover last following insulin treatment an may be the most susceptible to NE-induced downregulation. No significant differences were observed in β_3-AR expression between groups, but there may appear to be a trend toward an increase in β_3-AR expression in STZ-hyperglycemic animals. β_3-AR specific stimulation appears to mediate negative ionotropic responses and vasodilation (Zhao et. al., 2012). Their expression is expected to be upregulated in conditions of SNS activation to help counteract the hyperstimulation of β_1-AR; however this increase has been observed to be much larger in other studies. Dincer et al. (2001) observed a doubling of β_3-AR expression in 14 week STZ hyperglycemics. This may suggest that the upregulation of β_3-AR is progressive and a later time point similar to

Dincer may yield a larger increase in β_3-AR expression. Lower β_3-AR expression similar to controls in both insulin treated groups supports this notion that upregulation is related to the progression of the diabetic phenotype. Upregulation of β_3-AR is not expected to have a large impact on [^{3}H]-CGP12177 binding to cardiomyocytes. Using a specific activity of 41.6μCi/nmol and an injected activity of 8μCi, we can calculate that 0.192nmol of [^{3}H]-CGP12177 was injected into each rat. Given the low affinity of [^{3}H]-CGP12177 for β_3-AR, with a K_d of 90nM compared to 0.3nM and 0.9nM for β_1-AR and β_2-AR respectively, this strongly suggests a very weak receptor-ligand interaction. Determining the percent of the total β_3-AR occupied by [^{3}H]-CGP12177 can be done in *in vitro* binding experiments where the concentration of [^{3}H]-CGP12177 interacting with β-AR can be calculated exactly. Percent occupied receptors can be estimated by dividing the ligand concentration by the sum of the ligand concentration and the K_d of the receptor (Davenport and Russel, 1995) (Equation 3). This may be of interest in future to determine if there is any specific influence of [^{3}H]-CGP12177 binding to myocardial β_3-AR. The *in vitro* Western blotting results appear consistent with *ex vivo* [^{3}H]-CGP12177 binding results and support the notion that [^{3}H]-CGP12177 can accurately quantify changes in cardiac β-AR expression in diabetic animals.

$$\%Occupied\,\mathrm{Re}ceptors = \frac{[Ligand]}{[Ligand] + Kd}$$

Equation 3: Estimation of percent occupied receptors in *in vitro* binding experiments.

5.1.5)Assessment of Systolic and Diastolic Function by Echocardiography

Echocardiography assessment of systolic and diastolic function yielded results similar to previous reports from our group (Thackeray et. al., 2011b). Hyperglycemic animals displayed significant reductions in HR and prolonged MVD at 6 and 8 weeks post STZ, with preserved %EF and E/A ratios. Prolonged MVD is indicative of slower diastolic filling in the left ventricle and may indicate the early development of heart disease. Diastolic dysfunction has been observed in animal models of DM (Kim et. al., 2003) and human patients (From et. al., 2010). Early insulin groups showed no significant differences from controls, while late insulin treatment groups displayed reduced HR at 6 and 8 weeks post-STZ similar to hyperglycemic animals. STZ hyperglycemic, but not late treatment had significantly prolonged MVD at 8 weeks post-STZ. While not significant, late insulin MVD appears prolonged. It is unclear if insulin has delayed the onset of prolonged MVD or improved diastolic function preventing the progression of MVD in this group. This suggest that while β-AR expression assessed by [^{3}H]-CGP12177 may be restored by short term insulin therapy, functional impairments of heart rate and diastolic filling may not be. This is similar to other reports on the effect of insulin on echocardiographic parameters in STZ rats. After 8 weeks of sustained hyperglycemia followed by 8 weeks of insulin therapy, presynaptic NET retention of [^{11}C]-HED was restored in STZ rats (Thackeray et. al., 2013). Despite the restoration of presynaptic SNS innervation, MVD and HR were still slow in both treatments relative to euglycemic controls. This coupled with our late insulin-treatment may suggest that insulin therapy can readily restored cardiac SNS receptor density but may not correct impairments in cardiovascular function STZ rats.

5.2)Myocardial β-AR Expression in Zucker Rats

5.2.1)Animal Model Characteristics of Zucker Rats

The significant elevation in blood glucose in ZDF animals at the onset of the experiment at 8 weeks compared to ZO, and ZL rats clearly delineates the specific obese and DM phenotypes exhibited by these genotypically identical, but phenotypically distinct models. The gradual increase in ZDF blood glucose to overtly hyperglycemic levels by 10 weeks of age, and its continuation toward a threshold of about 20mM from 12 to 16 weeks provides a much more progressive and milder form of hyperglycemia than is observed in high-fat fed STZ rats. While these observations are relatively consistent with previous reports of blood glucose in ZL and ZO rats (Fredersdorf et. al., 2004; Daniels et. al., 2012; Baynes and Murray, 2009), it is important to note that the extent of hyperglycemia in ZDF varies to some extent in the literature. Zhou et al. (2000), reported lower blood glucose level of 4.36, 12.22 and 11.54mM in 7, 14 and 20 week old ZDF rats. It is also unclear if the onset of hyperglycemia is consistent in this model, as most groups provide specific time points, rather than a serial assessment of blood glucose levels. Sustained euglycemia until 16 weeks of age in 31% ZDF rats in this study suggests a significant limitation in this model. The low penetrance of hyperglycemia indicates the type-2 DM phenotype exhibited by ZDF may not be robust and may foreshadow variable results within this model.

The progressive increase in ZO body mass compared to a gradual attenuation in ZDF body mass indicates body mass is inversely correlated to hyperglycemia. It can be speculated that as glucose utilization is perturbed and blood glucose increases, adipocyte lipolysis and increased FFA utilization may contribute to reduced body mass. These

findings, as with blood glucose, are similar to other reports in this model; however discrepancies remain in the temporal nature of these changes in body mass. Baynes and Murray (2009) indicate that ZDF animals are significantly heavier than ZL controls at 16 weeks, but significantly less at 36 weeks; similarly Fredersdorf et al. (2004) show significantly higher body mass in ZDF relative to ZL at 19 weeks. These discrepancies in body mass and blood glucose provide an indication that the nature and development of type-2 DM in this model can vary. Longitudinal studies serially assessing body mass and blood glucose over time in large populations could provide a clearer indication of when these changes typically occur in this model, and may provide greater insight into choosing specific time points for assessing relevant parameters and for commencing therapeutic interventions. The rapid attenuation of weight gain is disappointing in a model described as both type-2 DM and obese.

As discussed previously, increased diet consumption in DM animals occurs as insulin resistance and hyperglycemia reduce the effective calories that can be derived from carbohydrates. Diet consumption has been implicated in sympathetic activation, with feeding contributing to its activation, and fasting its suppression (Young and Landsberg, 1977a; Young and Landsberg, 1977b). The significant increase in ZO and ZDF calories consumed at 10 weeks could suggest augmented SNS tone in tandem with the progression of metabolic perturbations such as obesity and insulin resistance. This appears consistent with a greater increase in diet consumption in ZDF rats relative to ZO at 16 weeks, despite a significantly elevated body mass in the ZO. These effects are also explained by the absence of leptin signaling at its contribution to changes in adipostatic and insulin regulation (German et. al. 2010). These feeding patterns appear consistent

with other models of DM (Thackeray et. al., 2011a). Specific data relating to diet consumption in ZL, ZO, and ZDF rats are limited and made complicated by different time lines and studies assessing the effects of dietary additives on metabolic parameters.

5.2.2)Metabolic Markers

Plasma insulin and FFA were measured in ZL, ZO, and ZDF animals in fasted and fed states, at 10 and 16 weeks of age to help characterize the metabolic profiles of these groups in line with *ex vivo* biodistributions. Leptin measurements were also performed in the fasted state at both time points. A comparison of the fed and fasted state insulin measurements showed marked differences in the development of insulin resistance in ZO and ZDF rats. At 10 weeks of age fasted insulin levels were similar between ZO and ZDF rats, both significantly higher than ZL; however fed state measurements showed a 7-fold increase in ZO insulin compared to ZDF, both remaining significantly higher than ZL. At 16 weeks, the same trend remains, but increased fasted insulin in ZO animals and reduced fed state insulin in ZDF animals suggests a further progression of insulin resistance in both groups. ZO animals display a prediabetic characteristic, maintaining euglycemia through increased insulin output and hyperinsulinemia. ZDF animals, unable to maintain insulin output to the same extent when fed develop hyperglycemia. The fasted and fed insulin measurements help explain the differences in the development of insulin resistance and hyperglycemia in ZO and ZDF animals respectively. When profiling ZDF rats in their progression to the overt diabetic state, Etgen and Oldham (2000) identified that hyperglycemia in ZDF animals corresponded with a reduction in plasma insulin and increased fatty acid oxidation. This appears related to a reduction in pancreatic β-cell mass and insulin secretion, which are

reduced with age in ZDF rats compared to ZL. Unlike ZDF rats, ZO animals appear to maintain euglycemia through increased insulin secretion. Increased β-cell mass and insulin secretion have been observed in ZO (Milburn et. al., 1995; Chan et. al., 1999). This disruption of normal pancreatic β-cell function appears related to increased triglyceride content and subsequent lipotoxicity. ZDF rats display an increase in labeled triglyceride stores when cultured with [^{14}C]glucose or [^{14}C]palmitate indicating increased storage and reduced oxidation of fuels (Lee et. al., 1997). This increased deposition of triglyceride contributes to an increase in ceramide synthesis. Increased ceramide content in ZDF β-cells have been associated with increased DNA laddering – a measure of apoptosis. Ceramide content and DNA laddering can be attenuated with fumonisin B_1, a ceramide synthase inhibitor (Shimabukuro et. al., 1998). Large increases in fasted plasma FFA at 10 and 16 weeks in ZO and ZDF animals support the role of lipotoxicity in the development of insulin resistance and disrupted β-cell function. Interestingly, fed-state plasma FFA levels were lower in ZDF animals than in ZO. This may appear somewhat contradictory, but is likely the result of impaired carbohydrate metabolism in ZDF animals. While ZO animals can catabolise carbohydrates when fed, ZDF animals can not as illustrated by their hyperglycemic phenotype. ZDF rats rapidly uptake FFA into cells and catabolise them as energy after feeding. ZO animals can utilize carbohydrate much more effectively, reducing FFA catabolism and allowing more FFA to remain in circulation after feeding until stored as triglyceride. This altered lipid metabolism in ZDF and ZO animal's results from their lack of an intact leptin receptor, contributing to large increases in circulating leptin. Adenoviral over expression of wild type leptin receptors in islets isolated from ZDF animals effectively lowered triglyceride content and attenuated

apoptosis through upregulating oxidative enzymes increasing FFA catabolism (Wang et. al., 1998a; Wang et al. 1998b). It remains unclear why ZO β-cells appear to be able to hypertrophy and maintain euglycemia through increased insulin secretion while ZDF rapidly atrophy and progress to insulin insufficiency, since these animals both carry the same *fa/fa* mutation and truncated leptin receptor. This appears to be one of the fundamental differences between these genotypically identical models, and underlies the development of hyperglycemia in ZDF and euglycemia in ZO. Hyperglycemia does eventually develop in ZO animals, but not until much later than the 10 weeks of age observed in ZDF animals here, and remains milder around 11mmol/L (Munoz et. al., 2009). This discrepancy may be better understood by directly comparing triglyceride and ceramide content as well as the oxidative capacity and glucose sensitivity of ZO and ZDF pancreata.

No significant differences were apparent in ZDF NE, although plasma NE may be tending toward an increase in ZDF at 16 weeks of age suggestive of sympathetic activation and a similar but lesser trend toward elevated plasma NE may be developing in ZO animals at 16 weeks, but these observations are not significant. Comparing NE levels in ZDF and ZO at 16 weeks of age suggests greater sympathetic activation in ZDF may be contributing to reduced [^{3}H]-CGP12177 binding. These findings appear consistent with previous reports of plasma NE in Zucker rats, where the ZDF exhibit the greatest plasma NE concentration followed by ZO and with ZL animals having the least (Marsh et. al., 2007). If ZDF plasma NE is tending toward an increase it could be due to the added effect of overt hyperglycemia and insulin resistance on sympathetic activation. Since ZO animals can maintain euglycemia through hyperinsulinemia, greater plasma NE

could be expected in ZDF animals that are hyperglycemic. This may provide context for understanding why [^{3}H]-CGP12177 retention is reduced in ZDF but not ZO. Elevated cardiac NE was not evident in ZO or ZDF animals at 16 weeks. The absence of elevated cardiac NE is tenuous. Elevations in plasma NE occur as whole body NE production exceeds NE use and reuptake. This means the sum of NE produced by all organs and tissue contributes to elevations in plasma NE. Elevations in cardiac NE are more specifically related to increased cardiac NE production, use, reuptake, as well as the progression of cardiovascular dysfunction. A later time point may be necessary for perturbed cardiac metabolism to manifest as overt functional deficits and elevated cardiac NE contributing to greater reductions in [^{3}H]-CGP12177 binding.

5.2.3) Myocardial β-AR Expression

5.1.3.1)[^{3}H]-CGP12177 Uptake

At 10 weeks of age, β-AR expression as assessed by [^{3}H]-CGP12177 binding, showed similar receptor density in myocardial regions of ZL and ZDF animals. After 6 weeks of sustained overt hyperglycemia, ZDF animals showed a significant reduction in [^{3}H]-CGP12177 retention of 16-25% across myocardial regions. To the author's knowledge, no other studies have quantified β-AR in ZDF animals. Song et. al. (2008) did show that 20 week old ZDF rats have a reduced left ventricle developed pressure in response to the β_1-AR agonist dobutamine. This finding appears consistent with our results of reduced [^{3}H]CGP12177 binding; however, it is unclear if the reduced dobutamine response is the result of a reduction in β_1-AR expression or alternatively a reduced sensitivity to agonist stimulated increases in contractile force, with maintained receptor expression. Similar experiments with [^{3}H]-CGP12177 have been conducted in

other models of DM. Thackeray et al. (2011a) showed that high-fat fed STZ rats have normal [^{3}H]-CGP12177 uptake after 2 weeks of hyperglycemia, but after 8 weeks of hyperglycemia [^{3}H]-CGP12177 binding becomes reduced 34-40%. This is similar to our findings that [^{3}H]-CGP12177 retention is normal in ZDF at 10 weeks of age, but is reduced at 16 weeks of age after a sustained period of hyperglycemia. This suggests not only the presence of, but the duration of hyperglycemia and altered insulin signalling is critical to the increases in NE levels contributing to reduced cardiac β-AR expression in DM. More modest reductions in [^{3}H]-CGP12177 binding in ZDF animals may be attributed to differences in the development of hyperglycemia and insulin resistance. While ZDF animals displayed significantly elevated blood glucose for 8 weeks like the STZ model, only 6 weeks displayed overt hyperglycemia >11mM. Moreover, hyperglycemia in ZDF animals was not as profound, with a plateau ~20mM, compared to ~30mM in STZ-induced diabetics. There is also evidence of native insulin production and signalling as plasma insulin showed some modest increases in the fed state when compared to the fasted in ZDF animals. STZ animals in contrast are hypoinsulinemic and exogenous insulin but not the insulin sensitizer metformin can preserve NET and β-AR expression (Thackeray et al. 2013). More modest increases in ZDF glucose levels and differences in insulin production and signalling may reflect why cardiac NE was not significantly higher in ZDF rats compared to controls, as occurred in STZ animals. Observing ZDF animals at a later time point that allows for the progression of metabolic derangements and hyperglycemia should translate to greater SNS activation, increased in NE levels, and reduced [^{3}H]-CGP12177 binding.

In contrast to the hyperglycemic ZDF animals, euglycemic ZO animals showed an

unexpected increased in [^{3}H]-CGP12177 retention, which was significant across myocardial regions at 16 weeks of age. ZO animals display metabolic characteristics that are very similar to ZDF with the exceptions that ZO animals maintain euglycemia through hyperinsulinemia, while ZDF animals become rapidly hypoinsulinemic and hyperglycemic. This may suggest that the development of hyperglycemia has a pivotal role in the downregulation of cardiac β-AR, and in the absence of hyperglycemia, hyperinsulinemia may promote β-AR expression. One possible mechanism for increased receptor expression could be through increased cell size. Insulin signaling promotes hypertrophy in isolated cardiomyocytes and *in vivo* in rats (Belke et al. 2002). A post-natal knockout of the insulin receptor results in reduced heart size (Shiojima et al. 2002). Hypertrophy appears in tandem with increased expression of downstream insulin signaling pathways PI3K/Akt and mitogen-activated protein kinase (MAPK) pathways (Yu et al. 2010). PI3K/Akt signaling negatively regulates glycogen-synthase 3 and forkhead box-O expression, encouraging gene transcription, protein synthesis and hypertrophy (Heineke et al. 2006; Shurk et al. 2005; Liu et al. 2007). MAPK activation by insulin promotes cell proliferation and vasoconstriction in the heart. The Renin-Angiotensin System (RAS) is also implicated MAPK activation and vasoconstriction in the heart, predominantly through the binding of its active signaling molecule angiotensin II to the AT-1 receptor. RAS activation is pathological in obesity and metabolic syndrome, often found in tandem with hyperinsulinemia, hypertrophy, and hypertension (Yu etal. 2010). RAS is associated with the development pressure-volume overload and contributes to hypertrophy and cardiovascular dysfunction (Van Buren and Toto, 2013). Sethi et al. (2006) found that 4 weeks after an aortocaval shunt-induced volume overload

in the heart, rats exhibited increased [^{125}I]iodocyanopindolol binding to cardiac β-AR in isolated membrane fractions from the left ventricle and increased AC activity. After 24 weeks both binding and AC activity were reduced. This suggests changes in cardiac β-AR expression are related to disease progression, initially increasing to maintain cardiac output then failing as receptors decrease. This could explain the absence of an increase in cardiac β-AR in ZDF animals that exhibited a more advance DM phenotype with fasted hyperglycemia, potentially accelerating the downregulation of cardiac β-AR, such that this increase in β-AR expression was lost completely or occurred prior to our initial 10 week time point. The conflicting *ex vivo* and *in vivo* results make the true nature of ZO cardiac β-AR expression unclear in this study. Further studies assessing the effect of glycemic control and hypertension on cardiac β-AR expression may provide greater insight into the observed increase in ZO [^{3}H]-CGP12177 binding. Assessing [^{3}H]-CGP12177 expression in young or embryonic ZL, ZDF and ZO may also elucidate more clearly the temporal nature of this effect and its relationship with the progression of the hyperglycemic DM phenotype.

5.2.3.2)Western Blotting for β-AR Subtypes

ZO β_1-AR expression similar to ZL appears to contradict [^{3}H]-CGP12177 binding experiments, which suggests an increase in β_1-AR expression. Hydrophilic [^{3}H]-CGP12177 only binds to receptors present at the cell surface, while Western blotting performed on whole heart homogenates reflects both membrane and intracellular pools. This may suggest β-AR cell surface expression of capable of binding [^{3}H]-CGP12177 is increased in ZO animals compared to ZL, but that total β-AR expression including intracellular β-AR pools remain similar to ZL. ZO may recruit more β-AR to the cell

surface to maintain cardiac output, which can become depressed in obesity. As plasma and cardiac NE levels increase further, internalization and downregulation of these receptors may occur (Figure 1.5). Western blotting in ZDF animals confirmed the reduction in β-AR expression observed in *ex vivo* biodistributions as being the result of reduced β_1- and β_2-AR expression. β_1- and β_2-AR are known to exhibit Gs coupling, and their downregulation has been described previously as a compensatory measure for hyperstimulation by NE (Dincer et. al., 2002).

5.2.4)Assessment of Systolic and Diastolic Function by Echocardiography

We observed a significant reduction in HR in 10 week ZDF, but not in 16 week ZDF. While HR is reduced more at 16 weeks than 10 weeks in ZDF, greater standard deviation within ZO and ZDF animals at 16 weeks appears to have reduced significance. Increasing n values may help ameliorate this discrepancy. Reduced HR in ZDF animals appears to be the trend observed in the literature, but some inconsistencies exist. Baynes and Murray (2009), found no change in HR in ZDF rats at 16 and 36 weeks of age; however most echocardiographic assessments of ZDF rats have shown a reduction in HR relative to ZL at 14 (Marsh et. al., 2007), 19 (Fredersdorf et. al., 2004), and 20 weeks of age (Song et. al., 2007). This discrepancy may relate to the development of hyperglycemia and insulin resistance. While Baynes and Murray (2009) found significant hyperglycemia at 16 and 36 weeks of age, they also report significantly elevated body mass at 16 weeks. In our study increased body mass in ZDF was attenuated by 16 weeks as insulin resistance and hyperglycemia develop. This may suggest that the progression of insulin resistance and impaired weight gain in ZDF rats can be variable making comparisons difficult. HR was found to be normal in euglycemic ZO at 30 weeks of age

(Baretti et. al., 2012). Interestingly, in db/db mice HR was not reduced until 15 weeks of age, after the development of hyperglycemia (Buchanan et. al., 2005). Since ZDF and ZO possess the same leptin knockout receptor as db/db mice, and ZDF but not ZO display overt hyperglycemia at 16 weeks and elevated plasma NE, it suggests hyperglycemia and NE may be a contributing factor to this reduction in HR. This is supported by a reduction in HR in high-fat fed Sprague Dawley rats, as early as 2 weeks after STZ-induced hyperglycemia, but not in high-fat fed vehicle treated controls that are euglycemic (Thackeray et. al., 2011b).

ZDF MVD was not significantly prolonged at 16 weeks. van den Brom et al. (2009) found that MVD was significantly prolonged in 14 week ZDF, in conjunction with a decreased fractional area change. Other studies report that in 44 week old ZDF only mild diastolic dysfunction due to impaired left ventricular relaxation occurs as indicated by an increased relaxation time constant Tau with normal systolic function (Daniels et al. 2012). Our findings seem consistent with the development of impaired diastolic function, but not with the same severity or early onset observed by van der Brom. Abnormal acoustic properties, like the pulse wave Doppler assessment of MVD, correlate positively with the severity and duration of DM (Perez et. al., 1992). More severe hyperglycemia in ZDF rats in van der Broms study (30.2mM) compared to ours (21.8mM) at 16 weeks may provide some context for explaining the more prolonged MVD observed. No indication of prolonged MVD was evident in ZO animals. Since MVD is intimately related to HR, the preservation of HR in ZO and not ZDF animals may explain why ZO MVD is not reduced.

Reports comparing %EF in ZL and ZDF rats have shown a reduction as early as

14 weeks (Marsh et. al., 2011; van der Brom et. al., 2009). Other reports have shown normal %EF in young rats that becomes progressively impaired with age (Baynes and Murray, 2009; Tobill et. al., 2010). Daniels et al. (2012) found that systolic function was normal in 44w old ZDF, and Fredersdorf et al. (2004) displaying an increased %EF in 19w ZDF animals. Our group has previously identified a preserved %EF in high-fat fed STZ rats after 8 weeks of hyperglycemia (Thackeray et. al. 2011b), supporting the notion of preserved %EF in ZDF rats with milder hyperglycemia. A small but insignificant decreased in %EF in ZDF animals compared to ZL, and decreased %EF compared to ZO in our study suggests a progression toward systolic dysfunction in ZDF. Elevated %EF in ZO animals relative to ZDF is somewhat surprising. Isolated myocytes from ZO exhibit reduced peak shorting and calcium clearance (Ren et. al., 2000); however, echocardiographic assessment of 30 week old ZO found no change in %EF compared to ZL (Barretti et. al., 2012). In db/db mice it has been reported that elevated cardiac output at 4 weeks of age occurs prior to the onset of hyperglycemia, but reduced cardiac output develops by 15 weeks of age after the onset of hyperglycemia (Buchanan et. al., 2005), suggesting that systolic performance may be elevated prior to overt insulin resistance and hyperglycemia in leptin receptor knock-out models. Conflicting reports regarding echocardiographic assessment of systolic and diastolic function in ZO and ZDF makes interpretation difficult.

6)CONCLUSION

This work demonstrates that myocardial β-AR expression is reduced in hyperglycemic high-fat fed STZ and ZDF *(fa/fa)* models of hyperglycemia and DM, when measured in *ex vivo* biodistributions with [^{3}H]-CGP12177. Western blotting reveals that in both DM models, this reduction is in β_1- and β_2-AR, while β_3-AR is not significantly impacted. Hyperglycemia and reduced β-AR expression appear inversely correlated to plasma and cardiac NE, which are elevated in STZ hyperglycemic animals. Echocardiographic assessment demonstrates that while HR is reduced in both models of DM, systolic dysfunction with reduced %EF is not. Prolonged MVD in STZ rats suggests the development of diastolic dysfunction, and while a statistically significant increase was not observed in ZDF MVD, a trend toward longer MVD times suggests diastolic function may be deteriorating. Insulin treatment in the STZ model demonstrated that glycemic control reducing blood glucose at the onset of hyperglycemia or after a sustained period of hyperglycemia can restore euglycemia and β-AR expression in the myocardium of STZ hyperglycemic animals. This *ex vivo* work with [^{3}H]-CGP12177 demonstrates that [^{11}C]-CGP12177 PET may have the potential to characterize myocardial β-AR expression in DM animals and identify changes therein following intervention with glycemic control therapies, which could be applied as a guide to therapeutic intervention in treating cardiac disease in DM and metabolic syndrome.

7)FUTURE DIRECTIONS

The long term goal of this project is to characterize myocardial β-AR expression in animal models of type-2 DM with the PET tracer [^{11}C]-CGP12177, for future application in assessing the cardiac SNS in human DM and heart failure. This work provides the rationale that [^{3}H]-CGP12177, in *ex vivo* biodistributions, can be used to assess reductions in myocardial β-AR expression in high-fat fed STZ and ZDF models of DM. Assessing ZDF animals at a later time point may yield a more significant reduction in myocardial β-AR expression and a significant reductions in MVD and HR, potentially providing a more robust model for assessing cardiovascular function in type-2 DM. Insulin therapy in STZ animals supports that reducing blood glucose in hyperglycemic rats can restore myocardial β-AR expression, and that this effect may not be limited by a period of sustained hyperglycemia, as may be observed in human patients before being diagnosed with DM. Native insulin production in ZDF animals means insulin sensitizers may be effective in reducing blood glucose in this model, to determine the effects of glycemic control therapy on β-AR expression in this model. The efficacy of metformin and rosiglitazone in inducing euglycemia in ZDF animals and the effect on myocardial β-AR expression remains to be explored. In future work, autoradiographic assessment of receptor subtypes or Western blotting on isolated membrane fractions in conjunction with polymerase chain reaction determination of mRNA levels could provide additional insight into pre- and post-transcriptional regulation of $\beta_{1\text{-}3}$-AR subtype expression.

8)REFERENCES

Adams M, Montague CT, Prins JB, et. al. Activators of peroxisome proliferator activated receptor gamma have depot-specific effects on human preadipocyte differentiation. J Clin Invest. 1997. 100: 3149-3153.

Altan VM, Arioglu E, Guner S, Ozcelikay AT. The influence of DM on cardiac β-adrenoceptor subtypes. Heart Fail Rev. 2007. 12:58-65.

Agardh E, Allebeck P, Hallqvist J, Moradi T, Sidorchuk A. Type-2 DM incidence and socioeconomic position: a systematic review and meta-analysis. International journal of epidemiology. 2011. 40: 804-814.

Amitani M, Asakawa A, Amitani H, Inui A. The role of leptin in the control of insulin-glucose axis. Frontiers in Neuroscience. 2013. 7(51):1-15.

Appenzeller O, Oribe E. The Autonomic Nervous System: An introduction to basic and clinical concepts 5th ed. (Elsevier, Amsterdam, 1997).

Armitage JA et al. Rapid onset of renal sympathetic nerve activation in rabbits fed a high-fat diet. Hypertension. 2012. 60:163-171.

Baker SP, Boyd HM, Potter LT. Distribution and function of beta-adrenoceptors in different chambers of the canine heart. Br J Pharmacol. 1980; 68(1):57-63.

Banks WA, Jaspan JB, Kastin AJ. Selective, physiological transport of insulin across the blood-brain barrier: novel demonstration by species-specific radioimmunoassays. Peptides. 1997;18(8):1257-62.

Barrettu DLM, Magalhaes FC, Fernandes T, do Carmo EC, Rosa KT, Irigoyen MC, Negrao CE, Oliveira EM. Effects of aerobic exercise training on cardiac rennin-angiotensin system in an obese Zucker rat strain. PLoS ONE. 2012. 7(10):e46114.

Baynes J and Murray DB. Cardiac and renal function are progressively impaired with aging in Zucker diabetic fatty type II diabetic rats. Ox Med and Cell Longevity. 2009; 2(5):328-334.

Beck B. Neuropeptides and obesity. Nutrition. 2002; 16:916–923.

Benthem L et al. Excess portal venous long-chain fatty acids induce syndrome X via HPA axis and sympathetic activation. 2000. Am J Physiol Endocrinol Metab. 279:E1286-E1293.

Bohm SK, Grady EF, Bunnett NW. Regulatory mechanisms that modulate signalling by G-protein-coupled receptors. J Bioc. 1997. 322: 1-18.

Benomar Y, Naour N, Aubourg A, Bailleux V, Gertler A, Djiane J, Guerre-Millo M, Taouis M. Insulin and leptin induce Glut4 plasma membrane translocation and glucose uptake in a human neuronal cell line by a phosphatidylinositol 3-kinase- dependent mechanism. Endocrinology. 2006.147(5):2550-6.

Borg WP, Sherwin RS, During MJ, Borg MA, Shulman GI. Local ventromedial hypothalamus glucopenia triggers counterregulatory hormone release. Diabetes. 1995. 44(2):180-4.

Bouvier M, Hausdorff WP, De Blasi A, O'Dowd BF, Kobilka BK, Caron MG, Lefkowitz RJ. Removal of phosphorylation sites from the beta 2-adrenergic receptor delays onset of agonist-promoted desensitization. Nature. 1988. 333(6171):370-3.

Brodde OE. Beta-adrenoceptors in cardiac disease. Pharmacol Ther. 1993. 60: 405-30.

Buchanan J, Mazumder PK, Hu P, Chakrabarti G, Roberts MW, Yun UJ, Cooksey RC, Litwin SE, Abel ED. Reduced cardiac efficiency and altred subtrate metabolism precedes the onset of hyperglycemia and contractile dysfunction in two mouse models of insulin reisstance and obesity. Endocrinology. 146(12):5341-5349.

Bugger, H., & Abel, E. D. (2009). Rodent models of diabetic cardiomyopathy.Disease Models & Mechanisms, 2(9-10), 454-466.

Burguera B, Couce ME, Curran GL, Jensen MD, Lloyd RV, Cleary MP, Poduslo JF. Obesity is associated with a decreased leptin transport across the blood-brain barrier in rats. Diabetes. 2000;49(7):1219-23.

Camargo RL. et. al. An increase in glucose concentration in the lateral ventricles of the brain induces changes in autonomic nervous system activity. Neurol Res. 2013. 35(1):15-21.

Cartee GD, Wojtaszewski JF. Role of Akt substrate of 160 kDa in insulin-stimulated and contraction-stimulated glucose transport. Appl Physiol Nutr Metab. 2007. 32(3):557-66.

Chakraborti S, Chakraboti T, Shaw G. Beta-adrenergic mechanisms in cardiac disease: a perspective. Cell Signal. 2000. 12(8): 449-513.

Chan CB, MacPhail RM, Sheu L, Wheeler MB, Gaisano HY. β-cell hypertrophy in fa/fa rats is associated with basal glucose hypersensitivity and reduced SNARE protein expression. Diabetes. 1999; 48:997-1005.

Cheng KT. [11C]meta-Hydroxyephedrine. Molecular Imaging and Contrast Agent Database (MICAD). Bethesda (MD): National Center for Biotechnology Information (US); 2004-2013. 2006 Jan 19 [updated 2008 Jun 30].

Chess DJ and Stanley WC. Role of diet and fuel overabundance in the development and progression of heart failure. Cardiovasc Res. (2008) 79. 269-278.

Choi KM, Zhong Y, Hoit BD, Grupp IL, Hahn H, Dilly KW, Guatimosim S, Lederer WJ, Matlib MA. Defective intracellular Ca2+ signalling contributes to cardiomyopathy in Type 1 diabetic rats. Am J Physiol Heart Circ Physiol. 2002; 283: H1398-H1408.

Choy CK, Rodgers JE, Nappi JM, Haines ST. Type-2 DM mellitus and heart failure. Pharmacotherapy. 2008. 28(2):170-192.

Chua SC, Chung WK, Wupeng XS, et al. Phenotypes of mouse DM and rat fatty due to mutations in the OB (leptin) receptor. Science. 1996; 271, 994–996.(a)

Chua SC Jr, White DW, Wu-Peng XS, et al. Phenotype of fatty due to Gln269Pro mutation in the leptin receptor (Lepr). Diabetes. 1996; 45, 1141–1143.(b)

Cincotta AH et. al. Hyperinsulinemia increases norepinephrine metabolism in the ventromedial hypothalamus of rats. 1999. NeuroReport.II:383-387

Craft S. Insulin resistance syndrome and Alzheimer disease: pathophysiologic mechanisms and therapeutic implications. Alzheimer Dis Assoc Disord. 2006. 20:298-301.

Currie G, Freel EM, Perry CG, Dominiczak AF. Disorders of blood pressure regulation-role of catecholamine biosynthesis, release, and metabolism. Curr Hypertens Rep. 2012. 14(1):38-45.

Damon DH. Vascular-dependent effects of elevated glucose on postganglionic sympathetic neurons. 2010. Am J Heart Circ Physiol. 300:H1386-H1392.

Daniels A, Linz D, van Bilsen M, Rutten H, Sadowski T, Ruf S, Juretschke HP, Neumann-Haefelin C, Munts C, van der Vusse GJ, van Nieuwenhove FA. Long-term severe DM only leads to mild cardiac diastolic dysfunction in Zucker diabetic fatty rats. Eur J Heart Fail. 2012; 14:193-201.

de Jong A, Strubbe JH, Steffens AB. Hypothalamic influence on insulin and glucagon release in the rat. AM J Physiol. 1977. 233(5):E380-8.

de Jong RM, Blanksma PK, van Waarde A, van Veldhuisen DJ. Measurement of myocardial beta-adrenoceptor density in clinical studies: a role for positron emission tomography? Eur J Nucl Med Mol Imaging. 2002; 29(1):88-97.

Delforge J, Mesangeau D, Dolle F, Merlet P, Loc'h C, Bottlaender M, Trebossen R, Syrota A. In vivo quantification and parametric images of the cardiac β-adrenergic receptor density. J Nucl Med. 2002. 43:215-226.

Dincer UD, Bidasee KR, Guner S, Tay A, Ozcelikay AT, Altan VM. The effect of DM on expression of β1-, β2-, and β3-adrenoreceptors in rat hearts. Diabetes. 2002. 50: 455-461.

Doze P, Elsinga PH, van Waarde A, Pieterman RM, Pruim J, Vaalburg W, Willemsen AT. Quantification of beta-adrenoceptor density in the human heart with (S)-[11C]CGP 12388 and a tracer kinetic model. Eur J Nucl Med Mol Imaging. 2002; 29(3):295-304.

Drake MT, Shenoy SK, Lefkowitz RJ. Trafficking of G Protein-Coupled Receptors. Circ Res. 2006. 99:570-582.

Dyntar D et al. Glucose and palmitic acid induce degredation of myofibrils and modulate apoptosis in rat adult cardiomyocytes. 2001. Diabtes. 50:2105-2113.
Elsinga PH, et al. Imaging of β-adrenoceptors in the human thorax using (S)-[11C]CGP12388 and positron emission tomography. Eur J Pharmacol. (2001). 433: 173-176.

Dzimiri N. Regulation of β-adrenoceptor signalling in cardiac function and disease. Pharmacological Reviews. 1999; 51(3): 465-501.

Esler M, Rumantir M, Wiesner G, Kaye D, Hastings J, Lambert G. Sympathetic nervous system and insulin resistance: from obesity to DM. American Journal of Hypertension. 2001. 14:304s-309s.

Esler M, Jennings G, Korner P, Willett I, Dudley F, Hasking G, Anderson W, Lambert G. Assessment of human sympathetic nervous system activity from measurements of norepinephrine turnover. Hypertension. 1988. 11(1):3-20.

Etgen GJ, Oldham BA. Profiling of Zucker Diabetic Fatty Rats in Their Progressio to the Overt Diabetic State. Metabolism. 2000; 49(5):684-688.

Evans ML, McCrimmon RJ, Flanagan DE, Keshavarz T, Fan X, McNay EC, Jacob RJ, Sherwin RS. Hypothalamic ATP-sensitive K + channels play a key role in sensing hypoglycemia and triggering counterregulatory epinephrine and glucagon responses. Diabetes. 2004. 53(10):2542-51.

Falcao-Pires I, Leite-Moreira AF. Diabetic cardiomyopathy: understanding the molecular and cellular basis to progress in diagnosis and treatment. Heart Fail Rev. 2012; 17(3):325-344.

Ferrannini E. Insulin Therapy Physiology of Glucose Homeostasis and Insulin Therapy in Type 1 and Type 2 Diabetes. Endo and Metab Clin. 2012. 41(1): 25-39.

Fonseca VA, Kulkarni KD. Management of type-2 DM: oral agents, insulin and injectables. J Am Diet Assoc. 2008. 108:S29-S33.

Fonesca V, Rosenstoack J, Patwardhan R, Salzman A. Effect of metformin and rosiglitazone combination therapy in patients with type-2 DM mellitus: a ranomized controlled trial. JAMA. 2000. 283:1695-1702.

Fredersdorf S, Thumann C, Ulucan C, Griese DP, Luchner A, Riegger GA, Kromer EP, Weil J. Myocardial hypertrophy and enhanced left ventricular contractility in Zucker diabetic fatty rats. Cardiovasc Pathol. 2004. 13(1): 11-19.

From AM, Scott CG, Chen HH. The development of heart failure in patients with DM mellitus and pre-clinical dysfunction a population based study. J Am Coll Cardiol. 2010. 55(4):300-305.

Fu WJ, Haynes TE, Kohli R, Hu J, Shi W, Spencer TE, Carroll RJ, Meininger CJ, Wu G. Dietary L-arginine supplementation reduces fat mass in Zucker diabetic fatty rats. J Nutr. 2005. 135(4):714-21.

Galderisi M. Diastolic dysfunction and diabetic cardiomyopathy: Evaluation by Doppler echocardiography. Journal of the American College of Cardiology. 2006; 48(8):1548-1551.

Ganguly PK, Beamish RE, Dhalla KS, Innes IR, Dhalla NS. Norepinephrine storage, distribution, and release in diabetic cardiomyopathy. Am J Physiol. 1987. 252:E734-739.

Gauthier C, Rozee B, Manoury B, Balligand JL. Beta-3 Adrenoceptors as New Therapeutic Targets for Cardiovascular Pathologies. Curr Heart Fail Rep. 2011. 8:184-192.

German JP, Wisse BE, Thaler JP, Oh-I S, Sarruf DA, Ogimoto K, Kaiyala KJ, Fischer JD, Matsen ME, Taborsky GJ Jr, Schwartz MW, Morton GJ. Leptin deficiency causes insulin resistance induced by uncontrolled diabetes. Diabetes. 2010. 59(7):1626-34.

Goldstein DS, Brush JE, Eisenhofer BG, Stull R, Esler M. In vivo measurements of neuronal uptake of norepinepherine in the human heart. Circulation. 1988. 78: 41-48.

Gosmanov A et al. Effects of oral and intravenous fat load on blood pressure, endothelial function, sympathetic activity, and oxidative stress in obese healthy subjects. In 13 obese normotensive subjects. 2010. Am J Physiol Endocrinol Metab. 299: E953-E958.

Hadcock JR, Malbon CC. Regulation of receptor expression by agonists: transcriptional and post-transcriptional controls. Trends Neurosci. 1991.14(6):242-7.

Haga K, Kameyama K, Haga T, Kikkawa U, Shiozaki K, Uchiyama H. Phosphorylation of human m1 muscarinic acetylcholine receptors by G protein-coupled receptor kinase 2 and protein kinase C. J Biol Chem.1996;271(5):2776-82.

Hardie LJ, Rayner DV, Holmes S, et al. (1996) Circulating leptin levels are modulated by fasting, cold exposure and insulin administration in lean but not Zucker (fa/fa) rats as measured by ELISA. Biochem Biophys Res Commun 223, 660–665.

Hausber M et al. Dissociation of sympathoexcitatory and vasodilator actions of modestly elevated plasma insulin levels. (1995) J Hypertens. 13:1015-1021

Hausdorff WP, Bouvier M, O'Dowd BF, Irons GP, Caron MG, Lefkowitz RJ. Phosphorylation sites on two domains of the beta 2-adrenergic receptor are involved in distinct pathways of receptor desensitization. J Biol Chem. 1989. 264(21):12657-65.

Haynes WG, Morgan DA, Walsh SA, Mark AL, Sivitz WI. Receptor-mediated regional sympathetic nerve activation by leptin. J Clin Invest. 1997. 100:270–278.

Hutchings M and Barrington SF. PET/CT for therapy response assessment in lymphoma. J Nuc Med. 2009. 50:21S-30S.

Hutcheson R and Rocic P. The metabolic syndrome, oxidative stress, environment, and cardiovascular disease: the great exploration. Exp Diabetes Research. 2012. 2012(271028):1-13.

International Diabetes Federation. (http://www.idf.org/DMatlas/5e/the-global-burden). Accessed September 17, 2013.

Jacobson AF, Senior R, Cerqueira MD, Wong ND, Thomas GS, Lopez VA, Agostini D, Weiland F, Chandna H, Narula J. Myocardial iodine-123 meta-iodobenzylguanidine imaging and cardiac events in heart failure. J Am Coll Cardiol. 2010; 55(20):2212-21.

Jain SK, Croad JL, Velusamy T, Rains JL, Bull R. Chromium dinicocysteinate supplementation can lower blood glucose, CRP, MCP-1, ICAM-1, creatinine, apparently mediated by elevated blood vitamin C and adiponectin and inhibition of NFkappaB, Akt, and Glut-2 in livers of zucker diabetic fatty rats. Mol Nutr Food Res. 2010. 54(9):1371-80.

Johnson D, Shepherd RM, Gill D, Gorman T, Smith DM, Dunne MJ. Glucose-dependent modulation of insulin secretion and intracellular calcium ions by GKA50, a glucokinase activator. Diabetes. 2007. 56(6):1694-702.

Kalsbeek, A., Fliers, E., Hofman, M. A., Swaab, D. F. & Buijs, R. M. Vasopressin and the output of the hypothalamic biological clock. J. Neuroendocrinol. 2010. 22: 362–372.

Kenk M, Greene M, Thackeray J, deKemp RA, Lortie M, Thorn S, Beanlands RS, DaSilva JN. In vivo selective binding of (R)-[11C]rolipram to phosphodiesterase-4 provides the basis for studying intracellular cAMP signalling in the myocardium and other peripheral tissues. Nucl Med Biol. 2007. 34(1):71-7.

Kenk M, Thomas A, Lortie M, Dekemp R, Beanlands RS, Dasilva JN. PET measurements of cAMP-mediated phosphodiesterase-4 with (R)-[11C]rolipram. Curr Radiopharm. 2011. 4(1):44-58.

Kern W, Peters A, Born J, Fehm HL, Schultes B.Changes in blood pressure and plasma catecholamine levels during prolonged hyperinsulinemia. Metabolism. 2005. 54(3):391-396.

Khong FL, Zhang Y, Edgley AJ, Qi W, Connelly KA, Woodman OL, Krum H, Kelly DJ. 3', 4'-Dihydroxyflavonol Antioxidant Attenuates Diastolic Dysfunction and Cardiac Remodeling in Streptozotocin-Induced Diabetic m(Ren2)27 Rats. PLoS ONE. 2011; 6(7) e22777.

Kim SK, Zhao ZS, Lee YJ, Lee KE, Kang SM, Choi D, Lim SK, Chung N, Lee HC, Cha BS. Left ventricular diastolic dysfunction may be prevented by chronic treatment with PPAR-alpha or –gamma agonists in type 2 diabetic animal model. Diabetes Metab Rex Rev. 2003; 19(6):487-493.

Kishi, T. et al. Expression of melanocortin 4 receptor mRNA in the central nervous system of the rat. J. Comp. Neurol. 2003; 457, 213–235.

Kostis JB and Sanders M. The association of heart failure with insulin resistance and the development of type 2 DM. Am J Hypertens. 2005;18(5 Pt 1):731-737.

Kuo JJ, Jones OB, Hall JE: Chronic cardiovascular and renal actions of leptin during hyperinsulinemia. Am J Physiol Regul Integr Comp Physiol. 2003. 284:R1037–R1042.

Kuschel M, Zhou YY, Cheng H, Zhang SJ, Chen Y, Lakatta EG, Xiao RP. Gi protein mediated functional compartmentalization of cardiac β2-Adrenerfic Signalling. J Bio Chem. 1999; 274(31): 22048-22052.

Kraegen EW and Cooney GJ. Free fatty acids and skeletal muscle insulin resistance. Curr Opin Lipidol. 2008. 19(3):235-41.

Kramer HF, Witczak CA, Taylor EB, Fujii N, Hirshman MF, Goodyear LJ. AS160 regulates insulin- and contraction-stimulated glucose uptake in mouse skeletal muscle. J Biol Chem. 2006.20;281(42):31478-85.

Kuschel M, Zhou YY, Cheng H. Gi protein-mediated functional compartmentalization of cardiac β2-adrenergic signalling. J Biol Chem. 1999. 274: 22048-22052.

Landsberg L, Greff L, Gunn S, Young JB. Adrenergic mechanisms in the metabolic adaptation to fasting and feeding: effects of phlorizin on diet-induced changes in sympathoadrenal activity in the rat. (1980). 29: 1128-1137.

Lee Y, Hirose H, Zou YT, Esser V, McGarry JD, Unger RH. Increased lipogenic capacity of the islets of obese rats. Diabetes. 1997. 46:408-413.

Lee Y, Yu X, Gonzales F, Mangelsdorf DJ, Wang MY, Richardson C, Witters LA, Unger RH. PPAR alpha is necessary for the lipopenic action of hyperleptinemia on white adipose and liver tissue. Proc Natl Acad Sci U S A. 2002 Sep 3;99(18):11848-53.

Lefkowitz RJG. Protein-coupled receptors. III. New roles for receptor kinases and beta arrestins in receptor signalling and desensitization. J Biol Chem. 1998. 272: 18677-18680.
Lenzen, S. Alloxan and streptozotocin DM. Diabetology. 2008. 51: 216-226

Lenzen S. The mechanisms of alloxan- and streptozotocin-induced DM. Diabetology. 2008. 51:216-226

Levin BE. Glucose increases rat plasma norepinepherine levels by direct action on the brain. Am J Physiol. 1991. 261(6 Pt 2):R1351-7.

Lips MA et al. Autonomic nervous system activity in diabetic and healthy obese and the effect of distinct weight loss strategies. 2013. Eur Soc Endoc. [Epud ahead of print].

Liu X, Perusse F, Bukiwiecki LJ. Mechanisms of the antidiabetic effects of the β3-adrenergic agonist CL-316243 in obese Zucker-ZDF rats. Am J Physiol. 1998. 274:R1212-1219.

Lohse MJ, Benovic JL, Caron MG, Lefkowitz RJ. Mutiple pathways of rapid β_2-adrenergic receptor desensitization. J Biol Chem. 1990. 265(6): 3202-3209.

Lourenco CM, DaSilva JN, Warsh JJ, Wilson AA, Houle S. Imaging of cAMP-specific phosphodiesterase-IV: comparison of [11C]rolipram and [11C]Ro 20-1724 in rats. Synapse. 1999 ;31(1):41-50.

Lourenco CM, Kenk M, Beanlands RS, DaSilva JN. Increasing synaptic noradrenaline, serotonin and histamine enhances in vivo binding of phosphodiesterase-4 inhibitor (R)-[11C]rolipram in rat brain, lung and heart. 2006. Life Sci. 79(4): 356-364.

Lyon AR, Rees PS, Prasad S, Poole-Wilson PA, Harding SE. Stress (Takotsubo) cardiomyopathy--a novel pathophysiological hypothesis to explain catecholamine-induced acute myocardial stunning. Nat Clin Pract Cardiovasc Med. 2008;5(1):22-9.

Maison, P., Byrne, C. D., Hales, C. N., & Wareham, N. J. Hypertension and its treatment influence changes in fasting nonesterified fatty acid concentrations: A link between the sympathetic nervous system and the metabolic syndrome?. Metabolism,. 2000. 49(1), 81-87.

Massion PB, Feron O, Dessy C, Balligand JL. Nitric oxide and cardiac function: ten years after, and continuing. Circ Res. 2003;93(5):388-98.

Maric-Bilkan C. Obesity and Diabetic Kidney Disease. Med Clin NA. 2013. 97(1):59-74.

Marsh SA, Powell PC, Agarwal A, Dell'Italia LJ, Chatham JC. Cardiovascular dysfunction in Zucker obese diabetic fatty rats: role of hydronephrosis. Am J Physiol Heart Circ Physiol. 2007. 293: H292-298.

Matthews PM, Rabiner I, Gunn R. Non-Invasive imaging in experimental medicine for drug development. Curr Opin Pharmacol. 2011. 11:501-507.

McCance AJ and Forfar JC. Cardiac and whole body [^{3}H]noradrenaline kinetics in ischaemic heart disease: contrast between unstable angina syndromes and pacing induced ischemia. Br. Heart J. 1989. 61: 238-247.

McCully BH, Hasan W, Streiff CT, Houle J, Woodward WR, Giraud GD, Brooks VL, Habecker BE. Sympathetic cardiac hypperinnervation and atrial autonomic imbalance in diet-induced obesity promotes cardiac arrythmias. Am J Heart Circ Physiol. 2013. [Epub ahead of print].

McGuire DK, Inzucchi SE. New drugs for the treatment of DM mellitus. Part I. Thiazolidinediones and their evolving cardiovascular implications. Circulation. 2008. 117: 440-449.

McTernan PG, Harte AL, Anderson LA, Green A,Smith SA, Holder JC, Barnett AH, Eggo MC, Kumar S. Insulin and Rosiglitazone Regulation of Lipolysis and Lipogenesis in Human Adipose Tissue In Vitro. Diabetes. 2002. 51:1493-1498.

Merlet P, Delforge J, Syrota A, Angevin E, Mazière B, Crouzel C, Valette H, Loisance D, Castaigne C and Randé JL. Positron emission tomography with 11C CGP-12177 to assess beta-adrenergic receptor concentration in idiopathic dilated cardiomyopathy. 1993. 87:1169-1178.

Milburn JL, Hirose H, Lee YH, Nagasawa Y, Ogawa A, Ohneda M, BeltrandelRio H, Newgard CB, Johnson JH, Unger RH. Pancreatic β-Cells in Obesity. J Biol Chem. 1995; 270(3):1295-1299.

Minhas KM et al. Leptin repletion restores depressed β-adrenergic contractility in ob/ob mice independently of cardiac hypertrophy. J Physiol. 2005. 565(2):463-474.

Mohell N, Dicker A. The beta-adrenergic radioligand [3H]CGP-12177, generally classified as an anatagonist, is a thermogenic agonist in brown adipose tissue. Biochem J, 1989. 261:401-405.

Momose M, Reder S, Raffel DM, Watzlowik P, Wester HJ, Nguyen N, Elsinga PH, Bengel FM, Remien J, Schwaiger M. Evaluation of cardiac beta-adrenoreceptors in the isolated perfused rat heart using (S)-11C-CGP12388. J Nucl Med. 2004 Mar;45(3):471-7.

Morin D, Zini R, Urien S, Sapena R, Tillement JP. Labelling of rat brain beta-adrenoceptors: (3H)CGP-12177 or (125I)iodocyanopindolol? J Recept Res. 1992;12(3):369-87.

Münch G, Nguyen NT, Nekolla S, Ziegler S, Muzik O, Chakraborty P, Wieland DM, Schwaiger M. Evaluation of sympathetic nerve terminals with [(11)C]epinephrine and [(11)C]hydroxyephedrine and positron emission tomography. Circulation. 2000; 101(5):516-23.

Munoz MC, Giani JF, Dominici FP, Turyn D, Toblli JE. Long-term treatment with an angiotensin II receptor blocker decreases adipocyte size and improves insulin signalling in obese Zucker rats. J of Hypert. 2009. 27:2409-2420.

Munzberg H, Flier JS, Bjørbaek C. Region-specific leptin resistance within the hypothalamus of diet-induced obese mice. Endocrinology. 2004. 145(11): 4880-4889.

Muntzel MS et al. Cafeteria diet increases fat mass and chronically elevates lumbar sympathetic nerve activity in rats. Hypertension. 2012. 60:1498-1502.

Naya M, Tsukamoto T, Morita K, Katoh C, Nishijima K, Komatsu H, Yamada S, Kuge Y, Tamaki N, Tsutsui H. Myocardial beta-adrenergic receptor density assessed by 11C-CGP12177 PET predicts improvement of cardiac function after carvedilol treatment in patients with idiopathic dilated cardiomyopathy. J Nucl Med. 2009; 50(2):220-5.

Nicholson G, Hall GM. Diabetes mellitus: new drugs for a new epidemic. British Journal of Anaesthesia. 2011. 107(1):65-73.

Nissen SE, Wolski K. Effect of rosiglitazone on the risk of myocardial infarction and death from cardiovascular causes. N Engl J Med. 2007. 356:2457-2471.

Nunn N, Womack M, Dart C, and Barrett-Jolley, R. Function and pharmacology of spinally-projecting sympathetic pre-autonomic neurones in the paraventricular nucleus of the hypothalamus. 2011. Current neuropharmacology, 9(2), 262.

Olivetti G, Abbi R, Quaini F, et al. Apoptosis in the failing heart. N Engl J Med. 1997;336:1131-1141.

Oppermann M, Freedman NJ, Alexander RW, Lefkowitz RJ. Phosphorylation of the type 1A angiotensin II receptor by G protein-coupled receptor kinases and protein kinase C. J Biol Chem.1996; 271(22):13266-72.

Oral, EA. Leptin for type 1 diabetes: coming onto stage to be (or not?). Pediatric Diabetes. 2012. 13:68-73.

Paillole C et al. Prevalence and significance of left ventricular filling abnormalities determined by Doppler echocardiography in young type I (insulin-dependent) diabetic patients. Am J Cardiol. (1989). 64(16):1010-1016.

Palomares SM, Sweet JG, Cipolla MJ. Acute rosiglitazone treatment during reperfusion after hyperglycemic stroke is neuroprotective not vascular protective. Transl Stroke Res. 2012; 3(3):390-396.

Park JY, Chong AY, Cochran EK, Kleiner DE, Haller MJ, Schatz DA, Gorden P. Type 1 diabetes associated with acquired generalized lipodystrophy and insulin resistance: the effect of long-term leptin therapy. .J Clin Endocrinol Metab. 2008. 93(1):26-31

Park S et al. Central infusion of leptin improves insulin resistance and suppresses β-cell function, but not β-cell mass, primarily through the sympathetic nervous system in type-2 diabetic rat model. Life Sci. (2010). 86: 854-862.

Perez JE, McGill JB, Santiago JV, et al. Abnormal myocardial acoustic properties in diabetic patients and their correlation with the severity of disease. J Am Coll Cardiol. 1992;19:1154-1162.

Phillips LS, Grunberger G, Miller E, Patwardhan R, Rappaport EB, Salzman A. Once- and twice-daily dosing with rosiglitazone improves glycemic control in patients with type-2 DM. Diabetes Care. 2001. 24: 308-315.

Phillips MS, Liu QY, Hammond HA, et al. Leptin receptor missense mutation in the fatty Zucker rat. Nature Gen. 1996; 13, 18–19.

Piacentino V 3rd, Weber CR, Chen X, et al. Cellular basis of abnormal calcium transients of failing human ventricular myocytes. Circ Res. 2003; 92:651-658.

Pico C, Sanchez J, Oliver P, et al. Leptin production by the stomach is up-regulated in obese (fa/fa) Zucker rats. Obesity Res. 2002. 10, 932–938.

Radovits T, Korkmaz S, Loganathan S, Barnuez E, Bomicke T, Arif R, Karck M, Szabo G. Comparative investigation of the left ventricular pressure-volume relathionship in rat models of type 1 and type-2 DM mellitus. 2009. 297:H125-H133.

Raffel DM, Chen W. Binding of [3H]mazindol to cardiac norepinephrine transporters: kinetic and equilibrium studies. Naunyn Schmiedebergs Arch Pharmacol. 2004; 370(1):9-16.

Rahmim A, Zaidi H. PET versus SPECT: strengths, limitations and challenges. Nucl Med Commun. 2008. 29(3):193-207.

Ramanadham S, Decker P, Tenner TE, Jr. Effect of insulin replacement on streptozotocin-induced effects in the rat heart. Life Sci. 1983;33(3):289-296.

Reed MJ, Meszaros K, Entes LJ, Claypool MD, Pinkett JG, Gadbois TM, Reaven GM. A new Rat model of type-2 DM: the fat-fed streptozotocin-treated rat. Metabolism. 2000. 49: 1390-1394.

Ren J, Sowers JR, Walsh MF, Brown RA. Reduced contractile response to insulin and IGF-I in ventricular myocytes from genetically obese Zucker rats. Am J Physiol Heart Circ Physiol. 2000. 279: H1708-1714.

Roes SD, Dehnavi RA, Westenberg JMJ, Lamb HJ, Mertens BJA, Tamsma JT, de Roos A. Effect of lifestyle intervention plus rosiglitazone or placebo therapy on left ventricular mass assessed with cardiovascular magnetic resonance in the metabolic syndrome. J Cardiovasc Magn Reson. 2011;13(1):65.

Roof SR, Shannon TR, Janssen PM, Ziolo MT. Effects of increased systolic Ca and phospholamban phosphorylation during B-adrenergic stimulation on Ca transients kinetics in cardiac myocytes. Am J Physiol. 2011. 301(4):H1570-1578.

Rozec B, Erfanian M, Laurent K, Trochu JN, Gauthier C. Nebivolol, a vasodilating selective beta(1)-blocker, is a beta(3)-adrenoceptor agonist in the nonfailing transplanted human heart. J Am Coll Cardiol. 2009. 28;53(17):1532-8.

Salem KA, Kosanovic M, Qureshi A, Ljubisavljevic M, Howarth FC. The direct effects of streptozotocin and alloxan on contractile function in rat heart. Pharmacological Research. 2009; 59: 235-241.

Sauter, A., Goldstein, M., Engel, J., & Ueta, K. (1983). Effect of insulin on central catecholamines. Brain research, 260(2), 330-333.

Sherma V, Dhillon P, Wambolt R, Parsons H, Brownsey R, Allard MF, McNeill JH. Metoprolol improves cardiac function and modulates cardiac metabolism in the streptozotocin-diabetic rat. Am J Physiol Heart Circ Physiol. 2008. 294(4): H1609-1620.

Shimabukuro M, Zhou YT, Levi M, Unger RH. Fatty acid-induced β-cell apoptosis: A link between obesity and DM. Proc Natl Acad Sci. 1998. 95:2498-2502.

Shoghi KI, Finck BN, Schechtman KB, Sharp T, Herrero P, Gropler RJ, Welch MJ. In vivo metabolic phenotyping of myocardial substrate metabolism in rodents. Circ Cariovasc Imaging. 2009. 2: 373-381.

Sloan C, Tuinei J, Nemetz K, Frandsen J, Soto J, Wride N, Sempokuya T, Alegria L, Bugger H, Abel ED. Central Leptin Sinaling is Required to Normalize Myocardial Fatty Acid Oxidation Rates in Caloric-Restricted ob/ob mice. Diabetes. (2011). 60: 1424-1434

Song D, Kuo K-H, Tao R, Hutchings SR, Pang CCY. Inducible nitric oxide synthase depresses cardiac contractile function in zucker diabetic fatty rats. Eur J Pharmacol. 2008. 579:253-259.

Srinivasan K, Viswanad B, Asrat L, Kaul CL, Ramarao P. Combination of high-fat diet-fed and low-dose streptozotocin-treated rat: a model for type-2 DM and pharmacological screening. Pharmacol Res. 2005. 52: 313-320.

St-Pierre J, Tremblay ML. Modulation of leptin resistance by protein tyrosine phosphatases. Cell Metab. 2012;15(3):292-7.

Stevens MJ, Raffel DM, Allman KC, Schwaiger M, Wieland DM. Regression and progression of cardiac sympathetic dysinnervation complicating DM: An assessment by C-11 hydroxyephedrine and positron emission tomography. Metabolism. 1999. 48(1):92-101.

Straznicky NE, Grima MT, Sari CI, Eikelis N, Lambert EA, Nestel PJ, Esler MD, Dixon JB, Chopra R, Tilbrook AJ, Schlaich MP, Lambert GW. Neuroadrenergic Dysfunction Along the Diabetes Continuum: A comparative study in obese metabolic syndrome subjects. Diabetes. (2012). 61(10):2506-2516.

Straznicky NE, Grima MT, Sari CI, Karapanagiotidis S, Wong C, Eikelis N, Richards KL, Lee G, Nestel PJ, Dixon JB, Lambert GW, Schlaich MP, Lambert EA. The relation of glucose metabolism to left ventricular mass and function and sympathetic nervous ystem activity in obese subjects with metabolic syndrome. J Endocrinol Metab. 2013. 98: E227-E237.

Stucchi P, Guzmán-Ruiz R, Gil-Ortega M, Merino B, Somoza B, Cano V, de Castro J, Sevillano J, Ramos MP, Fernández-Alfonso MS, Ruiz-Gayo M. Leptin resistance develops spontaneously in mice during adult life in a tissue-specific manner. Consequences for hepatic steatosis. Biochimie. (2011). 93: 1779-1785.

Stumvoll M, Haring H-U, Matthaei S. Metformin. Endocr Res. 2007. 32:39-57.

Taegtmeyer H, McNulty P, Young M. Adaptation and maladaptation of the heart in DM: Part I: General concepts. 2002. 105: 1727-1733.

Tempel DL, Leibowitz SF. Glucocorticoid Receptors in PVN: Interactions with NE, NPY, and Gal in Relation to Feeding. Am J Physiol. 1993. 265:E794-E800.

Thackeray JT, Beanlands RS, Dasilva JN.Am J Nucl Med Mol Imaging. Altered sympathetic nervous system signaling in the diabetic heart: emerging targets for molecular imaging. 2012;2(3):314-34.

Thackeray JT, Beanlands RS, Dasilva JN. Presence of specific 11C-meta-Hydroxyephedrine retention in heart, lung, pancreas, and brown adipose tissue. 2007. J Nucl Med. 48(10):1733-40.

Thackeray JT, Dekemp RA, Beanlands RS, Dasilva JN. Insulin restores myocardial presynaptic sympathetic neuronal integrity in insulin-resistant diabetic rats. J Nucl Cardiol. 2013. [Epub ahead of print]

Thackeray JT, Parsa-Nezhad M, Kenk M, Thorn SL, Kolajova M, Beanlands RS, DaSilva JN. Reduced CGP12177 binding to cardiac β-adrenoceptors in hyperglycemic high-fat-diet-fed, streptozotocin-induced diabetic rats. Nucl Med Biol. 2011. 38(7):1059-66. (a)

Thackeray JT, Radziuk J, Harper ME, Suuronen EJ, Ascah KJ, Beanlands RS, DaSilva JN. Sympathetic nervous dysregulation in the absence of systolic left ventricular dysfunction in a rat model of insulin resistance with hyperglycemia. Cardiovascular Diabetology. 2011. 10(75): 1-13. (b)

Thomas AJ, DaSilva JN, Lortie M, Renaud JM, Kenk M, Beanlands RS, deKemp RA. PET of (R)-11C-rolipram binding to phosphodiesterase-4 is reproducible and sensitive to increased norepinephrine in the rat heart. J Nucl Med. 2011. 52(2):263-9.

Toblli JE, Cao G, Rivas C, Munoz M, Giani J, Dominici F, Angerosa M. Cardiovascular protective effects of nebivolol in Zucker diabetic fatty rats. J of Hypert. 2010. 28:1007-1019.

Unger RH. The physiology of cellular liporegulation. Annu Rev Physiol. 2005. 65:333-347.

Uyama, N., Geerts, A. & Reynaert, H. Neural connections between the hypothalamus and the liver. Anat. Rec. A Discov. Mol. Cell. Evol. Biol. 2004. 280, 808–820.

van der Brom CE, Huisman MC, Vlasblom R, Boontje NM, Duijst S, Lubberink M, Molthoff CFM, Lammertsma AA, van der Velden J, Boer C, Ouwens DM, Diamant M. Altered myocardial substrate metabolism is associated with myocardial dysfunction in early diabetic cardiomyopathy in rats: studies using positron emission tomography. Cardiovascular Diabetology. 2009. 8:39.

Van Waarde A, Meeder JG, Blanksma PK, Brodde OE, Visser GM, Elsinga PH, Paans AMJ, Vaalburg W, Lie KI. Uptake of radioligands by rat heart and lung in vivo: CGP 12177 does and CGP 26505 does not reflect binding to β-adrenoceptors. Cardiovascular Diabetology. 1992. 22: 107-112.

Viollet B, Guigas B, Leclec J, Herbrard S, Lantier L, Mounier R, Andreelli F, Foretz M. AMP-activated protein kinase in the regulation of hepatic energy metabolism: from physiology to therapeutic perspectives. Acta Physiol. 2009.196(1):81-98.

Wallukat G. The β-adrenergic receptors. Herz. 2002. 27:683-690.

Wallum BJ, Taborsky Jr GJ, Porte Jr D, Figlewicz DP, Jacobson L, Beard JC et. al. Cerebrospinal fluid insulin levels increase during intravenous insulin infusions in man. J Clin Endocrinol Metab. 1987. 64:190-194.

Wang M-Y, Koyama K, Shimabukuro M, Mangelsdorf D, Newgard CB, Unger RH. Role of peroxisome proliferators-activated receptor α in disease of pancreatic β cells. Proc Natl Acad Sci USA. 1998; 95:11921-11926. (a)

Wang M-Y, Koyama K, Shimabukuro M, Newgard CB, Unger RH. OB-Rb gene transfer to leptin-resistant islets reverses diabetogenic phenotype. Proc Natl Acad Sci USA. 1998. 95:714-718. (b)

Wang Y, Fice DS, Yeung KF. A simple high-performance liquid chromatography assay for simultaneous determination of plasma norepinephrine, epinephrine, dopamine and 3,4-dihydroxyphenyl acetic acid. J Pharm and Bio Anal. 1999. 21:519-525.

Wang P and Chatham JC. Onset of DM in Zucker diabetic fatty (ZDF) rats leads to improved recovery of function after ischemia in the isolate perfused hearts. Am J Physiol Endocrinol Metab 286: E725-E736.

Wasserfall CH, Mathews CE, Schatz DA. The use of leptin as treatment for type 1 diabetes mellitus: counterpoint. Pediatric Diabetes. 2012. 13:74-76.

Weiss R, Bremer AA, Lustig RH. What is metabolic syndrome and why are children getting it. Ann. N.Y. Acad Sci. 2013. 1281:123-140.

Welch MJ, Lewis JS, Kim J, Sharp TL, Dence CS, Gropler RJ, Herrero P. Assessment of myocardial metabolism in diabetic rats using small-animal PET: a feasibility study. J Nucl Med. 2006; 47(4):689-97.

Wild S, Roglic G, Green A, Sicree R, King H. Global prevalence of DM: estimates for the year 2000 and projections for 2030. Diabetes Care. 2004; 27:1047-53.

Woo V. Important differences; Canadian Diabetes Association 2008 clinical practice guidelines and the consensus statement of the American DM association and the European association for the study of DM. Diabetologia. 2009. 52: s52-s53.

Young JB and Landsberg L. Impaired suppression of sympathetic activity during fasting in the gold thioglucose-treated mouse. (1980). J Clin Invest. 65:1086-1094.

Young JB and Landsberg L. Stimulation of the sympathetic nervous system during sucrose feeding. Science. 1977; 196:1473-1475. (a)

Young JB and Landsberg L. Suppression of sympathetic nervous system during fasting. Science. 1977; 196:1473-1475. (b)

Young JB and Landsberg L. Sympathoadrenal activity in fasting pregnant rats: dissociation of adrenal medullary and sympathetic nervous system responses. (1979). J Clin Invest. 64:109-116.

Young M, McNulty P, Taegtmeyer H. Adaptation and maladaptation of the heart in DM: Part II: Potential mechanisms. 2002. 105: 1861-1870.

Yu M, Bozek J, Lamoy M, Guaraldi M, Silva P, Kagan M, Yalamanchili P, Onthank D, Mistry M, Lazewatsky J, Broekema M, Radeke H, Purohit A, Cdebaca M, Azure M, Cesati R, Casebier D, Robinson SP. Evaluation of LMI1195, a novel 18F-labeled cardiac neuronal PET imaging agent, in cells and animal models. Circ Cadiovasc Imaging. 2011; 4:435-443.

Zarich SW et al. Diastolic abnormalities in young asymptomatic diabetic patients assessed by pulsed Doppler echocardiography. J Am Coll Cardiol. 1988; 12(1):114-120.

Zhang F, Ye C, Li G, Ding W, Zhou W, Zhu H, et. al. The rat model of type-2 diabetic mellitus and its glycometabolism characters. Exp Anim. 2003. 52:401-7.

Zhang M, Turnbaugh D, Cofie D, Dogan S, Koshida H, Fugate R, Kem DC. Protein kinase C modulation of cardiomyocyte angiotensin II and vasopressin receptor desensitization. Hypertension.1996; 27(2):269-75.

Zhang P, Mende U. Regulators of G-protein signalling in the heart and their potential as therapeutic Targets. Circ Res. 2011; 109:320-333.

Zhao Q, Zeng F, Liu JB, He Y, Li B, Jiang ZF, Wu TG, Wang LX. Upregulation of β3-Adrenergic Receptor expression in the atrium of rats with chronic heart failure. J Cardiov Pharm and Therap. 2012; 18(2):133-137.

Zhou YY, Grayburn P, Karim A, Shimabukuro M, Higa M, Baetens D, Orci L, Unger RH. Lipotoxic heart disease in obese rats: Implications for human obesity. PNAS. 2000. 97(4): 1784-1789.

Zucker LM & Zucker TF. Fatty, a new mutation in the rat. J Heredity. 1961. 52, 275–278.